Techno-Economics of Green Hydrogen

Production, Compression, Transportation and Storage

Soham Saraf

TUDelft

Techno-Economics of Green Hydrogen

Production, Compression, Transportation and Storage

by

Soham Saraf

in partial fulfillment of the requirements for the degree of

Master of Science
in Mechanical Engineering

at the Delft University of Technology

Student number: 5540445
Project duration: January 2023- September 2023
Thesis committee: Dr. M. Ramdin (Supervisor)
                     Prof.dr.ir. TJH Vlugt
                     Dr. A.M.J. Felden

Faculty of Mechanical, Maritime and Materials Engineering

Acknowledgements

Abstract

To comply with the Paris Agreement, the Dutch government has launched an energy transition process, with the goal of replacing coal and natural gas-based electricity with renewable sources. The intermittent nature of renewable electricity necessitates the installation of an energy storage system to balance supply and demand.Hydrogen is a potential energy storage and transport medium. However, its production is currently more expensive than natural gas, and storage and transport are energy-intensive due to its low density. Because the infrastructure necessary for the hydrogen supply chain necessitates significant capital investments, a techno-economic analysis of various techniques of hydrogen production, compression, storage, and transport is required.

The aim of this thesis was to evaluate the levelized costs of hydrogen at various phases of supply chain, from hydrogen production to utilization. In order to accomplish this task, a literature review was conducted to identify the most promising methods in hydrogen production, compression, storage and transport followed by developing mathematical models of various technologies. According to the literature review, water electrolysis using electrolyzers such as alkaline, polymer electrolyte membrane (PEM), and solid oxide was shown to be techno-economically feasible.The literature review also revealed that centrifugal and diaphragm compression, pipeline transmission, and salt cavern storage were all techno-economically feasible technologies.These technologies' steady-state mathematical models were built for scaling and techno-economic analysis.In the end, learning curves were applied for electrolyzers to predict the cost reductions in future.

According to the results of mathematical modeling, hydrogen production contributes the most to total levelized costs of supply chain followed by overall compression costs. Moreover, capital costs of electrolyzer stack and electricity costs significantly influence the levelized costs of hydrogen production. For 1 MW electrolyzer capacity and average capital and operating costs of electrolyzer stack, alkaline electrolysis is currently the most cost-effective technique of producing hydrogen with levelized cost of hydrogen (LCOH) calculated to be 3.69 €/ kg, followed by solid oxide electrolysis (4.55 €/kg).However, the use of learning curves indicates that by 2050, solid oxide electrolysis may be the most cost-effective technique of producing hydrogen with projected levelized cost of 1.72 €/kg. The pipeline compression costs were found to be around 0.065 €/ kg whereas diaphragm compression costs were found to be in the range of 0.55 to 1.2 €/ kg depending on the outlet pressure. While hydrogen storage and transportation require substantial capital investment, their overall impact on levelized costs was found to be minimal compared to production and compression expenses, with storage costs averaging around 0.8 €/kg and transportation costs at approximately 0.0007 €/kg per kilometer.The same mathematical model was used to analyze two hydrogen utilization scenarios: fuel for fuel cell vehicles and feed for industry. Both pessimistic and optimistic cases were examined by varying cost-influencing parameters to predict the possible range of total levelized costs for the supply chain. The results showed that hydrogen as a fuel for fuel cell vehicles will stay more expensive than hydrogen as a feed for industry.

Contents

Nomenclature

List of Abbreviations

CAPEX Capital costs

CEPCI Chemical engineering and plant cost index

EPC Engineering, procurement and construction

GHG Greenhouse gas

KS Knowledge stock

LBD Learning by doing

LBS Learning by searching

LCOE Levelized cost of electricity ($/MWh)

LCOH Levelized costs of hydrogen (€/kg H_2)

LR Learning rate

MFLC Multi factor learning curve

MOF Metal organic framework

OFLC One factor learning curve

OPEX Operating costs

PEM Proton Exchange Membrane

PR Progress rate

SOE Solid oxide electrolyzer

TFLC Two factor learning curve

TRL Technology readiness level

List of Figures

List of Tables

<div align="right">

1

</div>

Introduction

1.1. Climate Change and Energy Transition

In 2015, the Paris agreement was signed by 196 countries to maintain the global temperature rise below 2°C. Moreover, European Union intends to become carbon neutral by 2050. In order to achieve these targets, the Dutch government introduced the climate act in 2019 which aims to reduce the Netherlands' GHG emissions by 49% by 2030 and 95% by 2050 as compared to 1990 levels [1]. The CO_2 emissions from the Dutch energy sector is the largest source of GHG emissions in the Netherlands and accounts for 83% of total Dutch emissions [2]. The Netherlands produced about 40% of its electricity from natural gas and 21% from coal [3] in 2020. To comply with the climate act while maintaining energy security, it has been planned to reduce the consumption of natural gas and completely phase out the coal based energy supply [3]. To fulfill the energy demands, renewable electricity is set to gradually replace the conventional sources of energy as seen from Table 1.1 [2].

Table 1.1: Installed electricity generation capacity by type in the Netherlands, 2005-2030 (GW)[2]

	2005	2010	2015	2020	2025	2030
Natural gas	10.3	14.1	17.7	17.1	16.4	15.4
Coal	9.5	8.9	11.2	4.1	3.4	0.0
Nuclear	0.4	0.5	0.5	0.5	0.5	0.5
Wind	1.2	2.2	3.4	6.4	12.6	16.6
Solar PV	0.1	0.1	1.5	9.0	19.2	26.1
Biomass and waste	0.5	0.8	0.9	0.5	0.5	0.4
Hydro	0.04	0.04	0.04	0.04	0.04	0.04
Total	21.9	26.6	35.2	37.6	52.7	59.0

Although the renewable energy will play a significant role in decarbonising the energy sector, it will also introduce new challenges. One of the challenges of incorporating renewable electricity is the intermittent energy generation. Solar and wind farms are two of the main renewable energy producing technologies in the Netherlands. Electricity generated from both of these methods is dependent on daily and seasonal variations in solar irradiation and wind speed respectively. Moreover, electricity produced from renewable sources does not match the demand curve, i.e peak and valley periods of energy generation do not match with peak and valley periods of energy consumption [4]. To alleviate the aforementioned challenges, energy storage becomes a vital component in renewable energy systems. Although there are many energy storage methods available such as compressed air storage, pumped hydropower, batteries, hydrogen etc., batteries and hydrogen have been the focus of academia and industry [5]. Although batteries are more mature technology as compared to hydrogen, batteries self-discharge over a period of time making them unsuitable for long term storage. Hydrogen produced from wind/solar based electricity (known as green

hydrogen) addresses most of the problems posed by renewable electricity. Moreover, hydrogen also has uses in heating and chemical industries. Due to these reasons, hydrogen is one of the most promising energy storage and carrier method currently available.

1.2. Role of Green Hydrogen in Energy Transition

As discussed in the previous section, renewable energy will be the most contributing energy supply method in upcoming years. Green hydrogen is a viable option in the Netherlands due to two factors: the North Sea's potential for wind energy and the country's already-existing gas infrastructure, primarily because of the Groningen gas field. The wind power can be converted into green hydrogen by electrolysis process and existing natural gas pipeline network can be repurposed for the hydrogen transport. As hydrogen gas can be used for variety of applications such as heating, feed, fuel etc., an integrated energy system can be constructed which could lead to more efficient production and distribution of energy [6].

But, use of green hydrogen also introduces some challenges in the supply chain. First one is the highly energy intensive nature of green hydrogen production through the process of water electrolysis. As hydrogen is the element with lowest density, compression and storage are complex and energy intensive as compared to natural gas. And since most of the energy supply infrastructure in existence today is designed for natural gas and oil, energy transition could prove to be trickier. The extent and rate of energy transition is dependent on variables such as technical development and deployment, infrastructure development and economical feasibility of associated components. Economic viability for energy carriers is especially important since energy costs have influence on many sectors such as manufacturing, transport, services etc. Therefore, to understand the costs of green hydrogen to the consumer, a detailed techno-economic analysis is necessary. In this thesis, the techno-economical aspects of green hydrogen are studied in detail.

1.3. Research Questions

The main research question addressed in this thesis is:
How the costs associated with green hydrogen production, storage and transportation will change with time?
To answer the main question, following sub-objectives were identified:

1. Creating a python model incorporating production, storage and transportation stages to evaluate the levelized cost of hydrogen on the basis of mass and energy balances, capital and operating costs.

2. Evaluation of economics involved and generate learning curves to predict the cost of hydrogen in future.

3. Performing the sensitivity analysis using the python model to assess the impact of some input parameters such as electricity costs, operating pressures, temperatures etc.

1.4. Research Methodology

In the hydrogen supply chain, multiple options exist for hydrogen production, compression, storage, and transportation. To determine the most viable approaches, a comprehensive literature review was conducted. Based on the technological maturity and economic feasibility information found in the literature,the components depicted in Figure 1.1 were considered in the techno-economic analysis of the green hydrogen supply chain.
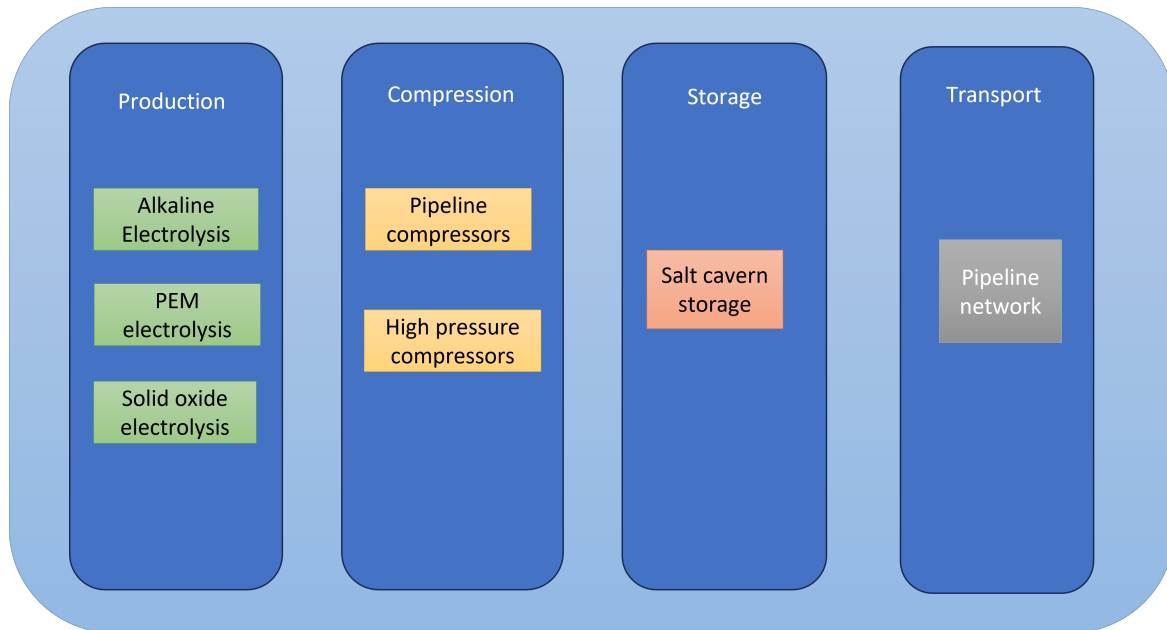
Figure 1.1: Components considered in the techno-economic analysis of green hydrogen supply chain

Based on the components shown in Figure 1.1,following tasks are identified:

1. **Hydrogen Production**:
   Alkaline, PEM, and solid oxide electrolyzers were identified as more feasible technologies from the literature. Therefore, techno-economic models using Python were built to assess the impact of operating conditions, scale, etc. on levelized costs of hydrogen production.

2. **Hydrogen Compression**:
   Hydrogen needs to be compressed several times during the supply chain. Mainly, compression is needed before storage, before transport, and for the refueling of fuel cell vehicles. As the production-transport-storage components are interlinked, scenario building was done to calculate the LCOH for the particular scenario.

3. **Hydrogen Storage**:
   From the literature, it was determined that underground storage in salt caverns is one of the ideal options for the Netherlands due to availability. Therefore, a techno-economic model similar to electrolyzers was built using Python.

4. **Hydrogen transport**:
   A techno-economic model for the pipeline network in the Netherlands was constructed in Python. The levelized costs of hydrogen per kilometer transported were calculated.

5. **Scenario building and integration of models**:
   Several scenarios will be constructed encompassing different utilization scenarios, storage cycles, etc., and production, transportation, and storage models constructed before were used to predict the levelized costs of hydrogen to the consumer.

6. **Application of learning curves**:
   Based on the learning rates for various components, learning curves were applied to predict how total LCOH will change with time.

7. **Sensitivity analysis**:
   During the literature study, it was identified that there is a wide range of predicted capital costs for electrolyzers. Also, the electricity costs, learning rates, etc. vary over a certain range. A sensitivity analysis using models constructed was performed to estimate the impact of different parameters.

1.5. Report Outline

This thesis comprises eight chapters. Chapter 2 provides a summary of the literature review conducted, along with the resulting conclusions. Chapter 3 discusses the equations employed in the electrochemical and techno-economic modeling of alkaline, PEM, and solid oxide electrolyzers. Chapter 4 centers on the compression system, explaining the assumptions made and the equations utilized to calculate the levelized costs associated with centrifugal and diaphragm compressors. Chapter 5 is about the equations and assumptions applied in the techno-economic analysis of a hydrogen pipeline network. Chapter 6 is dedicated to the equations used in the salt cavern storage of hydrogen and the associated costs. Chapter 7 involves the analysis of results obtained from models developed using equations discussed in Chapters 3-6. It presents the levelized costs of hydrogen production, compression, storage, and transport under a variety of conditions. Towards the chapter's end, various scenarios are assessed to demonstrate the total levelized costs of hydrogen for consumers. Chapter 8 provides a comprehensive discussion of the conclusions and recommendations derived from the analysis of results.

2

Literature Review

In this chapter, the state of the art of various components of the supply chain is discussed. In section 2.1, a brief overview of some physical and chemical properties of hydrogen is given. In section 2.2, various components involved in the supply chain are explained. In section 2.3, some important parameters such as the capacity factor for the Netherlands and levelized costs of electricity are described. Section 2.4 covers hydrogen production by electrolysis. Some types of electrolyzers are also discussed. Section 2.5 gives a general overview of available hydrogen storage technologies and their suitability for the Dutch hydrogen infrastructure. In section 2.6, different methods of hydrogen transport are discussed with some emphasis on the Dutch pipeline network. Section 2.7 gives a brief overview of different types of compressors while in section 2.8, some economic parameters and learning curves are explained.

2.1. Physical and chemical properties of hydrogen

The physical and chemical properties of hydrogen influence the design and sizing of different components of the green hydrogen supply chain. Therefore, a short summary of the relevant properties of hydrogen is given in this section.

Hydrogen is the first element in the periodic table with a molecular weight of 2.016 g/mol. It is a colorless and odorless gas at ambient conditions and burns with a pale blue flame that is nearly invisible in daylight [7]. The relevant properties are given in Table 2.1.

Property	Value
Lower heating value (LHV, MJ/kg)	120
Higher heating value (HHV, MJ/kg)	142
Density at 273 K (kg/m^3)	0.09
Boiling point at atmospheric pressure (K)	20.3
Liquid density (kg/m^3)	70.8
Flammability concentration limits in air (vol %)	4-75
Diffusion coefficient in air (cm^2/s)	0.61

Table 2.1: Physical and chemical properties of hydrogen [7][8]

The density of hydrogen is very low as seen from Table 2.1. For comparison, natural gas has a density of 0.65 kg/m^3 [9]. But at the same time, lower heating value of hydrogen is 120 MJ/kg while that of natural gas is 52 MJ/kg [9]. Thus, hydrogen offers higher gravimetric energy density (MJ/kg) but poor volumetric energy density (MJ/l) as compared to natural gas.

2.2. Main components of green hydrogen supply chain

A general overview of components involved in the green hydrogen supply chain is given in Figure 2.1.The components discussed will be expanded on in the next sections. All of these components add to the final cost of green hydrogen.
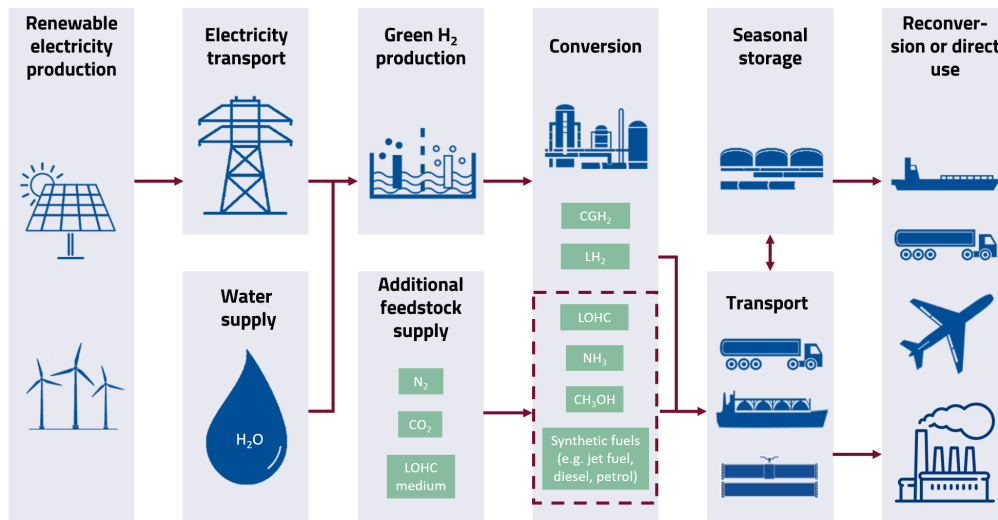
Figure 2.1: The green hydrogen supply chain incorporates essential components like electricity and water supply, green hydrogen production, conversion alternatives, as well as storage and transportation of hydrogen as shown in this figure. [10]

As seen from the Figure 2.1, there are seven major steps involved:

1. **Renewable electricity production**: Various energy forms, such as mechanical energy, solar radiation, and so on, are turned into electrical energy in this process. There are multiple sources of renewable energy generation such as solar, wind, biogas, tidal power etc.

2. **Electricity transport and water supply**: Renewable electricity produced has to be transported to the electrolyzer location by means of a grid network. Moreover, desalinated water is required as a feed for green hydrogen production.

3. **Green H_2 production**: In this step, desalinated water is decomposed to form hydrogen and oxygen by electrolysis process.The device used for this process is known as an electrolyzer. Based on materials of construction and working fluids, there are various types of electrolyzers available. In section 2.4, working and state of the art of some electrolyzers is explained in detail.

4. **Conversion**: Due to the low density of hydrogen at ambient pressure and temperature, a conversion step is often necessary before storage. There are many conversion methods such as high pressure compression, liquefaction, chemicals such as methanol etc.

5. **Storage**: Depending on the utilization route of green hydrogen, hydrogen storage can be broadly classified as short term and long term storage. Compressed hydrogen storage in tanks or salt caverns, liquefied hydrogen storage, chemical storage are some examples of hydrogen storage methods.

6. **Transport**: Hydrogen transport methods vary on the basis of hydrogen storage methods. For example, compressed hydrogen can be transported via pipelines and tube trailers. Ammonia and methanol can be transported in the steel tanks by ships.

7. **Utilization**: Currently, hydrogen in mainly used as a feed in chemical industries. But in the near future, hydrogen will also be utilized for heating. In the next few decades, depending on the development in fuel cell technologies and hydrogen combustion, hydrogen could be a potential fuel source for vehicles. These utilization methods will also have an influence on total green hydrogen cost to the consumer as some additional steps are involved in the utilization.

2.3. Renewable electricity generation

2.3.1. Renewable electricity in the Netherlands

The levelized costs of green hydrogen production (LCOH) depend heavily on the annual operating hours of the electrolyzer. Since electrolyzers use renewable electricity, intermittency involved in renewable energy generation influences the annual operating hours of the electrolyzer. Although it is possible to obtain the weather data for a particular location and calculate the hourly energy generation from wind and solar sources on an annual basis, it adds complexity and computation time for the total electrolyzer operation time. Therefore, a term called "capacity factor" is introduced to predict the renewable energy output per annum. The capacity factor can be defined by the following equation:

$$\text{Capacity factor} = \frac{\text{Actual energy output}}{\text{Theoretical maximum energy output}} \qquad (2.1)$$

In Figure 2.2 and 2.3, the capacity factor for solar PV and wind farms for Europe are shown. It can be seen that the solar capacity factor for Europe varies between 0.07 and 0.21 whereas, for the onshore and offshore wind farms, it varies between 0.12 and 0.7. For the Netherlands, the solar capacity factor is around 0.12 and the wind capacity factor is around 0.4.
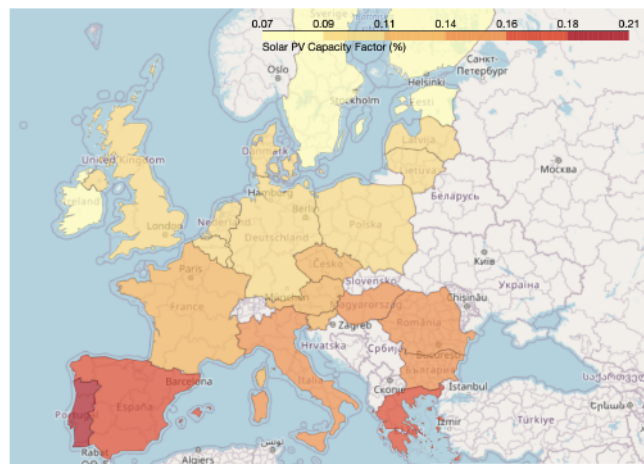
Figure 2.2: Capacity factor for solar PV systems in Europe [11]
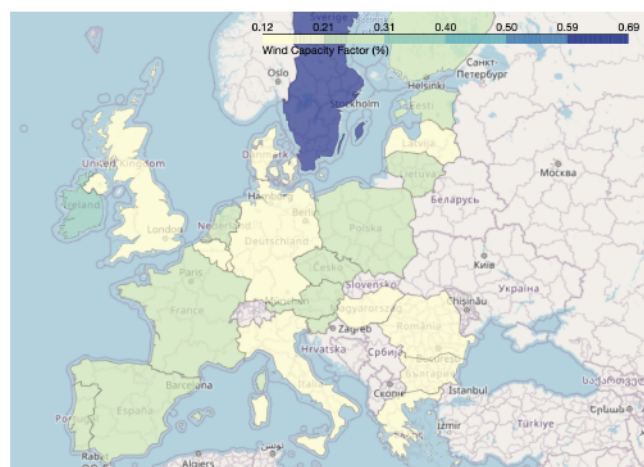
Figure 2.3: Capacity factor for onshore and offshore systems in Europe [11]

Therefore, wind energy is a more favorable option for the Netherlands due to the higher capacity factor which is dependent on geological location and weather patterns.

2.3.2. Levelized cost of electricity

The levelized cost of electricity (LCOE) depends on the capital and operating costs of wind farms, the lifespan of components, and capacity factor [12].

According to the IRENA report [12], LCOE for onshore wind farms decreased by 90% for the period from 1984 to 2021. Factors behind this decline are [12]:

1. Turbine technology improvements: Over the last few decades, turbine sizes have increased along with several optimizations in rotor diameter and specific power. Moreover, with the use of electronic systems, research in suitable geographic locations, etc., the cost of electricity generation has been reduced

2. Economies of scale: As the cost of manufacturing and installation per turbine is reduced with the increase in scale, its contribution towards LCOE has decreased as well.

3. O&M costs

4. Competitive procurement

In figure 2.4, LCOE from onshore wind farms, as predicted by IEA [13], is given. In this graph, the dotted light green line represents the global average LCOE while the CAPEX cost of wind turbine ($/MWh) is represented by the dark green line. The blue bars represent the global range of LCOE. According to Figure 2.4, the LCOE was 76.21 $/MWh. IEA has predicted that in 2025, the LCOE will be 44.6 $/MWh.
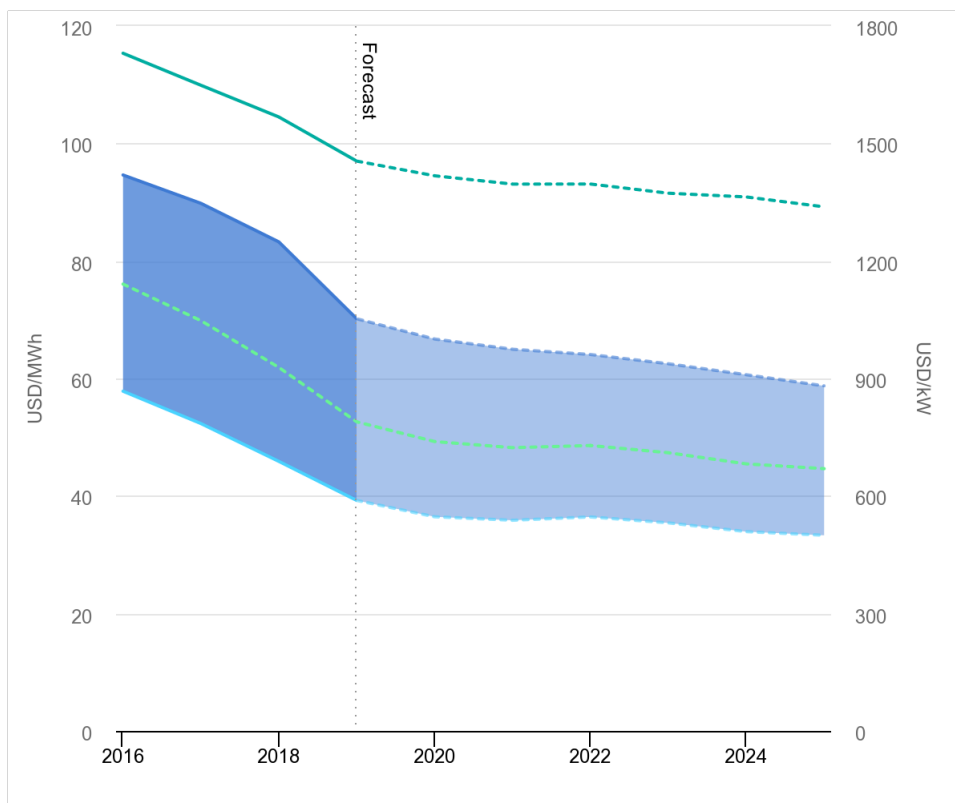
Figure 2.4: Actual and forecast onshore wind costs,2016-2025 [13]

But, as these predictions depend on a multitude of factors, various sources such as Bloomberg, and IRENA [14] differ in the predicted LCOE.

2.4. Hydrogen Production

2.4.1. Water Electrolysis

Hydrogen gas can be created by the electrolysis process, a process in which water molecules are decomposed into hydrogen and oxygen molecules. Figure 2.5 depicts a simple cell diagram of an electrolyzer.
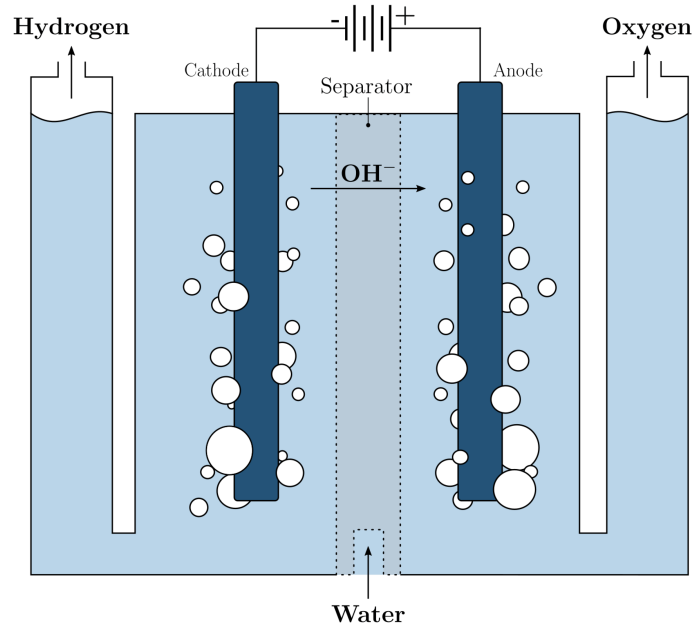
Figure 2.5: A schematic of an alkaline electrolyzer cell is shown in the figure. Voltage is applied across the electrodes to decompose water. Hydrogen and oxygen bubbles are formed at cathode and anode respectively. [15]

An electrolyzer consists of the following main components:

1. **Electrodes**: A direct current is applied to the electrodes which dissociate the water molecules on the electrode surface. Based on the charge of electrodes, they are classified as anode and cathode. In the case of water electrolysis, hydrogen is formed at the cathode and oxygen is formed at the anode.
2. **Electrolyte**: Electrolyte materials/solutions carry the ions to complete the circuit
3. **Separator**: Separator serves many purposes such as selective permeability of ions, gas diffusion barrier and prevents the risk of short circuiting.

This water splitting reaction is an example of redox reaction. The overall reaction can be written as follows:

$$2\,H_2O\,(l) \longrightarrow 2\,H_2(g) + O_2(g)$$
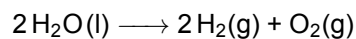
The reversible cell voltage, U_{rev} can be calculated by the formula given below:

$$U_{rev} = -\frac{\Delta G}{zF} \tag{2.2}$$

Here, z is the number of electrons transferred and is equal to 2 and the Faraday's constant (F = 96485 Cmol^{-1} [16].At a temperature of 25 °C and ambient pressure, the free reaction enthalpy ΔG is 237 kJ/mol [16]. It corresponds to the cell voltage of -1.23 V. The Gibbs free energy can be correlated to reaction enthalpy by the following formula:

$$\Delta G = \Delta H - T\Delta S \tag{2.3}$$

As the reaction is non spontaneous and to account for the entropy, cell voltage higher than the reversible voltage needs to be applied and is known as thermoneutral voltage since no heat is generated at this

voltage. This thermoneutral voltage is a function of reaction enthalpy as seen in the equation 2.4

$$U_{th} = -\frac{\Delta H}{zF} \tag{2.4}$$

At normal temperature and pressure, the thermoneutral voltage is -1.48 V [16]. The actual cell voltage is the summation of thermoneutral voltage and overpotentials which accounts the different resistances involved.These overpotential values depend on the materials of construction, composition of electrolyte etc.Thermoneutral voltage also varies with operating conditions such as temperature and pressure. There are many different types of electrolyzers available such as alkaline, PEM, SOEC etc. These types differ from each other in terms of electrode materials, working fluid and operating parameters. In further subsections, working of these electrolyzers is explained in detail.

2.4.2. Alkaline Electrolyzer

Alkaline water electrolysis is the most mature technology as compared to other types. Alkaline electrolyzer operates at lower temperature ranges such as 30 - 80 °C [17] and 1-10 bar pressure. In Figure 2.6, a simple schematic of an alkaline electrolyzer is shown.
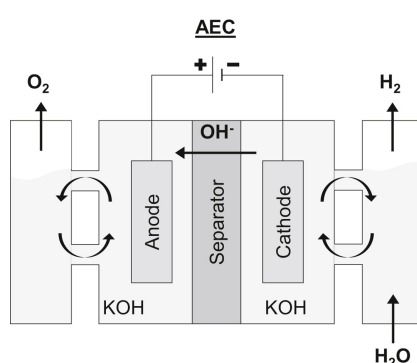
Figure 2.6: Schematic of alkaline electrolyzer [18]

The half cell reactions occurring at electrodes can be written as follows:

Cathode:

$$2\,H_2O\,(l) + 2\,e^- \longrightarrow H_2(g) + 2\,OH^-$$

Anode:

$$2\,OH^- \longrightarrow 0.5\,O_2\,(g) + H_2O\,(l) + 2\,e^-$$
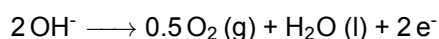
In this electrolyzer,20-40 % liquid sodium hydroxide or potassium hydroxide solution acts as an electrolyte [19]. These electrodes are separated by diaphragm (made of materials such as Zirfon [20] or NiO$_2$ [21]. Diaphragm allows water molecules and hydroxide ions to pass through. It also acts as a barrier between hydrogen and oxygen molecules and thereby improves purity. Purity of hydrogen produced is between 99.5 to 99.9 % [19].

Although alkaline electrolysis is a mature technology, some drawbacks still remain such as limited current density and relatively low energy efficiency [17]. As this electrolyzer usually operates at ambient pressure, there are some positive and negative aspects associated with it. Due to the operation at ambient pressure, the walls of electrolyzer don't need to have higher tensile strength and therefore plastics can be used which reduce the capital costs. At the same time, hydrogen produced at ambient pressure requires extra compression work and thus compression costs are increased.

2.4.3. Proton Exchange Membrane (PEM) Electrolyzer

PEM is a relatively new electrolysis technology as compared to alkaline electrolyzers. But, it has been introduced commercially in the past few years.PEM differs significantly from alkaline electrolyzers in terms

of electrode and electrolyte materials, operating pressure and temperature range, and response rate. A schematic of the PEM electrolyzer is shown in the Figure 2.7
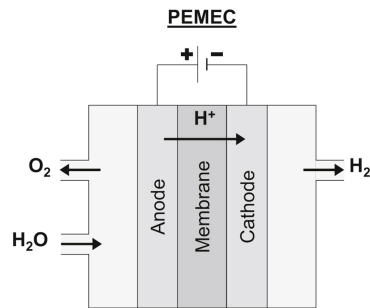
Figure 2.7: Schematic of PEM electrolyzer [18]

The half cell reactions occurring at electrodes can be written as follows:

Cathode:

$$2\,H^+ + 2\,e^- \longrightarrow H_2$$
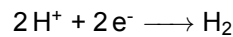
Anode:

$$H_2O \longrightarrow 0.5\,O_2 + 2\,H^+ + 2\,e^-$$

Electrodes in the PEM electrolyzer are made of noble metals such as platinum, iridium, ruthenium and platinum on carbon [19]. As the name suggests, solid polysulfonated membranes (Nafion, fumapem) are used as electrolytes [17]. These membranes have low gas permeability and high proton conductivity [17]. PEM electrolysis has some advantages as compared to alkaline electrolysis such as compact design, high efficiency, fast response rate to intermittency and better purity of hydrogen and oxygen streams [17]. Despite these advantages, due to the involvement of noble materials in the construction, the levelized cost of hydrogen production is generally higher for PEM as compared to alkaline electrolysis. Moreover, the stack lifetime is also lower in the case of PEM electrolysis [19].

2.4.4. Solid Oxide Electrolyzer (SOE)

This technology is still in the pilot commercial phase with some projects such as Hydrohub [22] being implemented in the Netherlands. One key feature of SOE is the operation at higher temperatures (500-850 °C [17]. Due to high operating temperatures, achieving higher efficiencies as compared to alkaline and PEM electrolyzers is possible as thermoneutral voltage required reduces with temperature. At the same time, degradation of electrode materials [17] is an issue which needs to be addressed for commercial success of the technology. A schematic of solid oxide electrolyzer cell is shown in Figure 2.8.
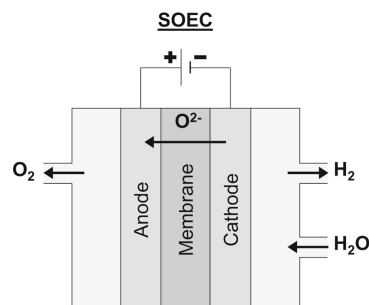
Figure 2.8: Schematic of solid oxide electrolyzer [18]

The half cell reactions occurring at electrodes can be written as follows:

Cathode:

$$H_2O + 2\,e^- \longrightarrow H_2 + O^{2-}$$
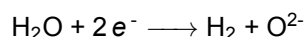
Anode:

$$O^{2-} \longrightarrow 0.5\,O_2 + 2\,e^-$$
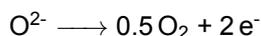
Due to higher heating efficiency, levelized costs of hydrogen production are lower as compared to alkaline or PEM electrolyzers. Therefore, research is being done to improve the lifespan of electrodes.

Some general information about the electrolyzers discussed above is summarized in Table 2.2. For these electrolyzers, operating conditions have an impact on operating voltages which in turn directly influence the economical aspects. Therefore, optimization and sensitivity analysis of various operating parameters is necessary to identify the best electrolyzer type for the given scenario.

Specification	PEM	AWE	SOE
Maturity	Commercial	Commercial	Early Commercial
Electrolyte	Solid polymer	aqueous solution of KOH/NaOH	Solid ceramic
Charge carrier	H^+	OH^-	O^{2-}
Anode material	Pt, Ir, Ru	Ni	LSMYSZ, $CaTiO_3$
Cathode material	Pt, Pt=C	Ni	Nicermets
Temperature, °C	65-100	30-80	500-850
Operating pressure (bar)	15-30	1-10	<30
Efficiency, HHV (%)	67-84	62-82	$\sim$90
Cell voltage, V	1.80-2.40	1.80-2.40	0.95-1.30
Current density (A/cm^2)	0.6-2	0.2-0.4	0.3-1
Startup duration	<15 minutes	15 minutes	>60 minutes
Stack lifetime (hr)	<40,000	<90,000	<40,000
Advantages	Compact design; fast response; high hydrogen purity	Low capital cost; no use of noble material	High efficiency; low capital cost
Disadvantages	Use of noble materials; low stack life	Slow response; low current density	Degradation of electrodes; safety and scaling problems

Table 2.2: Summary of electrolyzer specifications

2.5. Hydrogen storage

Hydrogen storage methods can be broadly classified into two categories: physical and chemical hydrogen storage. In physical hydrogen storage methods, hydrogen is stored in its pure molecular form. Whereas in chemical hydrogen storage, the stored hydrogen atoms have strong interactions with atoms of other elements. Figure 2.9 shows some hydrogen storage methods according to the classification.
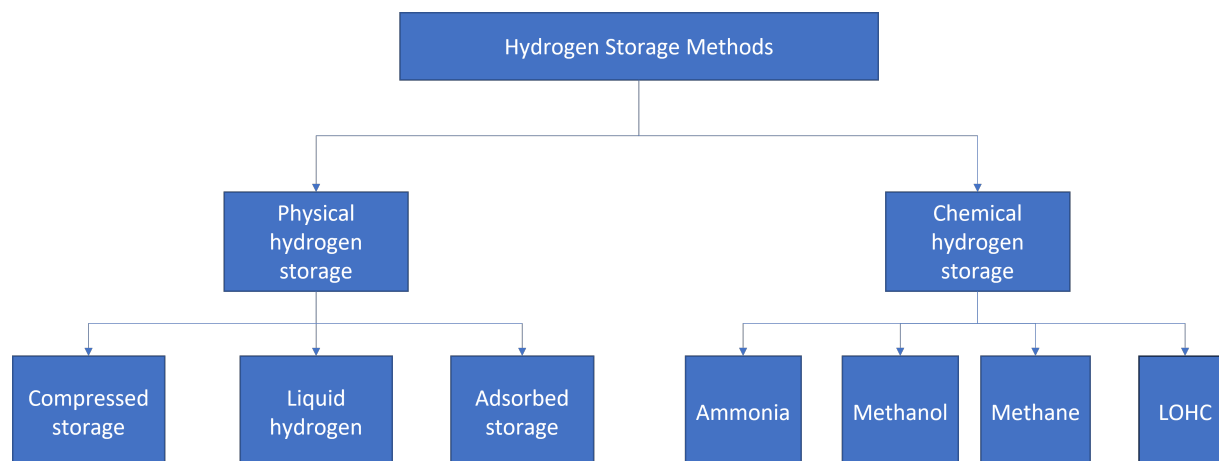
Figure 2.9: Classification of hydrogen storage methods

Summary of these storage methods is given below:

1. **Compressed storage**: This method involves compressing the hydrogen gas to 250-700 bar and storing it in tanks or underground in geological formations such as salt caverns, rock formations and depleted gas fields. Usually a multistage reciprocating or centrifugal compression system is used to compress the hydrogen. A detailed overview of this storage method is given in the next subsection.

2. **Liquid hydrogen**: In this method, hydrogen is cooled to -253 °C by passing the hydrogen feed stream through a series of heat exchangers and expanding it in a valve which causes cooling of the feed stream. The liquid hydrogen formed is then stored in an insulated tank. As the hydrogen is stored at ambient pressure in a liquid phase, thickness, internal volume and thereby weight of the storage tank is reduced. But, the liquefaction of hydrogen is a complex and expensive process. Moreover, due to ortho-para conversion inside the storage tanks, boiloff losses are present in the system [23]. Thus, this method is not suitable for long-term storage.

3. **Adsorbed storage**: This is a category of hydrogen storage that uses porous materials for storage using the physisorption phenomenon [24]. Some examples in this category are metal-organic frameworks (MOF), carbon materials, silica and alumina. In the case of MOFs, hydrogen is stored at 77K and 20 bar. Capacities of 4.5 wt% at 78 K [25] have been reported. For carbon nanostructures, at 298 K and 100 bar pressure, a gravimetric energy density of 2% has been observed [25]. These methods are costly because of involvement of either high pressures or low temperatures.

4. **Ammonia**: Ammonia (NH_3) is a carbon free hydrogen storage method. Ammonia can be synthesized from hydrogen and nitrogen using Haber Bosch process which has been used in the industry for over 100 years [26]. Ammonia can be stored at lower pressures (2-15 bar) in steel tanks [26]. Ammonia also has higher volumetric energy density as compared to liquid hydrogen (7.1 vs 2.9 MJ/L) [26].

5. **Methanol**: Methanol (CH_3OH) can be produced by reductive hydrogenation using CO_2. As CO_2 is being consumed in production, this method can be used to solve global warming issues by reducing the emission of CO_2 [27]. As methanol is in the liquid phase at ambient temperature and pressure, storage of methanol is less complicated than physical hydrogen storage methods. Direct methanol fuel cells can be used to convert methanol back into electricity.

6. **Methane**: Methane (CH_4) can be produced by a process called methanation. After producing hydrogen from electrolysis, catalytic hydrogen-carbon dioxide methanation is performed to convert electricity into methane [25]. Methane can be either compressed or liquefied for storage. As natural

gas has about 75% methane (mol%), the existing natural gas technologies can be used to predict the methane potential [25]. The liquefied natural gas boils off due to heat penetration into the tanks. Methane is also a GHG gas and boiloffs would lead to GHG emissions into the environment. Recovering hydrogen from methane is done by a steam methane reforming process which is an endothermic reaction. Therefore, additional energy is required to recover the hydrogen.

7. **LOHC**: Liquid organic hydrogen carriers (LOHC) are hydrocarbon molecules that can be hydrogenated and dehydrogenated as required [25]. The hydrogenation and dehydrogenation processes for LOHC are usually endothermic and exothermic respectively. One example of LOHC is dodecahydro-N-ethylcarbazole. When dehydrogenated, it becomes N-ethylcarbazole [25]. LOHCs can be stored and transported using normal tankers making storage and transport cheaper. But, hydrogenation and dehydrogenation steps require necessary infrastructure and adds to the costs.

Apart from these methods, some other methods such as metal borohydrides, Kubas-Type hydrogen,etc. [25]. Kubas Type hydrogen and metal borohydrides are still in the research phase. All the methods discussed have their own set of advantages and disadvantages. Chemical hydrogen storage requires process plants for methanol or ammonia generation. Moreover, hydrogen recovery requires additional steps which lead to additional losses in the conversion efficiency. Among the physical hydrogen storage methods, liquid hydrogen requires liquefaction plants to be set up and boiloff issues are difficult to control. Compressed storage is the most mature hydrogen storage technology but storage in artificial tanks is expensive. Storage in salt caverns and depleted gas fields depends on the availability, and requires geological surveys and storage preparations. Therefore, capital costs are higher. Despite these challenges, salt cavern storage is becoming the major hydrogen storage method in the Netherlands due to the availability of abundant salt caverns in the North of the Netherlands [22].

2.5.1. Underground hydrogen storage (UGS)

For physical hydrogen storage methods, UGS allows for large-scale hydrogen storage (in TWh scale) at lower levelized costs of storage as compared to other storage methods [6]. The UGS options include [28]

- Salt caverns: Cavities in rock salt formations created by the solution mining process.
- Depleted gas fields: Void formations from which natural gas was extracted.
- Aquifiers: Porous rock formations that contain water. Gases like hydrogen are naturally trapped in such rock formations.

Among these three options, storage in salt caverns is a more mature technology for natural gas with several salt caverns in the Netherlands already being in use for natural gas storage [22]. For hydrogen storage in salt caverns, Table 2.3 shows the already existing operational caverns across the world.

Parameter	Clemens Dome	Moss Bluff	Spindletop	Teesside
Geology	Salt diapir	Salt diapir	Salt diapir	Bedded salt
Operator	Conoco Phillips	Praxair	Air Liquide	Sabic Petrochemicals
Start	1983	2007	2016	1972
Geom. vol. [m3]	580,000	566,000	906,000	3 * 70,000
Avg. depth [m]	1,000	1,200	1,340	365
Press. range [bar]	70-137	55-152	68-202	45

Table 2.3: Operational hydrogen storage caverns in the world [28]

Storage volumes depend on the geological data but the general range for Europe is between 100,000 m^3 to 1000,000 m^3 [6]. For salt cavern storage, techno-economic feasibility analysis has to be done accounting for various parameters. Figure 2.10 shows the methodology applied in the derivation of the technical potential of salt caverns. As compared to other UGS methods, salt caverns have long-term structural stability, low cushion gas requirements, and saline nature reduces the microbiological activities [29]. However, due to the large amount of stored gas, the structural safety of the salt cavern becomes an

important parameter. Moreover, the construction of salt caverns requires a lot of water which becomes an influencing parameter in regions with water scarcity [29]. These factors need to be accounted for in the land eligibility criteria.
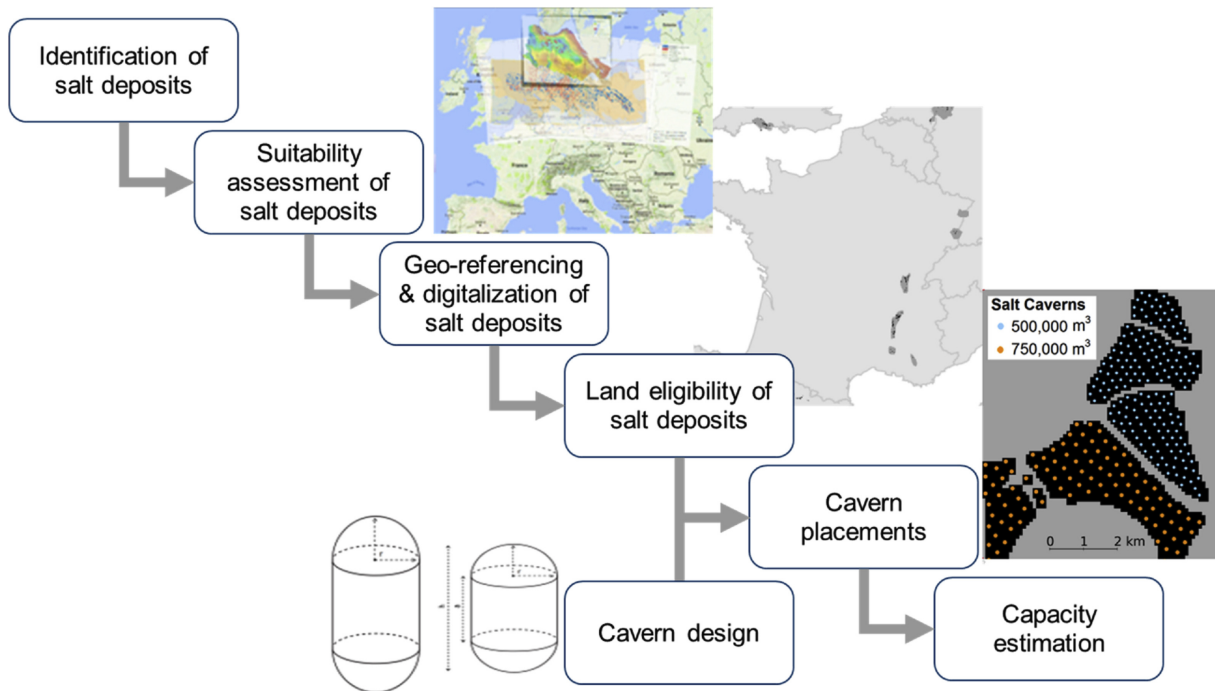
Figure 2.10: General methodology to evaluate the technical feasibility [30]

Land Eligibility

Apart from the safety and water scarcity factors, surveys of geological structure in potential storage location also needs to be done. Based on the geological structure, two types of salt caverns can be utilized: domal salt caverns and bedded salt caverns [29]. A normal salt cavern is a more suitable choice because it is built completely inside a rock salt structure. Whereas in bedded caverns, there are several layers of rock salt embedded into some other materials. Figure 2.11 depicts the differences between these two salt structure types.

(a) domal salt cavern (b) bedded salt cavern
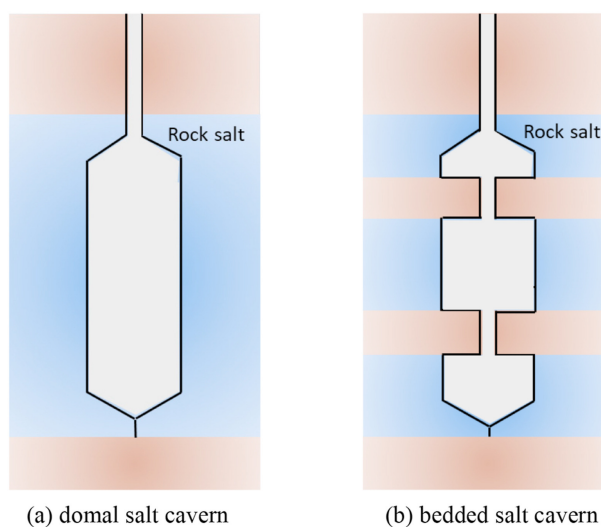
Figure 2.11: Domal and bedded salt caverns [29]

In the case of the Netherlands, the salt structures suitable for underground storage are shown in Figure 2.12. As seen in the figure, there are some potential storage locations in the northern part of the Netherlands. There are some potential storage locations in the North sea as well which could be utilized for offshore energy storage (for example: offshore standalone windfarms).
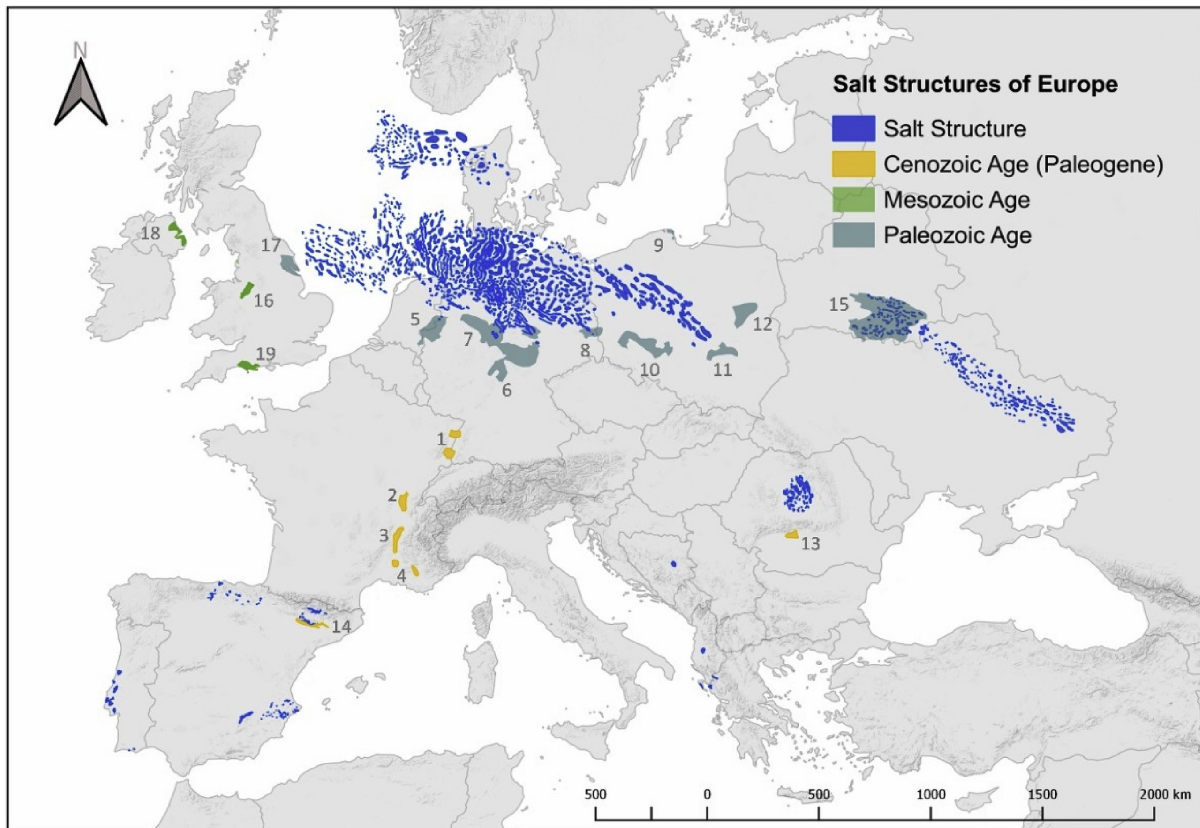
Figure 2.12: Suitable salt structures in Europe [30]

The national storage potential of some major European nations is shown in Figure 2.13. In Europe, Germany, and the Netherlands have the highest salt cavern storage potential in Europe.
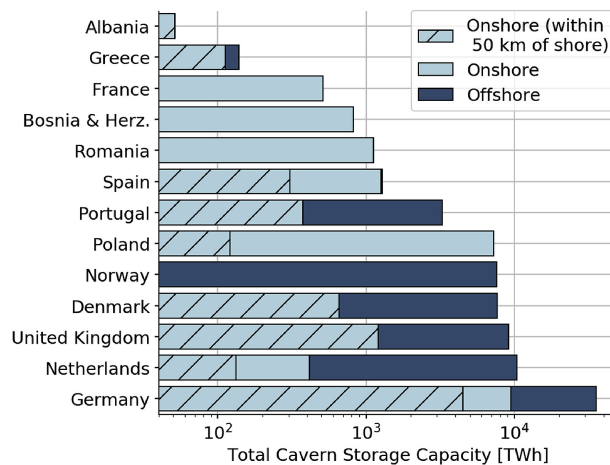
Figure 2.13: National storage potential [30]

Cavern construction
Salt caverns are constructed by a process known as solution mining. There are several steps involved in this process and are outlined below [6]:

1. A well is drilled in the salt deposit and the outer casing is placed in the well to prevent seepage. Inside this casing, two concentric tubes are placed.

2. Freshwater or undersaturated brine is circulated in the salt deposit through one of the tubes and recovered back through the other tube.

3. After some time, when the cavern has reached the desired volume, the cavern must be depleted of brine. For this, leaching tubes are removed and a gas injection string and a brine string are inserted.

4. By injecting hydrogen gas at high pressure, brine is removed from the cavity. For structural stability, the cavity needs to have a "cushion gas" which keeps the internal pressure of the cavern above minimum operating pressure.

Operation of salt caverns

Components involved in the salt cavern storage system are shown in Figure 2.14. The salt cavern storage systems are usually connected to the hydrogen transportation network which links hydrogen production to hydrogen utilization. When demand is lower than supply, the hydrogen is removed from the network to be stored in the caverns. The salt cavern storage system consists of one or more salt caverns, wellheads (for injection and withdrawal), and gas processing equipment.
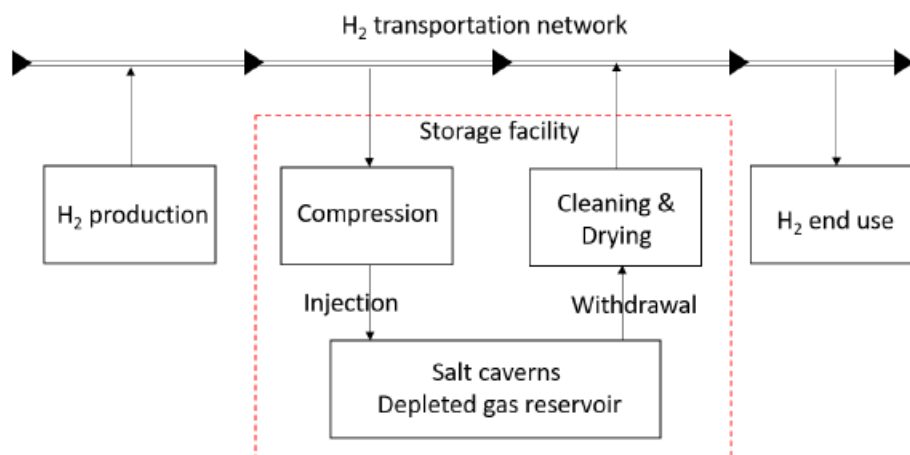
Figure 2.14: Components involved in the salt cavern storage [28]

Some processes shown in Figure 2.14 are:

1. Gas injection: In the injection phase, hydrogen from the pipeline network arrives at the facility at a pressure of around 30-80 bar. Depending on the depth of the salt cavern, storage pressures inside the cavern range between 80-200 bar [28]. Therefore, hydrogen is compressed from pipeline pressure to the cavern's operating pressure. Since compression causes an increase in temperature, the gas is cooled using a heat exchanger and then injected into the facility through the wellhead.

2. Gas withdrawal: Hydrogen gas stored in salt caverns might contain some impurities and moisture depending on the geology of the salt cavern. Mainly, sulphur impurities and moisture are observed in the hydrogen gas withdrawn from salt caverns [31]. To remove the sulphur impurities which exist in the H_2S form, the gas sweetening process can be used [31]. The chemical adsorption process with amines [31] can be used to remove sulphur impurities. For the drying process, another chemical adsorber is required to obtain gas with the acceptable concentration limits of moisture.

2.6. Hydrogen transport

Hydrogen can be transported in its pure form or using ammonia or methanol. Currently, transportation can be subdivided into three options: road, pipeline, and shipping as shown in Figure 2.15. Among these options, compressed hydrogen transport is the most mature technology followed by liquid hydrogen transport [32].

For road transport, hydrogen is compressed to 350-700 bar and transported by tube trailers. According to [32], 380-900 kg of compressed hydrogen can be transported by tube trailers. Liquid hydrogen is also transported by tube trailers but it is unsuitable for long-distance transport due to boiloff issues. But as the volumetric density of liquid hydrogen is much higher than compressed hydrogen, larger amounts of hydrogen can be transported. The cryogenic tank provided by Linde AG can transport around 4000 kg of hydrogen [32].
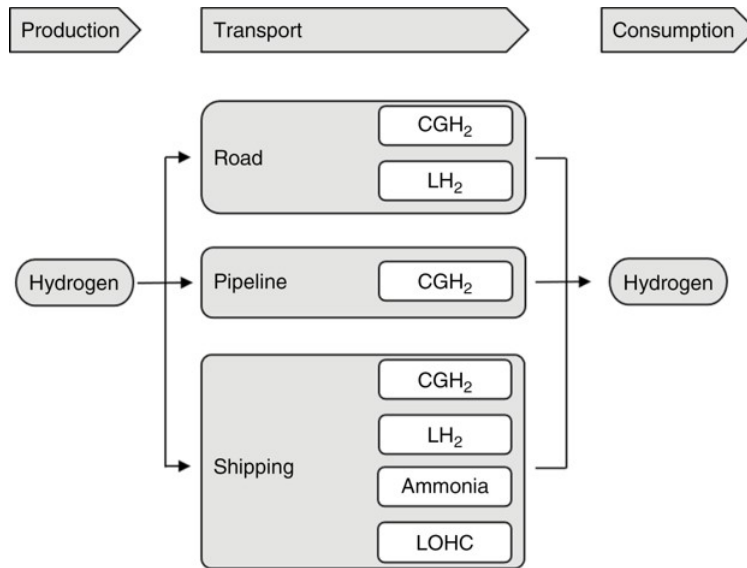
Figure 2.15: Transport options for hydrogen [32]

The second option for hydrogen transport is using ships. Ammonia is easier to transport by ships as compared to compressed or liquid hydrogen because of its higher density. But, conversion to ammonia incurs additional costs, and re-conversion back to hydrogen also adds to the costs. Also. technology readiness level (TRL) of green ammonia transport and reconversion is still low as compared to other transport methods [32].

The use of a pipeline network is another transport option in which compressed hydrogen (30-80 bar) is transported similarly to natural gas. Natural gas distribution via pipeline infrastructure is already highly mature in the Netherlands and most other regions of the world, and many countries, including the Netherlands, have substantial pipeline infrastructure as seen from Table 2.5. All of these transport methods have advantages and disadvantages which are summarized in Table 2.4

	Road	Pipeline	Shipping
Advantages	Flexibility, accessibility and quick deployment	LCOH are lower, high transport capacities	Ideal for longer distances, high transport capacity
Disadvantages	LCOH are higher, transport capacity is limited	Higher infrastructure costs and deployment time	Access to waterways is required, additional conversion costs in case of chemical hydrogen

Table 2.4: Advantages and disadvantages of transport methods

Country	Gas pipeline length (in km)
The United States	548,665
Russia	158,767
Canada	74,980
China	28,132
Ukraine	33,327
Argentina	28,657
Australia	26,719
Germany	25,094
Mexico	22,705
Iran	19,161
The Netherlands	~11,000 [33]

Table 2.5: Natural gas pipeline lengths in some countries[34]

The transportation options discussed above have their own advantages and limitations. For example, road transport is more expensive in terms of levelized costs as compared to pipelines but requires less capital investment and installation time. In the end, the decision to select one of the transportation options depends on the costs, distance and geography of the location [35].
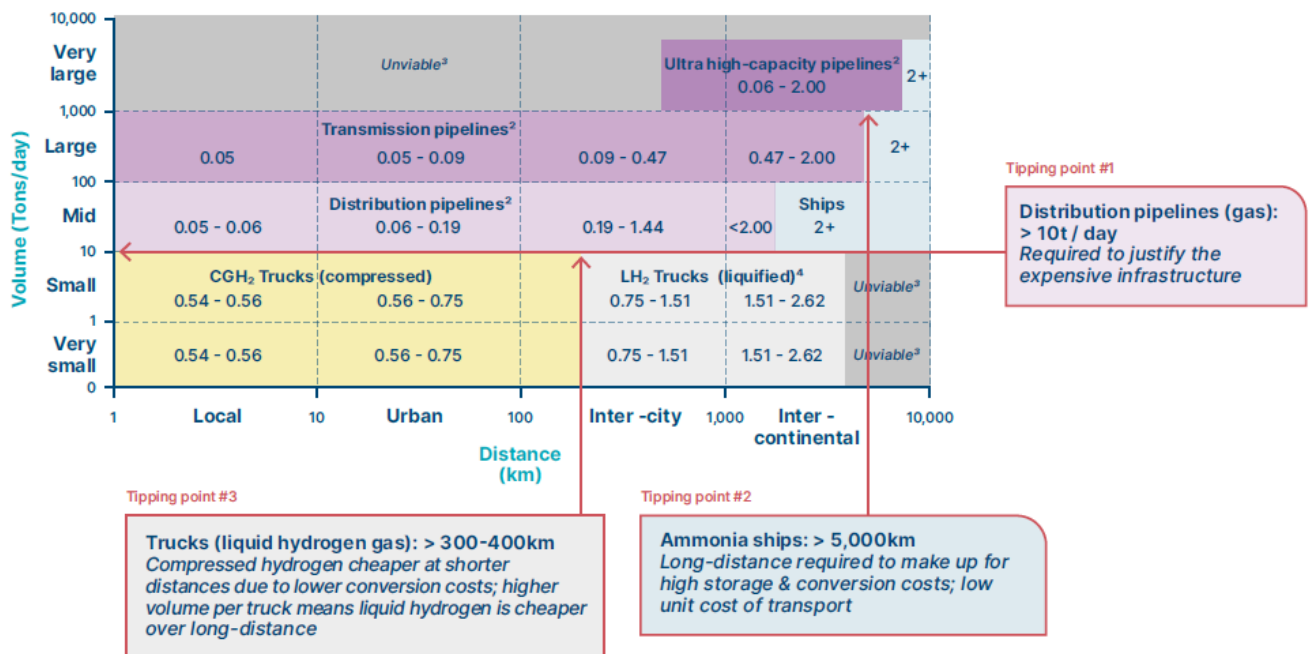
NOTE: [1] Including conversion and storage; [2] Assumes salt cavern storage for pipelines; [3] Ammonia assumed unsuitable at small scale due to its toxicity; [4] While LOHC (liquid organic hydrogen carrier) is cheaper than liquid hydrogen for long distance trucking, it is unlikely to be used as it is not commercially developed.

Figure 2.16: Transportation costs as a function of volume and distance [35]

In Figure 2.16, the levelized costs of different transportation types are shown as a function of distance and volume. Moreover, it can be observed that road transport (compressed and liquid hydrogen) is viable for a very small volume/day. For small to very large scale volumes and larger distances, pipelines are more viable. Delivery by ships is only viable for very large distances and medium to large transport volumes.

Although Figure 2.16 gives a general idea of the decision-making process, it doesn't account for the geography between transport locations.

2.6.1. Overview of pipeline network
Types of pipelines
Based on the operating pressure ranges and volumetric flow rates, pipelines can be subdivided into three categories as shown in Figure 2.17. The hydrogen pipeline network is mostly based on the natural gas network and therefore, the pipeline diameters, operating pressure ranges, etc. are similar to the natural gas network.
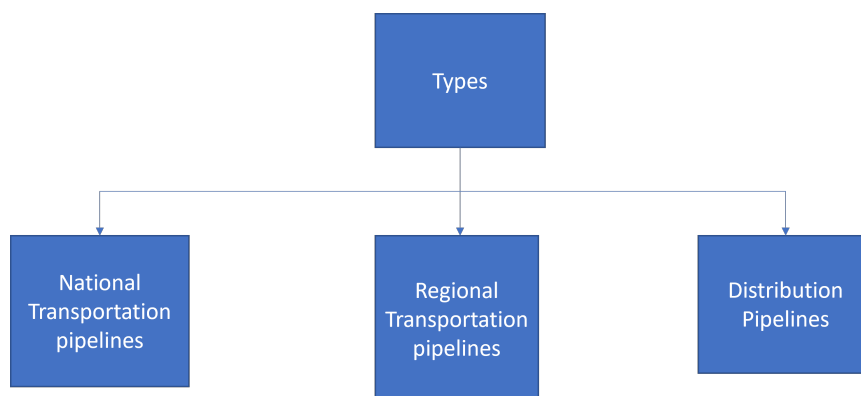
Figure 2.17: This figure shows three major types of pipelines in use.The types differ from each other in terms of flow rates and internal pressure

An overview of these categories is given below:

1. **National transportation pipelines**: These pipelines carry gases over longer distances or from the production facility to distribution hubs. The operating pressure in these pipelines ranges between 43-63 bar [36]. The diameter of these pipelines ranges between 24 -36 inches [37]. Currently, the Dutch natural gas infrastructure of national transportation pipelines is 4000 km in length [36]

2. **Regional Transportation pipelines**: These pipelines are used to connect the major distribution centers to refueling stations or industrial clusters. Their operating pressure range is 16-40 bar and the current Dutch infrastructure of these types of pipelines is about 6000 km in length [36].

3. **Distribution pipelines**: These pipelines are used to transport hydrogen to homes and industries. They operate near atmospheric pressure [36]. The diameter of these pipelines is around 2 inches [38]. Currently, the natural gas infrastructure of 85,000 km of these types of pipelines exists in the Netherlands.

The national transportation lines are made of steel because of high pressures and distribution pipelines are made of PVC, steel or cast iron [34]. The pipes serve two purposes: to transport the gas and to store the gas (known as linepack).

Compression stations
Due to gas viscosity and friction with the insides of the pipe, the pressure drop over the length of the pipeline can be observed [34]. Thus to maintain the operating pressure range, compressor stations are installed. The distance between two compressor stations is usually 80-100 km [34]. Figure 2.18 shows the general working of compression stations.
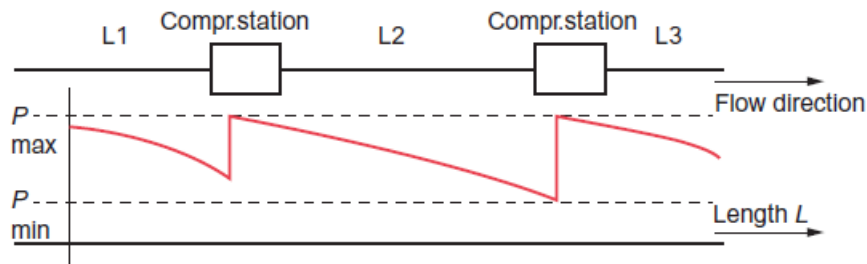
Figure 2.18: Compression station overview [34]

Pressure reduction stations
When connecting two different types of pipelines, for example, a national transportation line to an interstate line, the pressure difference between the lines needs to be equalized. Thus, pressure reduction stations are installed. In these stations, a throttle valve is used to expand the gas. [34]

2.6.2. Hydrogen infrastructure in the Netherlands
In the Netherlands, due to low elevation changes and the availability of natural gas pipeline infrastructure, developing a hydrogen pipeline network is a currently preferred choice according to [39]. The Dutch hydrogen infrastructure is supposed to be completed by 2031 [39]. Gasunie is currently repurposing the natural gas infrastructure to be used for hydrogen transport [40]. Figure 2.19 shows the proposed hydrogen network. Gasunie plans to connect the industrial hubs with this hydrogen infrastructure. Also, as shown in Figure 2.12, most salt caverns are concentrated in the northern part of the Netherlands. Therefore, this pipeline network will connect the large-scale UGS to the utilization hubs.

Figure 2.19: Proposed hydrogen network by Gasunie [40]

Some new sections of pipelines need to be constructed to complete this network. The northern parts of this network are supposed to be available by 2025 and will be initially used to transport natural gas between 2026 and 2028 [39]. As the demand for natural gas falls, this network will start transporting hydrogen.

2.7. Hydrogen Compression

Hydrogen compression is used both in storage (high-pressure storage in salt caverns) and transport (pipeline and road transport) and therefore is one of the vital contributing factors to the cost of hydrogen. Figure 2.20 shows the schematic of compression systems used in the hydrogen supply chain.
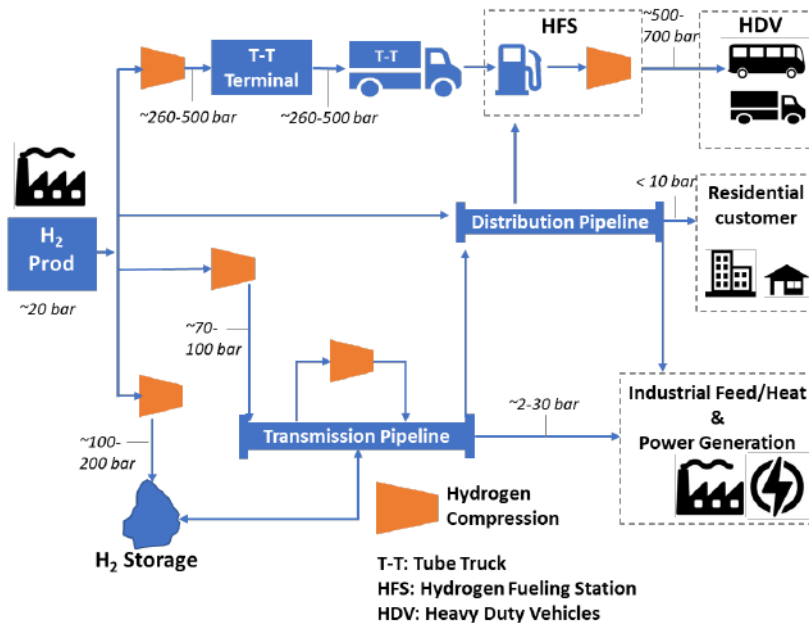
Figure 2.20: Schematic of compression systems used in the hydrogen supply chain [41]

2.7.1. Compression Methods

Compression methods can be broadly classified into two categories: mechanical and non-mechanical. Mechanical compression involves reducing the volume or increasing the density of a substance or material through physical force or pressure. Whereas, non-mechanical compression refers to the reduction in volume or increase in density of a substance or material without the use of external mechanical force or pressure. Some examples of non-mechanical compression involve metal hydride compressors, electrochemical compression, adsorption compressors and cryogenic compression [42]. Mechanical compressors can be further subdivided into subcategories as shown in Figure 2.21
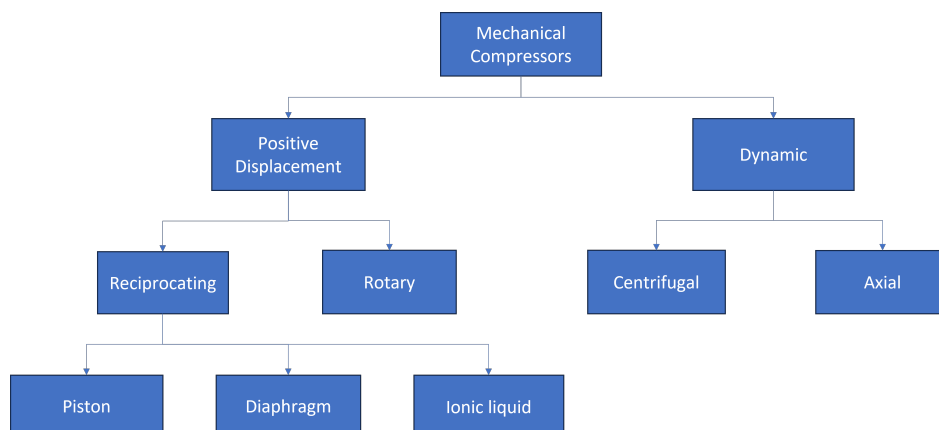
Figure 2.21: Types of mechanical compression

Positive displacement compressors work by trapping a fixed volume of gas in a chamber and then

reducing the volume to compress the gas. These compressors use mechanical components such as pistons, vanes, or scrolls to achieve compression. Dynamic compressors, also known as rotary compressors operate using a different principle. They use rotating components, such as impellers or screws, to generate kinetic energy in the gas, which is then converted into pressure. Some common compressor types, their advantages, and disadvantages are discussed below:

- **Reciprocating piston compressors**:
  This type of compressor is used in hydrogen compression when the desired level of pressure is more than 30 bar [43]. They are ideal for moderate flow and high-pressure applications such as refueling fuel cell vehicles [43]. Moreover, multiple stages can be used to increase the pressure.
  Some advantages of this type are [43]:

  - Mature technology
  - Useful over a larger range of flowrates
  - High discharge pressures

  Some disadvantages of this type are :

  - Several moving parts [43]
  - Presence of vibrations and noise [44]
  - Manufacturing complexity

- **Diaphragm compressors**:
  Due to high flow rates, lower specific power consumption and relatively low cooling requirements, these types of compressors are suitable for handling chemically pure gases[45]. Some advantages of this compressor are [43]:

  - High flowrate
  - Low specific power consumption
  - Low cooling requirements as compared to reciprocating compressor

  Some disadvantages of this compressor are [43]:

  - Low durability of diaphragm
  - Complex design

- **Ionic liquid compressors** [46]:
  Instead of using a conventional metal piston, an ionic liquid compressor utilizes a specifically engineered, nearly incompressible ionic liquid. The compression of gas within the cylinder occurs through the vertical movement of the liquid column, resembling the reciprocating motion of a typical piston. One notable advantage of this system is that the ionic liquid remains separate from the gas, eliminating the requirement for seals and bearings in the compressor. Some advantages of this compression type are :

  - High volumetric efficiency [47]
  - High compression ratio[47]
  - Relatively small number of moving parts[43]

  Some disadvantages of this compression type are [43]:

  - Liquid leaks
  - Cavitation
  - Corrosion due to ionic liquids

- **Centrifugal compressors**:
  Belonging to the dynamic class of compressors, centrifugal compressors are used when flowrates are high and compression ratios are moderate [48]. A rotating impeller is used to increase the velocity of gas which increases the kinetic energy of gas. This kinetic energy then leads to increase in pressure when the gas is passed through diffuser [41]. Some advantages of this type of compressor are as follows:

- High flowrates are possible as compared to mechanical compressors
- Low number of moving parts as compared to reciprocating compressor
- High durability

Some disadvantages of this compressor are as follows:

- Low tech maturity for hydrogen compression (In prototype phase [41]
- Not suitable for high-pressure compression

Among the compressors discussed above, the selection of compressor type depends on the following factors:

1. Flow rate of gas
2. Inlet and outlet pressures
3. specific gravity of the gas [41]

Figure 2.22 shows the suitable type of compressor for particular outlet pressure and volumetric flow rate.
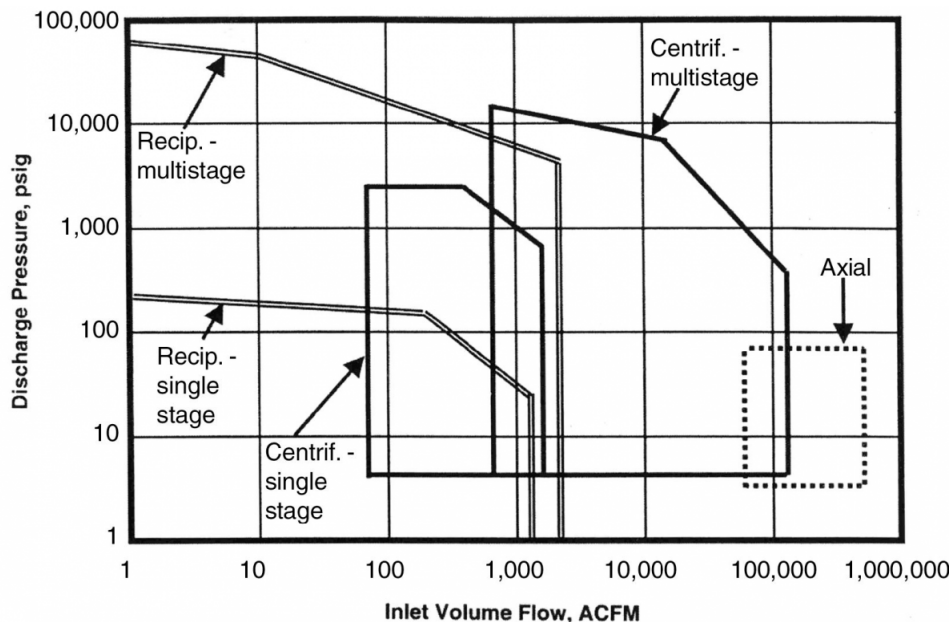
Figure 2.22: Compressor selection on the basis of outlet pressure and volumetric flow rate [41]

Also, there are some auxiliary components involved in the compression system such as prime movers and heat exchangers. Prime movers are used to drive the compressor. Electric motors, gas turbines, or internal combustion engines could be used as prime movers. The compression of gas causes an increase in the temperature. Moreover, the work required to compress the gas increases with an increase in temperature. Therefore, heat exchangers are installed between two compression stages to cool the gas.

2.8. Economic modelling

In this section, the general economic modeling approach and application of the learning curve are discussed.

2.8.1. System costs calculation

To analyze the impact of different components involved in the hydrogen supply chain on the total costs of hydrogen to the consumer, an economic model can be constructed accounting for capital and operating costs.

Capital costs

Capital costs or more commonly known as CAPEX include the following components [49]:

- Cost of the equipment:
  This includes the cost of the construction of equipment which involves labor, materials, processes, etc.

- Direct costs:
  Direct costs include the installation of the equipment, electrical, piping, service facilities, etc.

- Indirect costs:
  This includes the EPC (Engineering, procurement, and construction) costs and administrative costs.

To evaluate the capital costs, there are mainly two ways: quotations from vendors and cost correlations. Cost correlations available in books such as Sinott and Towler [50], Peters and Timmerhaus [51] can be used to predict the capital costs of equipment. The cost estimation correlations given by these books and research papers are for a particular equipment size. To adjust the capital cost according to the scale, the following relation is used:

$$\frac{\text{Cost}_1}{\text{Cost}_2} = \left(\frac{\text{Size}_1}{\text{Size}_2}\right)^n \tag{2.5}$$

The exponent n ranges between 0.5 and 0.7 depending on the equipment type [52].
To account for the inflation over time, CEPCI (Chemical Engineering Plant Cost Index) is used. The correlations given by academia are usually for a particular year. The cost can be calculated using the following equation if both the CEPCI index for the specific year and the desired year are known:

$$\text{Cost}_2 = \text{Cost}_1 \frac{\text{CEPCI}_2}{\text{CEPCI}_1} \tag{2.6}$$

As the hydrogen supply chain is made up of several components with varying lifespans, CAPEX costs can be annualized by the following equation:

$$\text{CAPEX}_{\text{annualized}} = \text{CAPEX}\left(\frac{r}{1 - (1 + r)^n}\right) \tag{2.7}$$

In this equation, n stands for the lifetime of the equipment and r stands for the discount rate. Usually, the discount rate is taken as 5% per year [49],

Operating costs

Operating costs, also known as OPEX consists of the following components:

- Electricity costs
- Maintenance costs
- feed costs

Based on the annual CAPEX and OPEX costs, levelized costs of hydrogen (€/kg) for various components such as production, compression, etc. can be calculated as follows:

$$\text{LCOH} = \frac{\text{CAPEX}_{\text{annualized}} + \text{OPEX}}{M_{H_2}} \tag{2.8}$$

In this equation, M_{H_2} stands for the amount of hydrogen passing through the system annually.

2.8.2. Learning curves

Learning curves can be used to predict future cost reductions in technology due to ongoing research or production and deployment of the technology. Zauner et. al [53] defines the learning curves as follows: "Learning curves refer to an increase in performance per unit of a specific technology as the cumulative production of that technology increases."

As an example, a learning curve is given in Figure 4.1. In this figure, learning rates of wind farms and solar PV are shown along with their effect on LCOE as the cumulative installed capacity of electricity generation of both these types has increased over the years. In Figure 4.1, it can be observed that for wind, the learning rate was 16% for 1982-2006 and the learning rate was -10% for 2006-2010 but again saw an increase between 2010-2040 with 40% learning rate [54]. The negative learning rate between 2006-2010 was due to inflation in which the US dollar weakened and caused an increase in capital costs of wind turbines according to Bolinger et al. [54].
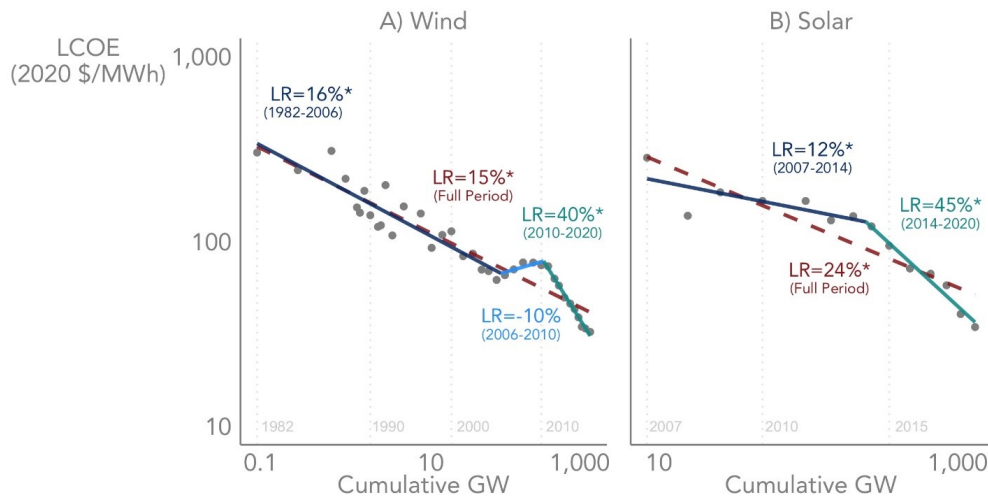
Figure 2.23: Learning curve for LCOE from solar PV and wind farms on the basis of cumulative installed capacity [54]

Based on the learning rates, future cost reductions can be predicted. There are several ways in which learning rates can be correlated with unit costs. One way to represent the relationship between cost and production is by means of power law and the equation can be written as follows [55]:

$$c_t = c_0 \left(\frac{P_t}{P_0} \right)^{-\alpha} \tag{2.9}$$

Here, the unit cost (c_t) and cumulative production (P_t) are related to the unit cost (c_0) and cumulative production (P_0) at some time t through the learning index α [55]. A progress ratio (PR) can be expressed in terms of learning index by the following equation [56]:

$$PR = 2^{-\alpha} \tag{2.10}$$

Learning rate (LR) can be then obtained as follows:

$$LR = 1 - PR \tag{2.11}$$

Equations 2.9, 2.10 and 2.11 represents the one-factor learning curve (OFLC) method [55]. In this method, the factor of α encapsulates all the influencing factors such as standardized manufacturing, development in design, etc. in a single variable. Advantages of this method are as follows[55]:

- Relatively simple and therefore convenient to use
- Resistant to overfitting

But several disadvantages are also present in this method:

- Accuracy is low [57]
- Can only accurately predict the technology that has reached the commercialization phase [58]

Although the OFLC method is easier to implement, several errors are introduced due to the merging of several different parameters. To minimize these errors. Kouvaritakis et al. [59] developed Two-factor learning curves (TFLC). In TFLC, learning is segregated into learning by searching (LBS, also referred to as learning by researching [55]) and learning by doing (LBD). As the names suggest, LBS accounts for cost reduction due to research, and LBD accounts for cost reduction due to experience gained during production. The equation for TFLC is given as follows:

$$c_t = c_0 \left(\frac{P_t}{P_0}^{-\alpha} \right) (KS)^{-\beta} \tag{2.12}$$

In this equation, *KS* is the knowledge stock (measured in R&D expenditures [55]) and β is the LBS index.

The advantages of this method are as follows:

- More accurate as compared to OFLC.
- Cost predictions for pilot phase technologies are also possible due to the segregation of LBS and LBD.

Some disadvantages of this method are as follows:

- Access to R&D expenditures is required for a particular technology.
- Harder to establish a correlation between R&D expenditure and improvement in technology.

In multi-factor learning curves (MFLCs), another parameter called learning by using (LBU) is added. This factor accounts for the cost reduction from user feedback and user experience [58]. Although this method is more accurate, it is also more complex as data collection is required for the LBU parameter.

3

Electrolyzer Modeling

The primary objective of the electrolyzer model is the evaluation of levelized costs associated with hydrogen production. This requires analysis of the influence of operational conditions and electrolyzer cell parameters on the Faradaic efficiency and the corresponding mass of generated hydrogen, both of which are inherently influenced by electrochemical processes. The amount of hydrogen generated is then linked to the capital and operating costs of the electrolyzer to compute the levelized costs.

The modelling process consists of two distinct sections:

- **Electrochemical model**: This section involves the analysis of the electrochemical processes that occur within the electrolyzers. In this model, underlying processes that influence the conversion of electricity into hydrogen gas are considered by analyzing their impact on cell voltage. The impact of operating characteristics such as temperature and pressure on cell voltages can also be analyzed in this model.

- **Economical model**: In this section, the emphasis shifts towards the assessment of economic aspects associated with hydrogen production through electrolyzer. The model takes into account the data obtained from the electrochemical model and incorporates additional factors such as energy costs, capital expenses, maintenance, and other operational costs. By integrating these factors, the levelized costs of hydrogen production are computed.

Main objective of these electrochemical models is to calculate the total cell voltage and Faradaic efficiency. While equation to calculate the total cell voltage is same for all three electrolyzers,parametric relations used to calculate Faradaic efficiency are different.

Cell voltage

The electrolyzer operates at a cell voltage which takes into account the various losses. The cell voltage can be calculated by the following equation [60]:

$$V_{\text{cell}} = V_{\text{oc}} + V_{\text{act}} + V_{\text{ohmic}} + V_{\text{conc}} \tag{3.1}$$

Here,

- V_{oc} is open circuit voltage
- V_{act} is activation overpotential
- V_{ohmic} is ohmic overpotential
- V_{conc} is concentration overpotential

It is assumed that concentration overpotential for all three types of electrolyzer cell remains zero for the operating range. This is because concentration overpotential only becomes significant at higher current densities and most commercial electrolyzers avoid operation at higher current densities due to increased ohmic losses.

As the operating parameters, materials involved in the construction vary significantly for these three electrolyzers, the equations involved in the calculation of overpotentials are also different and are discussed in sections 3.1, 3.2, 3.3.

3.1. Alkaline Electrolyzer

3.1.1. Open circuit voltage

Open circuit voltage is the ideal voltage required for the electrolysis process. It accounts for the temperature and pressure effects on the thermodynamic energy and eventually the ideal voltage value. A set of equations as reported by Adibi et al. [61] were used to calculate the open circuit voltage. Equation 3.2 is a modified form of the Nernst equation.

$$V_{\text{OC}} = V_{P_0,T}^{\text{rev}} + \frac{RT}{2F} \ln \left(\frac{p_{H_2}\sqrt{p_{O_2}}}{\alpha_{H_2O,KOH}} \right) = V_{P_0,T}^{\text{rev}} + \frac{RT}{2F} \ln \left(\frac{(p - p_{H_2O,KOH}^{\text{saturation}})^{3/2}}{\alpha_{H_2O,KOH}} \right) \tag{3.2}$$

- $V_{P_0,T}$ is the reversible voltage at standard conditions and is calculated as follows:

$$V_{P_0,T}^{\text{rev}} = 1.5184 - 1.5421 \times 10^{-3} \times T + 9.526 \times 10^{-5} \times T \ln T + 9.84 \times 10^{-8} \tag{3.3}$$

- p (in bar) denotes the partial pressures of the components involved. Since an alkaline electrolyzer contains a liquid electrolyte, molarity of the solution (mol/L) should be known and is calculated by Equation 3.4 [60] when weight percentage of KOH solution is known. Using Equation 3.5 ,the saturation pressure of steam can be calculated over KOH.

$$m = \frac{\text{Wt\%} \left(183.1221 - 0.56845T + 984.5679 \exp\left(\frac{\text{Wt\%}}{115.96277}\right) \right)}{5610.5} \tag{3.4}$$

$$
\begin{aligned}
p_{H_2O,KOH}^{\text{saturation}} &= \exp\left(2.302a + b \ln p_{Pure-H_2O}^{\text{saturation}}\right) \\
a &= -0.0151m - 1.6788 \times 10^{-3}m^2 + 2.2588 \times 10^{-5}m^3 \\
b &= 1 - 1.2062 \times 10^{-3}m + 5.6024 \times 10^{-4}m^2 - 7.8228 \times 10^{-6}m^3 \\
p_{Pure-H_2O}^{\text{Saturation}} &= \exp\left(81.6179 - \frac{709.68}{T} - 10.9 \ln T + 9.5891 \times 10^{-3}T\right)
\end{aligned} \tag{3.5}
$$

- $\alpha_{H_2O,KOH}$ is the water activity of KOH solution and is calculated by using Equation 3.6. But this equation is only valid for the temperature range of 0 - 250 °C, pressure range of 1 - 200 kPa, and molar concentration range of 2-18 mol/kg [61].

$$\alpha_{H_2O,KOH} = \exp\left(-0.05192m + 0.003302m^2 + \frac{(3.177m - 2.131m^2)}{T}\right) \tag{3.6}$$

3.1.2. Activation Overpotential

The activation overpotential accounts for the energy required to break chemical bonds prior to an electrochemical reaction [60]. It is usually given as a function of current density and exchange current density. At exchange current density, no electrolysis takes place and overpotential is zero. Due to the involvement of liquid electrolyte, gas bubbles forming at the electrode surface influence the activation and ohmic overpotentials. The bubble effect as a function of current density and partial pressures is calculated using the Equation 3.7 [61] at reference temperature of 50 °C.

$$\theta = \left[-97.25 + 182 \left(\frac{T}{T_{\text{ref}}} \right) - 84 \left(\frac{T}{T_{\text{ref}}} \right)^2 \right] \times \left(\frac{i}{i_{\text{lim}}} \right)^{0.3} \times \frac{P}{P - p_{H_2O,KOH}^{\text{saturation}}} \tag{3.7}$$

In the above equation, i_{lim} is the limiting current density with the value of 300 kA/m^2 and i is the current density of the electrolyzer.

For the calculation of activation overpotential, procedure and equations mentioned by Niroula et. al. [60] were used. Butler Volmer equations are used to calculate the activation overpotentials at the cathode and anode. Another term is added to the Butler Volmer relations to account for bubble effects as seen in

Equation 3.8.

$$V_{\text{act}-a} = b_{\text{a}}\log\left(\frac{j_{\text{a}}}{j_{\text{o}-a}}\right) + b\log(1-\theta)$$

$$V_{\text{act}-c} = b_{\text{c}}\log\left(\frac{j_{\text{c}}}{j_{\text{o}-c}}\right) + b\log(1-\theta)$$

(3.8)

In Equation 3.8,

- $b_{a,c}$ is Tafel slope and calculated by Equation 3.9.

$$b_{\text{a,c}} = \frac{RT}{nF\alpha_{\text{a,c}}}$$

(3.9)

The charge transfer coefficient is a function of temperature. The equation mentioned by Hammoudi et al [62] was used (Equation 3.10) and is valid only for the nickel electrode since it was correlated to the experimental data.

$$\alpha_a = 0.0675 + 0.000957T$$

$$\alpha_c = 0.1175 + 0.000957T$$

(3.10)

- The exchange current densities, $J_{0-c,a}$ [A/m^2] at anode and cathode are calculated by using Equation 3.11 [63]. These equations are only valid for HRI's electrolyzer cell.

$$J_{0-c} = 13.72491 - 0.09055T + 0.09055T^2$$

$$J_{0-a} = 30.4 - 0.206T + 0.00035T^2$$

(3.11)

- $j_{a,c}$ are current densities at anode and cathode respectively. It was assumed that current density at anode and cathode are equal and this is one of the sensitivity parameters in the model.

3.1.3. Ohmic overpotential

The components inside the electrochemical cell such as electrodes, electrolyte, separator membrane, etc. offer some resistance to the flow of current. To counteract the resistive losses, ohmic overpotential is added to the total cell voltage. The resistance offered by cell components is dependent on cell parameters. Thus for the analysis, cell parameters of HRI's electrolyzer were considered and are listed in Table 3.1.

Symbol	Description	Value
d_{ac}	Anode-cathode gap	2.5 mm
d_{am}	Anode-membrane gap	1.25 mm
d_{cm}	Cathode-membrane gap	1.25 mm
e_{m}	Membrane thickness	0.5 mm
$S_{\text{a}}, S_{\text{c}}$	Electrode surface area	0.03 m^2
$L_{\text{a}}, L_{\text{c}}$	Anode and cathode thickness	2 mm

Table 3.1: HRI's Electrolyzer cell parameters [63]

To calculate the voltage overpotential, the methodology used in Henao et al. [63] was followed. The equations for different components are as follows:

1. **Electrodes**:
   The electrical conductivity of nickel electrode in Scm^{-1} is given by Equation 3.12 as a function of temperature.

$$\sigma_{\text{Ni}} = 60000000 - 279650T + 532T^2 - 0.38057T^3$$

(3.12)

Then, the resistance of electrodes(cathode and anode) can be calculated by Equation 3.13 [63].

$$R_{\text{a}} = \frac{1}{\sigma_{\text{N}}}\left(\frac{L_{\text{a}}}{S_{\text{s}}}\right)$$

$$R_{\text{c}} = \frac{1}{\sigma_{\text{N}}}\left(\frac{L_{\text{c}}}{S_{\text{c}}}\right)$$

(3.13)

2. **Electrolyte**:
   The conductivity of the KOH solution is dependent on the molarity and temperature of the solution. Equation 3.14 correlates the conductivity to molarity and temperature.

$$\sigma_{\text{KOH}} = -2.04m - 0.0028m^2 + 0.005332mT + 207.2\frac{m}{T} + 0.001043m^3 - 0.0000003m^2T^2 \quad (3.14)$$

Formation of bubbles also influence the conductivity of electrolyte. Following relations are used to account for the bubble effects:

$$\frac{\sigma_{\text{KOH}-\epsilon}}{\sigma_{\text{KOH}}} = (1 - \varepsilon)^{\frac{3}{2}}$$

$$\varepsilon = \frac{2}{3}\theta \quad (3.15)$$

3. **Separator membrane**:
   HRI electrolyzer has a Zirfon based separator membrane to separate the anode and cathode. Equation 3.16 gives the resistance on the basis of temperature and membrane surface area [cm^2].

$$R_{\text{mem}} = \frac{0.060 + 80e^{T/50}}{10000S_{\text{m}}} \quad (3.16)$$

The resistances calculated by Equations 3.13, 3.15, 3.16 are added and multiplied with the operating current density and cell area as shown in Equation 3.17.

$$V_{\text{Ohmic}} = j_{\text{cell}}(R_{\text{electrode}} + R_{\text{electrolyte}} + R_{\text{Separator}})S_{\text{cell}} \quad (3.17)$$

In the above equation, j_{cell} is the operating current density in A/m^2 and S_{cell} is the cell area.

3.1.4. Faradaic efficiency

Faraday's efficiency is the ratio of actual hydrogen produced by an electrolyzer to the theoretical hydrogen production possible [61]. It was calculated by using the Equation 3.18

$$\eta_F = \left(\frac{j_{\text{cell}}^2}{f_{11} + f_{12}T + j_{\text{cell}}^2}\right) \cdot (f_{21} + f_{22}T) \quad (3.18)$$

In the above equation, f are the constants and are given by [61] as follows:

$$f_{11} = 50, f_{12} = 2.5, \ f_{21} = 1, f_{22} = -2.5 \times 10^{-4} \quad (3.19)$$

3.1.5. Voltage validation

The mathematical model developed in Python by using Equations 3.2 to 3.18 was validated by comparing the variation of voltage with respect to current density for the HRI electrolyzer cell. The experimental data was taken from Niroula et al. [60] and the comparison of experimental and simulated voltage values with respect to current densities is shown in Figure 3.1.
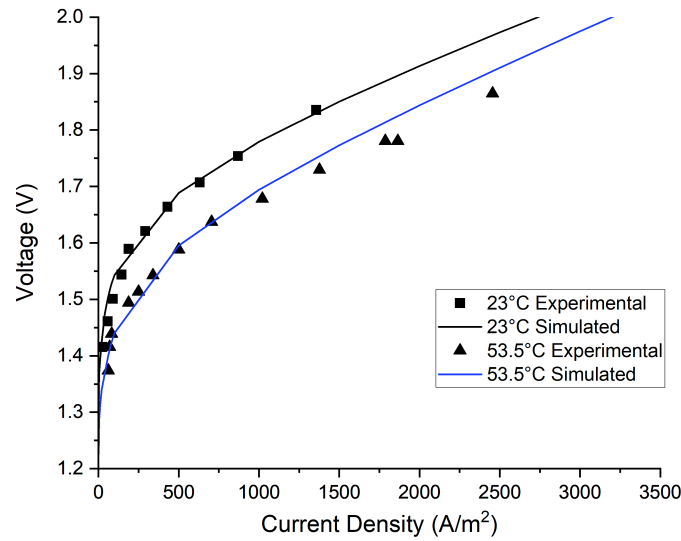
Figure 3.1: Comparison of experimental and simulated voltage values of HRI electrolyzer at 1 bar pressure

It can be observed from Figure 3.1 that for 23 °temperature, the simulated values correlate well with the experimental data. For 53.5 °operating temperature, slight deviation (Around 0.02 V) is observed at higher current densities.

3.2. Polymer Electrolyte Membrane (PEM) Electrolyzer

3.2.1. Open circuit voltage
By applying the Nernst equation for water electrolysis, the following equation can be obtained.

$$V_{\text{oc}} = V_0 + \frac{RT}{2F} \ln \left(\frac{p_{H_2} \sqrt{P_{O_2}}}{\alpha_{H_2O}} \right) \tag{3.20}$$

The reversible voltage, denoted as V_0, often holds a commonly used value of 1.23 V in the literature. This value is typically calculated under standard temperature and pressure conditions. But the operating temperature and pressure of the PEM electrolyzer are different and therefore, the value of 1.23 V for reversible voltage introduces errors in the value of open circuit voltage. To account for the temperature effects on reversible cell voltage, Equation 3.21 is used [64].

$$V_0 = 1.229 - 0.9 \times 10^{-3} \left(T - 298 \right) \tag{3.21}$$

3.2.2. Activation Overpotential
The methodology described by Abdin et al. [65] was used to compute the activation overpotentials. The activation overpotentials at the anode and cathode respectively can be calculated using Equation 3.22

$$V_{\text{act}}^{\text{an}} = \frac{RT}{\alpha_{\text{an}}F} \text{arcsinh} \left(\frac{j}{2j_{0,\text{an}}} \right)$$
$$V_{\text{act}}^{\text{cat}} = \frac{RT}{\alpha_{\text{cat}}F} \text{arcsinh} \left(\frac{j}{2j_{0,\text{cat}}} \right) \tag{3.22}$$

In Equation 3.22, α_{an} and α_{cat} are the charge transfer coefficients at the cathode and anode respectively. $j_{0,\text{an}}$ and $j_{0,\text{cat}}$ are the exchange current densities at anode and cathode. When it comes to the values of

charge transfer coefficients and exchange current densities, a significant variation in the values reported by the literature was observed. For example, Hwang et al. [66] reported the exchange current density at anode and cathode as 0.5 $\times 10^{-3}$ and 0.4 $\times 10^{-6}$ respectively. While Agbli et al. [67] reported the exchange current density at anode and cathode to be 1.548 $\times 10^{-3}$ and 3.539 $\times 10^{-2}$. A similar discrepancy can be observed in the values of charge transfer coefficients. The exchange current densities and charge transfer coefficients reported by different authors are tabulated by Falcao et al.[68]. In this project, values reported by Abdin et al. [65] were used to validate the voltage values and are given in Table 3.2.

Parameter	Value
$i_{0,an,ref}$	1 $\times 10^{-7}$ A/cm^2
$i_{0,cat,ref}$	1 $\times 10^{-1}$ A/cm^2
α_{an}	0.8
α_{cat}	0.25

Table 3.2: Exchange current density and charge transfer coefficient for PEM electrolyzer used in the model [62]

3.2.3. Ohmic Overpotential

Although many methods to calculate the ohmic overpotentials exist in the literature, method given by Abdin et al. [65] was followed. The total Ohmic overpotential can be calculated by Equation 3.23.

$$V_{ohm} = R_{cell} j_{cell} A \tag{3.23}$$

where R_{cell} is the total resistance of a cell and is comprised of three components.

$$\begin{aligned} V_{ohm} &= (R_{el} + R_{pl} + R_{mem})I \\ &= V_{ohm}^{el} + V_{ohm}^{pl} + V_{ohm}^{mem} \end{aligned} \tag{3.24}$$

In Equation 3.24 [65], R_{el}, R_{pl} and R_{mem} are the resistances of the electrodes, bipolar plates and membrane. The corresponding ohmic overpotentials in Equation 3.24 are dependent on geometric properties of the electrolyzer cell. The parameters and their values used in calculations are given in Table 3.3.

Resistivity of the electrodes is influenced by the electrode porosity and therefore effective resistivity, ρ_{eff} is used in the resistance calculations accounting the porosity [65].

$$\rho_{eff} = \frac{\rho_e}{(1 - \varepsilon)^{1.5}} \tag{3.25}$$

The total resistance in both the electrodes, R_{el} then can be calculated by Equation 3.26 [65]. Moreover, it was assumed that both anode and cathode electrodes are identical.

$$R_{el} = \frac{\rho_{eff}}{8L} \left[\frac{(w_c^{an} + w_s^{an})}{n_{ch}^{an} \delta_{el}^{an}} + \frac{(w_c^{cat} + w_s^{cat})}{n_{ch}^{cat} \delta_{el}^{cat}} \right] \tag{3.26}$$

For the bipolar plates, there are two types of resistances involved: resistance by flow field plate and resistance due to channel supports. Resistance due to the flow field plate can be calculated by using Equation 3.27 [65].

$$\begin{aligned} R_f^{an} &= \frac{\rho_p^{an} h_p^{an}}{WL} \\ R_f^{cat} &= \frac{\rho_p^{cat} h_p^{cat}}{WL} \end{aligned} \tag{3.27}$$

Symbol	Parameter	Value
A	Cell area	160 cm^2
δ_{mem}	Membrane thickness	0.0254 cm
δ_{el}	Electrode thickness	0.008 cm
ρ_{el}	Resistivity of Electrode	10.6$\times$10^{-6} Ω cm
ρ_{pl}^{an}	Resistivity of plate (Anode side)	43.1$\times$10^{-6} Ω cm
ρ_{pl}^{cat}	Resistivity of plate (Cathode side)	16.0$\times$10^{-6} Ω cm
ϵ	Porosity of electrode	0.4
n_{ch}	Number of flow channels	10
w_c	Width of flow channel	2 mm
h_c	Height of flow channel	2 mm
W	Plate length	50 mm
L	Plate width	50 mm

Table 3.3: Geometrical parameters of PEM electrolyzer cell used for the calculations [62]

Here, ρ_p is the resistivity of the electrode, and h_p^{an}, h_p^{cat} are the distances from outside the border to the anode surface. The resistance due to channel supports is calculated by Equation 3.28

$$R_s^{cat} = \frac{\rho_p^{cat} h_c^{cat}}{n_{ch,an}^s w_s^{cat} L}$$
$$R_s^{an} = \frac{\rho_p^{an} h_c^{an}}{n_{ch,cat}^s w_s^{an} L}$$

(3.28)

Here, h_c is the height of the channel. A square channel was assumed so that channel width and height are equal. n_{ch} is the number of flow channels. Using Equation 3.27 and 3.28, the total resistance due to the bipolar plate can be calculated by adding the resistances as shown in Equation 3.29.

$$R_{pl} = (R_s^{an} + R_s^{cat}) + (R_f^{an} + R_f^{cat})$$

(3.29)

The resistance due to the Nafion membrane can be calculated using Equation 3.30.

$$V_{ohm}^{mem} = \frac{\delta_{mem} j_{cell}}{\sigma_{mem}}$$

(3.30)

Here, δ_{mem} is the thickness of electrolyte membrane and σ_{mem} is the conductivity of electrolyte.

The membrane conductivity is dependent on water content and temperature as given in Equation 3.31 [69].

$$\sigma_{mem} = (0.005139\lambda - 0.00326) \exp\left[1268\left(\frac{1}{303} - \frac{1}{T}\right)\right]$$

(3.31)

In this equation, λ is defined as molecules of water per sulphonic group. The λ value is taken as 0.5 in dry conditions, 12-14 when exposed to water saturated gas and 22 when exposed to liquid water [65]. It can be observed that the membrane conductivity is low when conditions are dry and as the water content is increases, the membrane conductivity increases as well. Therefore, sufficient water level has to be maintained in the membrane for optimum working of the electrolyzer cell.

3.2.4. Faradaic Efficiency

To calculate the Faradaic efficiency of PEM electrolyzer, empirical relation given by Yodwong et al. [70] was used. This relation correlates the experimental data using coefficients given in Table 3.4.

Parameter	Value
a_1	-0.0034
a_2	-0.001711
b	-1
c	-1

Table 3.4: Fitted constants used in the calculation of Faradaic efficiency of PEM electrolyzer [65]

Equation 3.32 uses the coefficients to calculate the Faradaic efficiency as a function of current density and operating pressure.

$$\eta_{\mathsf{F}} = (a_1 p + a_2)\left(j_{\mathsf{el}}\right)^b + c \tag{3.32}$$

3.2.5. Voltage validation

Similar to the validation of alkaline electrolzyer model, PEM electrolyzer model was analyzed against the experimental data and results are shown in Figure 3.2. The experimental data was taken from Abdin et al. [65] for two distinct operating conditions.
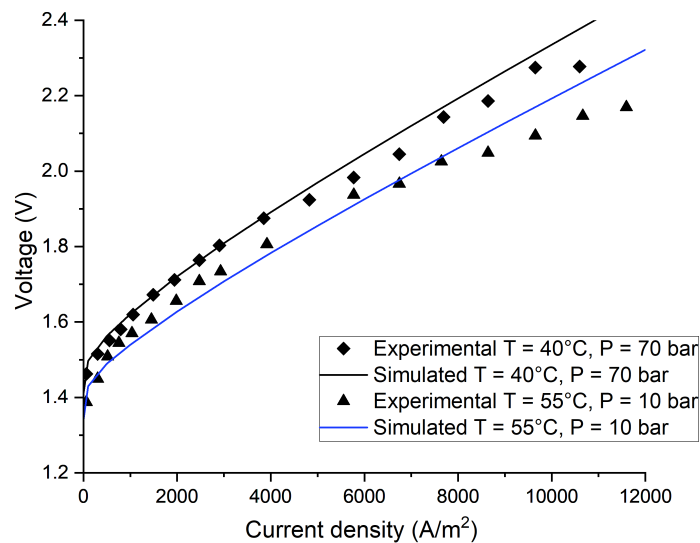
Figure 3.2: Comparison of experimental and simulated voltage values of PEM electrolyzer at different operating conditions

It can be observed from Figure 3.2 that the predicted voltages are closer to experimental data at lower current densities for both set of operating conditions. But a slight deviation of up to 0.1 V was observed as current density was increased. As current density increases, the influence of ohmic losses and activation overpotentials on cell voltage also increases. Therefore, the deviation can be attributed to several assumptions and factors as described below:

1. Number of cathodic and anodic channels used in the experimental data were not known. Therefore, total of 10 channels were assumed. Moreover, the dimensions of these channels was also not known and values from several different papers were used which could have resulted in the deviation.

2. There is a difference in reported values of reference current densities and charge transfer coefficients in the literature which are used to calculate the activation overpotential. This results in some uncertainty in the prediction of activation overpotential.

3. The parameter denoted as λ, representing the ratio of water molecules to sulphonic groups, was an initially undetermined quantity. Abdin et al.[65] established its value at 21 through fitting procedures.

3.3. Solid Oxide Electrolyzer (SOE)

3.3.1. Open Circuit Voltage
As both PEM and solid oxide electrolyzer cells have solid state electrolyte and higher operating temperature,Equation 3.1 is used to calculate the open circuit voltage. To calculate the reversible cell voltage at high operating temperatures, Equation 3.33 [71] is used.

$$V_0 = 1.253 - 2.4516 \times 10^{-4}T \tag{3.33}$$

3.3.2. Activation Overpotential
For computing the activation overpotential, Equation 3.34 [72] is used.

$$V_{\text{act,i}} = \frac{RT}{F}\text{arcsinh}\left(\frac{j}{2j_{0,\text{i}}}\right) \tag{3.34}$$

Here, $V_{\text{act,i}}$ is the activation overpotential for the cathode and anode. $j_{0,\text{i}}$ denotes the exchange current density at electrodes. The exchange current density can be calculated by using the Arrhenius relation as shown in Equation 3.35 [73].

$$j_{0,\text{i}} = k\exp\left(\frac{-E_{\text{act,i}}}{RT}\right) \tag{3.35}$$

In this equation, k stands for the pre-exponential factor and E_{act} stands for the activation energy. The pre-exponential factor and activation energy of the anode and cathode are given in Table 3.5 [72].

Parameter	Value	Unit
Activation energy for anode	1.2×10^5	J/mol
Activation energy for cathode	1×10^5	J/mol
Pre-exponential factor for anode	2.051×10^9	A/m^2
Pre-exponential factor for cathode	1.344×10^{10}	A/m^2

Table 3.5: Activation energy and pre-exponential factor used in solid oxide electrolyzer calculations [67]

3.3.3. Ohmic Overpotential
For calculating the ohmic overpotential, Equation 3.36 was developed by Ni et al. [72] on the basis of parameters listed in Table 3.6.

$$V_{\text{ohm}} = 2.99 \times 10^{-5}\exp\left(\frac{10300}{T}\right)jL \tag{3.36}$$

Here L is the thickness of electrolyte and j is the operating current density.

Parameter	Value	Unit
Cell area	0.04	m^2
Anode thickness	500×10^{-6}	m
Cathode thickness	50×10^{-6}	m
Electrolyte thickness	50×10^{-6}	m
Porosity	0.3	-
Tortuosity	5.0	-

Table 3.6: Solid oxide electrolyzer geometrical parameters used in calculations [67]

3.3.4. Voltage Validation

Comparison of reference voltage values and simulated values was done and results are shown in Figure 3.3. The reference data was taken from Udagawa et al. [74]. The operating conditions and feed compositions used are given in Table 3.7

Parameter	Value
Operating Temperature	1023 K
Operating pressure	1 bar
Cathode stream inlet composition	10 mol% H_2/ 90 mol% H_2O
Anode stream composition	100 mol% O_2

Table 3.7: Voltage validation input parameters
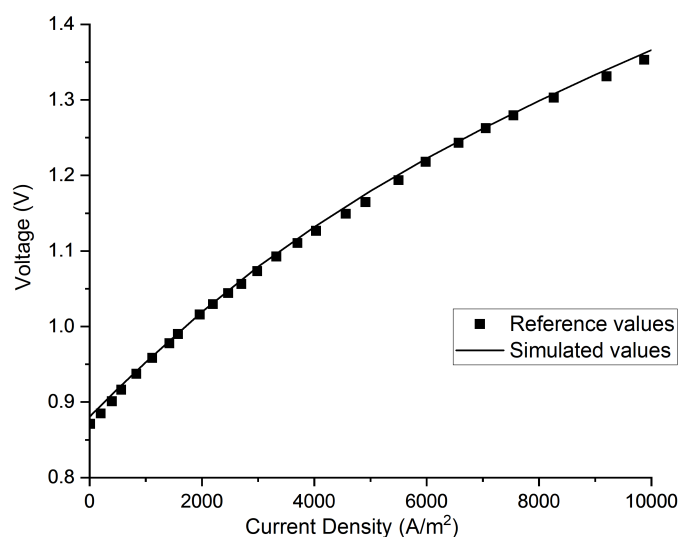
Figure 3.3: Comparison of reference and simulated voltage values for solid oxide electrolyzer

As seen from Figure 3.3, a good correlation between reference and simulated voltage was observed. But it should be noted that the reference data was a result of simulation and not an experiment. Moreover, the activation energy and pre-exponential factors reported by Ni et al. [72] were found to correlate better

with the reference data. With the activation energies and pre-exponential factors reported by Udagawa et al.[74], simulated voltage values were found to deviate from the reference values by around 0.04 V at higher current densities.

3.4. Mass flow rates

Using the cell voltage, electrolyzer capacity, operating current density and Faraday's efficiency, mass flow rates of generated hydrogen, oxygen and consumption of water can be calculated. Firstly, the specific power consumption (Wh/kg) was calculated using Equation 3.37

$$P_{\text{Cons}} = \frac{2V_{\text{Cell}}F}{M_{H_2}\eta_F \times 3600} \tag{3.37}$$

By dividing the known electrolyzer capacity with specific power consumption as seen in Equation 3.38, the mass flow rate of hydrogen produced (kg/h) was calculated.

$$m_{H_2} = \frac{E_{\text{Cap}}}{P_{\text{Cons}}} \tag{3.38}$$

Mass flow rate of oxygen generated and mass flow rate of water required was then calculated by mass balance of chemical equation of water electrolysis.

3.5. Economic Analysis of Electrolyzers

3.5.1. Capital Costs

Significant deviation can be observed in the literature for capital cost prediction of electrolyzer systems. This deviation can mainly be attributed to two factors [75]:

1. Novelty of electrolyzer technology drives companies to hide the cost data to retain the competitive advantage.

2. Boundaries for estimation of CAPEX costs are inconsistent.

In Christensen's report on hydrogen production costs [11], electrolyzer CAPEX costs from different reports, interviews and publications are summarized. It can be observed that CAPEX costs for alkaline and PEM electrolyzers have relatively lower deviation as compared to solid oxide electrolyzer costs. This is due to the fact that technology maturity of alkaline and PEM electrolysis is much higher. For alkaline and PEM electrolyzers, CAPEX costs given by Patonia et al.[75] were used since the division of costs according to the key components was given. For capital costs of solid oxide electrolyzer, costs given by Christensen [11] were used since there is significant deviation in the capital estimation in the literature. The component costs for 1 MW electrolyzer in 2019 USD as per Patonia et al. are shown in Table 3.8 along with solid oxide electrolyzer costs.

	Technologies		
Components	**Alkaline**	**PEM**	**Solid Oxide**
Stack ($/kW)	270-450	400-870	-
Power electronics ($/kW)	81-135	100-217.5	-
Gas conditioning ($/kW)	81-135	67-145	-
Balance of plant ($/kW)	108-180	100-217.5	-
Total ($/kW)	**540-900**	**667-1450**	**677-2285**

Table 3.8: Capital costs of electrolyzer stack [11], [75]

To calculate the total CAPEX costs of electrolyzer in euros, procedure described below was used:

- Calculation of current: The electron mole flow rate (electrons/s) was calculated from hydrogen mole flow rate. By multiplying the electron flow rate with Faraday's constant, the current (I) was calculated.
- Electrolyzer area: Electrolyzer area was then calculated by dividing the current with current density as shown in Equation 3.39.

$$A_{\text{Electrolyzer}} = \frac{I}{j_{\text{el}}} \tag{3.39}$$

- Power required per unit area: By multiplying the cell voltage with current density, power required per unit area was calculated.
- Total capital cost: The total capital cost of electrolyzer was calculated by Equation 3.40.

$$\text{CAPEX}_{\text{Total}} = \text{CAPEX}_{\text{Stack}} \times A_{\text{Electrolyzer}} \times \text{Power}_{\text{Area}} \tag{3.40}$$

In this equation, $\text{Power}_{\text{Area}}$ is the power required per unit area and is in kW/m^2.

Scaling effects

In the past few years, alkaline and PEM electrolyzer capacities have grown from kilowatt scale to megawatt scale and this growth in capacities can also be foreseen for the solid oxide electrolyzers. The impact of scale on CAPEX costs of electrolyzer can be given by Equation 3.41

$$C_b = C_a * \left(\frac{S_b}{S_a} \right)^f \tag{3.41}$$

Here, C_a and S_a are the capital cost and capacity of known reference component. C_b is the capital cost of component at capacity S_b. f is the scale factor. Bohm et al. [76] has summarized the scale factors and are given in Table 3.9.

	f (<5MW$_{el}$)	f(>5MW$_{el}$)
Alkaline	0.69	0.9
PEM	0.72	0.9
Solid oxide	0.6	0.9

Table 3.9: Scale factors for capital cost estimation of electrolyzers

It can be seen from Table 3.9 that scale factors for >5 MW electrolyzer capacity, the scale factor is assumed to be 0.9 for all three types. This is because at higher capacities, most electrolyzers are built by modular approach in which size and number of electrolyzer cells in a stack remains the same and stack numbers are increased for higher electrolyzer capacity. Increasing the individual cell size is not always feasible due to leakage issues [76]. Therefore, decrease in capital costs of electrolyzer with respect to capacity is quite low.

3.5.2. Levelized Costs

Firstly, the capital costs are annualized by Equation 3.42.

$$C_{\text{CAPEX}} = \frac{C_{\text{tot}} CRF}{CF \times 8760} \tag{3.42}$$

In this equation, C_{tot} stands for total capital costs while C_{CAPEX} stands for annualized capital costs. CRF stands for capital recovery factor and CF stands for the annual capacity factor of the system. The annual levelized costs of hydrogen production (LCOH) are calculated by Equation 3.43.

$$\text{LCOH}_{\text{Prod}} = \frac{C_{\text{CAPEX}} + C_{\text{Electricity}} + C_{\text{Water}} - C_{\text{O}_2}}{M_{H_2}} \tag{3.43}$$

Here $C_{\text{Electricity}}$, C_{Water} are annual electricity, desalinated water costs respectively while C_{O_2} is the selling price of produced oxygen and is assumed to be 0 for the initial analysis but in some cases, selling price of oxygen can be 0.1 €/kg [77]. But, selling oxygen is not always a possibility since availability of consumers is required.

<div align="right">

4

</div>

Compression System

4.1. Introduction

After hydrogen production, hydrogen compression is the most energy intensive process in the supply chain. Moreover, as evident from Figure 2.20, compression step is involved multiple times during the supply chain.Therefore, total compression energy required and subsequent costs need to be calculated to analyze the impact on supply chain.In this chapter, equations used to evaluate the energy consumption and economic analysis steps are discussed.

4.1.1. Compressor Selection

The choice of compressor selection was done on the basis of few parameters: tech maturity level, possible flow rate, compression ratio of single stage and durability. As hydrogen supply chain involved vast number of scenarios and requirements, a simplified model was assumed in which hydrogen compression for the supply chain was mainly divided into two categories and a type of compressor was selected for each category:

1. **High flow rate and moderate compression ratio**: This type of compression is needed in the transport of hydrogen using pipelines. Depending on the type of pipeline, the discharge pressure required range between 40-80 bar. To comply with this requirements, centrifugal compressors are selected as high flowrates are possible and their higher durability as compared to mechanical compression.

2. **Low flow rate and high compression ratio**: For fuel cell vehicles, the internal pressure of storage tank usually range between 350-700 bar due to space constraints. Also for salt cavern storage, the storage pressure usually range in 100-200 bar depending on the cavern depth. For this, two compressor types are feasible: reciprocating compressor and diaphragm compressor. In the end, diaphragm compressor was selected due to their higher reliability.

4.1.2. Assumptions

Following assumptions were made in the energy and cost related calculations:

1. Compressors are driven by electric motors with motor efficiency of 95%

2. For centrifugal compressors, the maximum isentropic efficiency was assumed to be 80% and maximum compressor capacity for a single stage to be 16 MW. This assumption was made on the basis of HDSAM model developed by Argonne National Laboratory [78].

3. For diaphragm compressors, the maximum isentropic efficiency was assumed to be 60% and maximum compressor capacity for a single stage to be 1 MW. Similar to the previous assumption, this assumption was also made on the basis of HDSAM model developed by Argonne National Laboratory [78].

4. Isentropic expansion factor, κ was assumed to be 1.41 [79].

For the power and cost calculations, methodology used by Khan et al. [41] was adapted. The equations involved are discussed in the next sections.

4.2. Power Calculations

4.2.1. Number of stages

Number of stages required for particular discharge pressure can be calculated by Equation 4.1.

$$N = \frac{\log\left(\frac{P_{\text{disc}}}{P_{\text{suc}}}\right)}{\log\left(x\right)} \tag{4.1}$$

Here, N signifies the number of stages, P_{disc} and P_{suc} are discharge and suction pressures respectively and x is the compression ratio of a single stage. The value of N obtained was then rounded to the next whole number to get required number of stages.

4.2.2. Discharge temperature

Discharge temperature value is needed for the calculation of compressor power. The discharge temperature can be obtained by manipulating the isentropic efficiency formula. Therefore, a constant isentropic efficiency was assumed and then discharge temperature can be calculated by Equation 4.2.

$$T_{\text{disc}} = T_{\text{suc}}\left(1 + \frac{\left(\frac{P_{\text{disc}}}{P_{\text{suc}}}\right)^{\frac{k-1}{Nk}}}{\eta_{\text{isen}}}\right) \tag{4.2}$$

4.2.3. Compressibility factor

Hydrogen gas deviates from ideal gas model and therefore, compressibility factor (Z) has to be introduced in the calculations to account for the deviation. As evident from Figure 4.1, the compressibility factor of hydrogen varies as a function of temperature and pressure. At higher pressures, the compressibility factor increases.
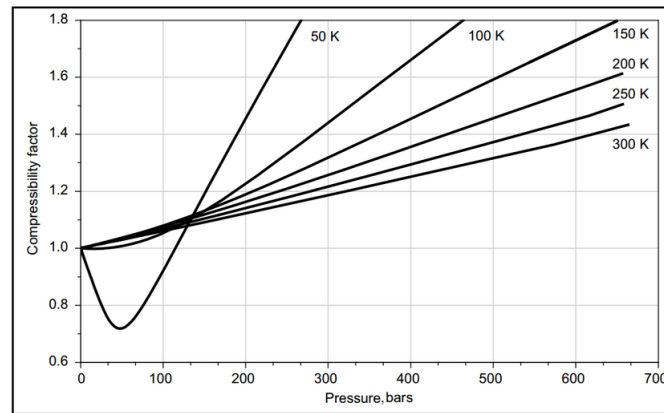
Figure 4.1: Compressibility factor of hydrogen as a function of temperature and pressure [80]

Coolprop library [81] in Python was used to calculate the compressibility factor at average temperature and pressure of the compressor. Average pressure was calculated using the Equation 4.3 [82] and Equation 4.4 was used for average temperature.

$$P_{\text{avg}} = \frac{2}{3}\left(\frac{P_{\text{disc}}^3 - P_{\text{suc}}^3}{P_{\text{disc}}^2 - P_{\text{suc}}^3}\right) \tag{4.3}$$

$$T_{\text{avg}} = \frac{T_{\text{disc}} + T_{\text{suc}}}{2} \tag{4.4}$$

4.2.4. Compressor power

For single stage compression, the power can be calculated by Equation 4.5 [41].

$$P_1 = \left(\frac{k}{k-1}\right)\left(\frac{Z}{\eta_{\text{isen}}}\right) T_{\text{suc}} \left(q_M\right) R \left[\left(\frac{P_{\text{disc}}}{P_{\text{suc}}}\right)^{\left(\frac{k-1}{k}\right)} - 1\right] \tag{4.5}$$

In this equation, P_1 stands for compression power required for one stage in Watts. q_M is the molar flow rate of hydrogen compressed (mol/sec). But since multiple stages are involved in the compression, Equation 4.6 was used.

$$P_N = N \left(\frac{k}{k-1}\right)\left(\frac{Z}{\eta_{\text{isen}}}\right) T_{\text{suc}} \left(q_M\right) R \left[\left(\frac{P_{\text{disc}}}{P_{\text{suc}}}\right)^{\left(\frac{k-1}{Nk}\right)} - 1\right] \tag{4.6}$$

Here, P_N is the total power required for the compression system. To account for the prime mover efficiency, rated compressor power was calculated by Equation 4.7.

$$P_{\text{Rated}} = \frac{P_N}{\eta_{\text{Motor}}} \tag{4.7}$$

4.3. Economical Calculations

For economical calculations, equations given by Khan et al. [41] were used. Since the paper calculated the capital costs in Canadian dollars in 2019, it was converted into Euros by using appropriate CEPCI indices and conversion ratio between C\$ and €. It is also important to note that rated compressor power (P_{Rated}) used in this section is in kilowatts.

4.3.1. Capital costs

The uninstalled costs (UC) for centrifugal compressor were calculated by Equation 4.8.

$$UC = 3083.3 \times P_{\text{Rated}}^f \tag{4.8}$$

In this equation, UC stands for uninstalled costs and f stands for scaling factor has a fixed value of 0.8335.

For the diaphragm compressor used at refuelling stations, there are two equations according to the discharge pressure:

1. **For 350 bar discharge pressure**:

$$UC = 63684.6 \times P_{\text{Rated}}^f \tag{4.9}$$

The scaling factor in this case is 0.4603.

2. **For 700 bar discharge pressure**:

$$UC = 62909.9 \times P_{\text{Rated}}^f \tag{4.10}$$

Here the scaling factor is 0.6038

Then total installed costs (TIC) were then calculated by Equation 4.11

$$TIC = UC \times IF \tag{4.11}$$

The installation factor (IF) for:

1. Centrifugal compressors is 2
2. Diaphragm compressors is 1.3

The total installed costs were multiplied with a factor of 1.4 and 1.28 for centrifugal and diaphragm

compressors respectively to account for the indirect costs [41]. These costs include factors such as site preparation, engineering and design, project contingency and permitting. The summation of installation costs and indirect costs is called as total capital investment (TCI). These capital costs were then annualized by multiplying with a capital recovery factor as shown in Equation 4.12

$$C_{\text{CAPEX}} = \text{TCI} \times \text{CRF} \tag{4.12}$$

Here C_{CAPEX} is the annual capital cost in €/year and CRF is the capital recovery factor.

4.3.2. Operating costs
Electricity costs
Annual electricity costs were calculated by Equation 4.13

$$C_{\text{Electricity}} = 8760 \times P_{\text{Rated}} \times CF \times C_{\text{Unit}} \tag{4.13}$$

In this equation. $C_{\text{Electricity}}$ is the total electricity cost per year (€/ year) and C_{Unit} is the unit electricity cost (€/ kWh).

O&M costs
Operating and maintenance costs were assumed to be 5% of the annual capital costs.

4.3.3. Levelized costs of compression
Levelized costs of compression were calculated by Equation 4.14.

$$\text{LCOH}_{\text{Comp}} = \frac{1.05 C_{\text{CAPEX}} + C_{\text{Electricity}}}{8760 \times CF \times M_{H_2}} \tag{4.14}$$

Here M_{H_2} is the flow rate of hydrogen compressed in kg/hr.

Hydrogen Transport by Pipeline Network

5.1. Introduction

Gases move through the pipeline network due to pressure differential. The pressure differential between inlet and outlet is caused due to friction between the internal pipe surface and flowing gas. If the pipeline length is longer, the pressure losses can be significant and compressor stations are installed every 100 to 500 km [83]. The overall design of hydrogen pipeline network is similar to natural gas but some modifications are needed and are described below :

1. **Hydrogen Embrittlement**:
   Most transmission pipelines for natural gas are made of steels with higher tensile strength. It has been observed that high strength steels are more susceptible to hydrogen embrittlement [84]. As a consequence, low tensile strength steels will have to be used for hydrogen transport. Due to this, either the operating pressures have to be kept lower or thickness of the pipe will have to be increased. The distribution lines for natural gas are made of low strength steels such as API 5L A, B, X42 and X46 are not susceptible to hydrogen embrittlement [**88**]. Therefore, a large section of existing natural gas infrastructure can be repurposed for hydrogen transport.

2. **Safety**:
   Due to low density of hydrogen, preventing leakages would be more challenging as compared to natural gas. Hydrogen also has a flammability range of 4% to 76% at normal temperature and pressure [85]. Hydrogen-air mixtures are also easy to ignite as compared to natural gas [83]. Hydrogen burns in air with pale blue flame which is almost invisible during the day. Therefore, more complex safety procedures are required.

3. **Odorization**:
   As natural gas is odourless, natural gas used for residential consumers is odorized using sulfur based compounds for making it easier to detect the leaks. Similarly, hydrogen gas is also odourless and will need to odorized. In the Netherlands, tetrahydrothiophene (THT) is used to odorize the natural gas. According to Huszal et al. [86], THT can also be used to odorize the hydrogen gas. But, there is absence of approval and regulation of odorization of hydrogen in Europe.

The analysis of hydrogen transport by pipeline network is mainly split into two sections: pipeline hydraulics and economical analysis.

5.2. Pipeline Hydraulics

In this section, gas hydraulics calculations done to calculate the total transport capacity of a pipeline network are discussed. Some assumptions and generalizations made during the calculation process are described below:

1. Ambient temperature and pressure are assumed to be constant across the length of the pipeline

2. The calculations are made considering the geography of the Netherlands. Elevation changes are assumed to be zero and burial depth of the pipeline is assumed to be constant.

3. In many cases, the discharge pressure of the pipeline is not known. Therefore, an initial discharge pressure was assumed and flow velocity was calculated. If the flow velocity was lower than maximum velocity (also known as erosional velocity), then the discharge pressure assumed initially was used in the next calculations.

The gas flow calculations are done using the equations and methodology discussed in the book "Gas Pipeline Hydraulics" by Sashi Menon[82].

5.2.1. Gas flow rate

General flow equation was used to calculate the gas flow rate in Sm^3/day.

$$Q = 1.1494 \times 10^{-3} \left(\frac{T_b}{P_b} \right) \left[\frac{(P_1^2 - e^s P_2^2)}{G T_f L_e Z f} \right]^{0.5} D^{2.5} \tag{5.1}$$

In Equation 5.1,

- Q is the gas flow rate per day [Sm^3/day]
- L is the pipeline length [km]
- L_e is the equivalent pipeline length [km]
- D is the internal diameter of pipe [mm]
- P_1 is the inlet pressure [kPa]
- P_2 is the outlet pressure [kPa]
- P_b is the ambient pressure (Assumed to be constant at 101.351) [kPa]
- T_b is the ambient temperature (Assumed to be 288 K) [K]
- T_f is average temperature of flowing gas [K]
- G is the specific gravity of hydrogen (0.0696 [83]).
- Z is the compressibility factor
- f is the friction factor
- s is the elevation adjustment parameter and was assumed to be zero.

5.2.2. Compressibility factor

To calculate the compressibility factor of hydrogen gas flowing through the pipeline, methodology discussed in Section 4.2.3 was followed.

5.2.3. Friction factor

One of the key parameters for calculating the friction factor is Reynolds number. According to Khan et al. [83], most gas pipelines operate at higher Reynolds numbers i.e in the turbulent regime. The Reynolds number was calculated by assuming an average velocity as shown in Equation 5.2.

$$Re = \frac{V_{avg} D \rho_{avg}}{\mu} \tag{5.2}$$

As turbulent flow is assumed, the Colebrook-White equation [82] was used to calculate the friction factor.

$$\frac{1}{\sqrt{f}} = -2\log_{10}\left(\frac{\varepsilon}{3.7 D} + \frac{2.51}{Re\sqrt{f}} \right) \tag{5.3}$$

In Equation 5.3, f is the friction factor, ε is the pipeline roughness (m). Explicit solution to this equation is not available and therefore, the equation was solved iteratively by process described below:

1. An initial starting value for friction factor was assumed.
2. The LHS and RHS of equation were solved for the assumed value of friction factor.
3. The process was repeated until the difference in the value of LHS and RHS was less than 0.001.

5.2.4. Average velocity of gas

Assuming steady stage conditions, the velocity of gas can be calculated from flow rate and pipe diameter as seen from Equation 5.4 [82]

$$V = 14.734 \left(\frac{P_b}{T_b}\right) \left(\frac{ZT}{P}\right) \left(\frac{Q}{D^2}\right) \tag{5.4}$$

5.2.5. Erosional velocity

Erosional velocity is the velocity of gas in a pipeline at which flow of gas starts causing erosion of pipe wall. Therefore, gas flow velocity should be lower than erosional velocity. Erosional velocity can be calculated by Equation 5.5 [83].

$$V_{max} = 100\sqrt{0.05131\frac{ZRT}{GP}} \tag{5.5}$$

5.2.6. Model Overview

It can be observed from previous sections that Reynolds number and subsequently the friction factor are dependent on assumed value of average velocity. The flow rate calculated therefore will be for assumed value of average velocity. But, during basic calculations it was observed that the calculated value of average velocity from Equation 5.4 varied significantly from assumed value. Thus, general methodology shown in Figure 5.1 was created to reduce the error in predicting the flow rate of pipeline.
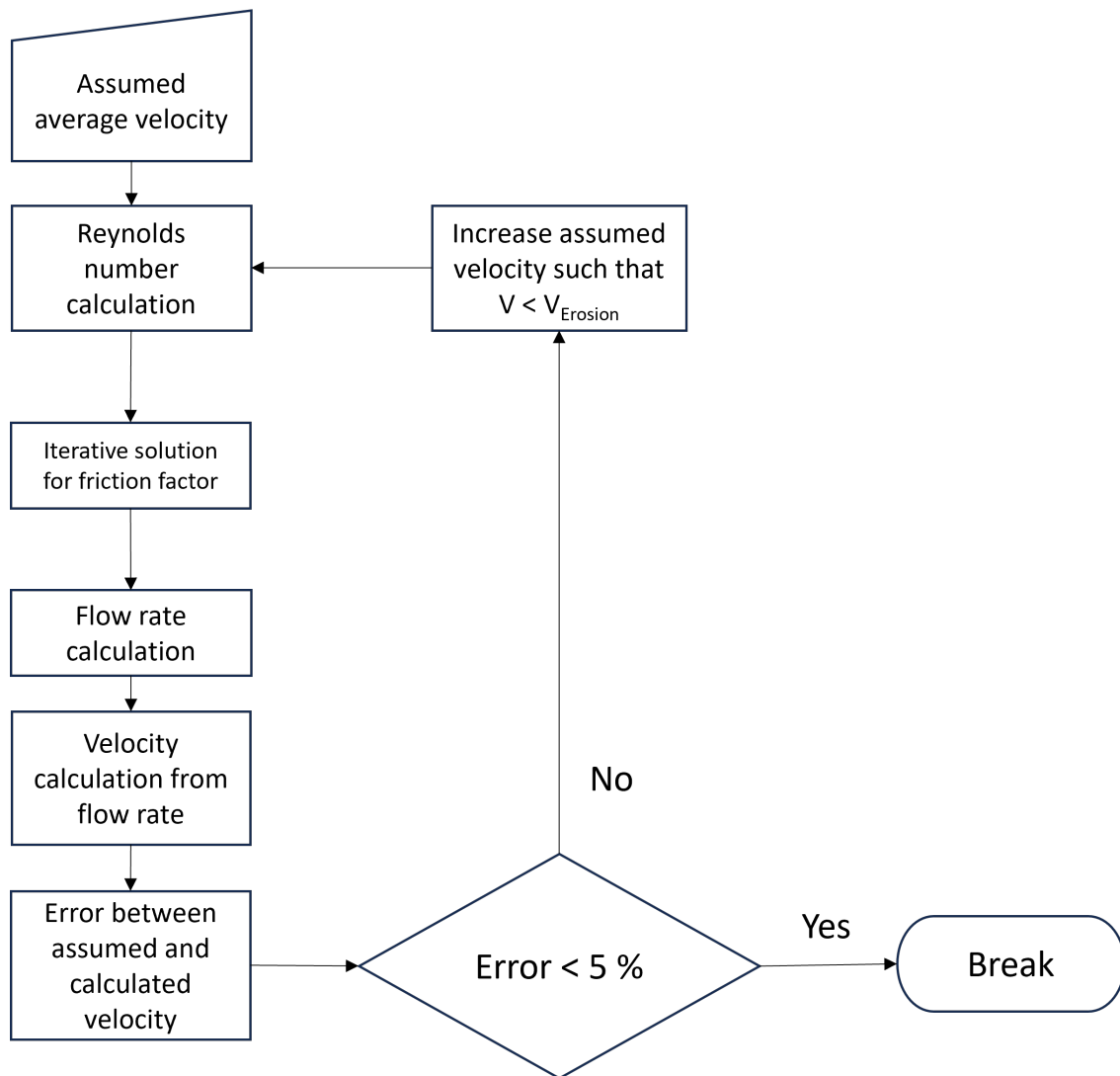
Figure 5.1: Methodology for flow rate and average velocity of hydrogen in the pipeline

The steps involved are briefly discussed below:

1. An initial average velocity was manually entered into the Python code.
2. The Python code calculated the Reynolds number on the basis of this initial velocity.
3. The friction factor was calculated iteratively on the basis of this initial assumed velocity.
4. Flow rate on the basis of friction factor was calculated.
5. Velocity was calculated on the basis of flow rate.
6. Error between assumed and calculated average velocity was evaluated.
7. If the error was more than 5%, the assumed velocity was given an increment and the process was repeated again until the error value was less than 5%

In this method, outlet pressure was initially assumed to be half of inlet pressure and was manually varied until $V < V_{\text{Erosion}}$ was satisfied.

As the flow rate calculated using Equation 5.1 is in Sm^3/day, it was converted to kg/day using Equation 5.6 [83].

$$\text{Capacity}_{\text{Pipe}} = Q * 0.0834 \tag{5.6}$$

5.3. Cost calculations

For the calculation of levelized cost of hydrogen transport, methodology from Khan et al. [83] was adapted. This paper based their calculations on the HDSAM model [78]. HDSAM model modified the natural gas pipeline cost calculations by multiplying the capital costs with a factor of 1.1. This was done to account for the involvement of low strength steel pipe with higher thickness (due to hydrogen embrittlement), valves capable of containing hydrogen etc. The equations used are discussed in this section. The costs calculated using the equations are in 2009 $. They were converted to 2022 €using appropriate CEPCI indices and conversion rates.

5.3.1. Total capital Investment

Total installed costs can be calculated by Equation 5.7.

$$\text{TIC}_{\text{pipe}} = \text{Material cost} + \text{Labour cost} + \text{Miscellaneous cost} + \text{Right of way cost} \tag{5.7}$$

Material costs and labor costs are influenced by the pipe diameter and pipeline length. Additionally, it's important to highlight that the equations employed in this section utilize inches for diameter and miles for pipeline length.

Material costs

$$\text{Material costs} = 1.1 \times 63027 \times e^{0.0697D} L_{\text{Pipeline}} \tag{5.8}$$

In this equation, D stands for diameter (in.) and L_{Pipeline} stands for pipeline length (miles).

Labour costs

$$\text{Labour costs} = 1.1 L_{\text{Pipeline}}(-51.393D^2 + 43523D + 16171) \tag{5.9}$$

Miscellaneous costs

$$\text{Miscellaneous} = 1.1 L_{\text{Pipeline}}(303.13D^2 + 12908D + 123245) \tag{5.10}$$

Right of way costs

$$\text{Right of way costs} = L_{\text{Pipeline}}(-9 \times 10^{-13}D^2 + 4417.1D + 164241) \tag{5.11}$$

Assuming indirect costs to be 40 % of TIC, total capital investment (TCI) was calculated using Equation 5.12.

$$\text{TCI} = \text{TIC} + 0.4 \times \text{TIC} \tag{5.12}$$

Total capital investment was then annualized by multiplying it with capital recovery factor (CRF) and assuming lifetime to be 50 years.

5.3.2. Operating costs

As reported by Khan et al.[83], the operating costs, expressed as a percentage of Total Capital Investment (TCI), are determined by the following parameters:

- O&M = 0.5% of TCI

- Insurance = 1% of TCI

- Property tax = 1 % of TCI

- License & permits = 0.1 % of TCI

Therefore, operating costs were assumed to be 2.6% of annualized TCI. In addition to these costs, compression costs are also involved which are calculated using the equations discussed in previous section.

5.3.3. Levelized costs

The levelized costs of hydrogen transport (LCOH$_{Pipeline}$ were calculated using Equation 5.13.

$$LCOH_{Pipeline} = \frac{CAPEX_{Annualized} + OPEX_{Annualized}}{UF \times Capacity_{Pipeline} \times 365} \tag{5.13}$$

In this equation, UF stands for utilization factor and was assumed to be 90% [83] for the initial analysis. It was later varied to study the effect on levelized costs. Capacity$_{Pipeline}$ is the flow rate of hydrogen per day (kg/day).

<div align="right">

6

</div>

Salt Cavern Storage

6.1. Introduction

In this chapter, assumptions and equations used to predict the levelized cost of hydrogen storage in salt caverns are discussed. While designing a salt cavern, several factors need to be considered to ensure safe operation. The first important factor is the operating pressure range which should be lesser than the overburden pressure. Overburden pressure can be defined as the pressure exerted on rock/sediment layer due to the weight of the material above it. Overburden pressure increases with depth and is a key defining factor in determining the operating pressure range.Figure 6.1 [30] shows the overburden pressure with respect to the depth of cavern. If the internal pressure of the cavern is too low as compared to overburden pressure, the cavern might collapse. To prevent this, cushion gas is added to the cavern (around 20-30% of cavern volume) to maintain the minimum required pressure.
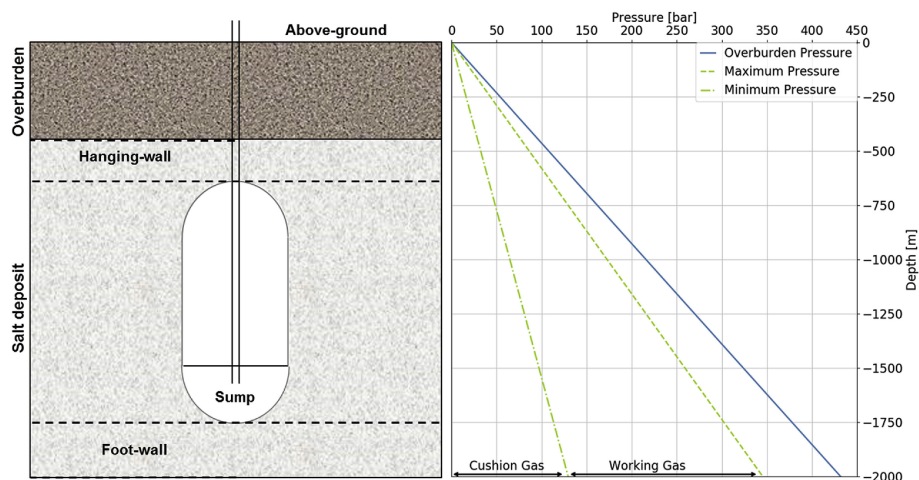
Figure 6.1: A simple representation of a salt cavern and estimated pressure limits as a function of cavern depth

The second important factor in cavern design is the dimensions of cavern. Considering the geomechanical safety, following recommendations are made by Wang et al. [87]:

- The minimum thickness of hanging wall should be 75% of cavern diameter.

- Minimum limit for height to diameter ratio of salt caverns is 0.5.

In Section 6.2, equations used to calculate the capacity and operating parameters are discussed. In Section 6.4, procedure used to calculate the levelized costs is discussed.

6.2. Cavern Design

6.2.1. Cavern shape and dimensions

For the cavern design, capsule shape was assumed as Ozarslan [88] stated that capsule shape is more stable than cylindrical or elliptical shape considering the stress risk. For cavern sizing, methodology suggested by Eradus [6] was followed. In capsule shaped cavern it was further assumed that top section is a dome with height being 1/6th of cavern diameter and bottom section is cone shaped with height being 1/3rd of cavern diameter. Then, cavern volume can be approximated as given by Equation 6.1.

$$V = \frac{\pi}{12} D_{\text{Cavern}}^2 (3H - D_{\text{Cavern}}) \tag{6.1}$$

In this equation, V is the cavern volume, D_{Cavern} is the diameter of cavern and H is the cavern height. To understand the impact of cavern volume on costs, cavern volume was given as an input and then cavern height and diameter were calculated by assuming that height to diameter ratio is 0.5. By manipulating the Equation 6.1, height of the cavern can be calculated on the basis of volume.

$$H = \sqrt[3]{\frac{3V}{\pi}} \tag{6.2}$$

6.2.2. Operating pressure

The operating pressure range is defined on the basis of overburden pressure. Overburden pressure was calculated using Equation 6.3 [6].

$$P_{\text{overburden}} = \rho_{\text{rock}} g (D_{\text{Cavern}} - H) \tag{6.3}$$

In this equation, ρ_{rock} is the average density of rock and was assumed to be 2300 kg/m^3 [88]. g is the gravitational acceleration constant. According to Caglayan et al.[30], cavern pressure range should be between 24% to 80% of the overburden pressure. Below 24% of overburden pressure, there is a risk of cavern collapse and above 80% of overburden pressure, could result in fracture.

6.2.3. Storage capacity calculations

To calculate the density of hydrogen gas stored, temperature of gas needed to be calculated. Assuming that the gas temperature is same as rock layer at that depth and geothermal gradient of 25 °Ckm^{-1} [6], the average gas temperature was calculated by Equation 6.4 [6].

$$T_{\text{Average}} = 288 + 0.025 \left(D_{\text{Cavern}} - \frac{H}{2} \right) \tag{6.4}$$

At this temperature and using lower and upper limits of operating pressure range, the minimum and maximum density of stored hydrogen was calculated using CoolProp library [81]. During the solution mining phase, some brine remains in the cavern and is accounted in the capacity calculations by introducing a safety factor, θ_{Safety} [30] and was assumed to be 70% [6]. Then, the amount of hydrogen stored in the cavern was calculated using Equation 6.5.

$$m_{\text{Hydrogen}} = (\rho_{\text{H}_2,\text{maximum}} - \rho_{\text{H}_2,\text{minimum}}) V_{\text{Cavern}} \theta_{\text{Safety}} \tag{6.5}$$

In salt caverns, cushion gas is required to maintain the safety limits of pressure. TNO report [89] suggested that hydrogen, nitrogen and carbon-dioxide can be used as cushion gas. Among these options, using nitrogen or carbon dioxide as cushion gas would reduce the costs but withdrawal of hydrogen would require an additional purification step. Using hydrogen gas for cushioning would eliminate the need of additional purification but is expensive. But, cushion gas was still assumed to be hydrogen since extra purification step is not needed. The amount of cushion gas needed was calculated by Equation 6.6 in which cushion gas volume was assumed to be 30% of the cavern volume.

$$m_{\text{Cushiongas}} = 0.3 (\rho_{\text{H}_2,\text{maximum}} - \rho_{\text{H}_2,\text{minimum}}) V_{\text{Cavern}} \tag{6.6}$$

6.3. Gas cleaning

Depending on the geology of cavern, the hydrogen stored might contain several impurities such as nitrogen, methane, carbon dioxide etc. Some major hydrogen consumers such as fuel cell based vehicles require a purity level of 99.999% [90]. Thus, a separation unit is required. In case of hydrogen, three purification technologies are viable: pressure swing adsorption (PSA), membrane adsorption and cryogenic distillation [91]. According to Yousefi et al. [90], PSA is the most optimum choice considering the factors such as energy consumption, feed rate, gas composition and withdrawal rate. In PSA, activated carbon (AC) and zeolite (ZE) are used as adsorbates for hydrogen purification since AC can separate organic compounds and ZE can separate nitrogen [90]. In this project, the detailed calculations for PSA were not performed since the exact feed composition needs to be known. Instead, following assumptions were made on the basis of work done by Yousefi et al.[90]:

1. Recovery of separated feed is 85%.
2. Hydrogen stored majorly consists of nitrogen, methane and carbon dioxide as impurities.

6.4. Cost analysis

6.4.1. Capital costs of salt cavern

Total capital cost of salt cavern storage consists of four categories: cushion gas costs, geologic site preparation cost, compressor capital cost and well capital cost. The capital and operating costs of compression are discussed in detail in Chapter 4. The contribution of other categories is summarized in Table 6.1 as adapted from Chen et al. [92].

Capital cost type	Name of capital cost	Salt cavern
Cushion gas cost	Cushion gas percentage (%)	30
	H2 cost (€/kg)	5 (base case)
Geologic site preparation cost	Mining cost ($/m^3)	25.53
	Site characterization ($)	127,650
	Leaching plant cost ($/kg)	5.55
	Mechanical integrity cost ($/kg)	2.553
Well capital cost	Well cost ($/well)	1,276,500

Table 6.1: Capital cost parameters and values for salt cavern [92]

The capex costs calculated were then annualized by assuming the lifetime of 50 years and discount rate of 5% [6] by using Equation 2.7.

6.4.2. PSA capital costs

The capital costs of PSA were calculated using Equation 6.7 given by Mivechian et al. [93]. Although there are several different capital cost estimation equations available in the literature, according to Yousefi et al. [90] the estimation given by Mivechian et al. [93] correlates well with the supplier quote for large scale PSA design for hydrogen purification.

$$\text{CAPEX}_{\text{PSA}} = C_{\text{ref}} \left(\frac{Q}{Q_{\text{ref}}} \right)^{0.66} Q_{\text{ref}} \tag{6.7}$$

In Equation 6.7,
Q_{ref} = 116 kmol/hr
C_{ref} = 1.74 M€

Then the total annual capital costs were calculated by summing the annualized capital costs of salt cavern, compressor and PSA.

6.4.3. Operating costs

Annual operating costs for salt cavern were assumed to be 2% of annualized capital cost of salt cavern [6]. For PSA, the operating costs are complex to evaluate due to the adsorbants.The effectivity of adsorbants decreases over time and need to be replaced every 3-5 years. Although Yousefi et al. [90] has done a detailed analysis about the impact, the operating costs were assumed to be 5% of annual capital costs of PSA. This was done because the detailed operating cost analysis require additional data such as feed composition and number of separation units involved.

6.4.4. Levelized costs

For the calculation of levelized costs, total amount of hydrogen stored annually inside a salt cavern needs to be known. Although Equation 6.5 gives total capacity of hydrogen that can be stored at a time, it doesn't account for the constant injection and withdrawal that happens over a year. Although it is difficult to predict the total amount due to constant injection and withdrawal, an estimation can be made by assuming a number of injection and withdrawal cycles a cavern goes through annually. Yousefi et al. [90] made two scenarios on the basis of storage cycles:

- **Seasonal storage**: Hydrogen stored for a long time. Only one cycle per year was assumed in this case.
- **Short term storage**: Constant injection and withdrawal of hydrogen. Two to six cycles were assumed in this case.

By using this simplification, the levelized costs of hydrogen stored were calculated by Equation 6.8.

$$\text{LCOH}_{\text{Storage,Annualized}} = \frac{\text{LCOH}_{\text{CAPEX}} + \text{LCOH}_{\text{OPEX}}}{m_{\text{Hydrogen}} \times n_{\text{cycles}}} \qquad (6.8)$$

In Equation 6.8, m_{Hydrogen} is the capacity of cavern and n_{cycles} is the number storage cycles.

7

Results and Discussion

In this chapter, results obtained from the hydrogen production, compression, storage and transportation models are discussed. In Section 7.1, the techno-economics of electrolyzers are discussed. Also, application of learning rates on the electrolyzers to predict the future costs of electrolyzers are also discussed in this section.

7.1. Hydrogen production

Using the electrochemical and economical models for alkaline, PEM and solid oxide electrolyzers discussed in Section 2.4, techno-economics of the electrolyzers were analyzed. Firstly, technical analysis was done and is discussed in detail in Subsection 7.1.1. In this subsection, impact of operating conditions on cell voltage is analyzed. In Subsection 7.1.2, the impact of current densities, electricity costs on levelized costs of hydrogen production is analyzed. In Subsection 7.1.3, prediction of levelized costs with respect to time is discussed.

7.1.1. Technical analysis

The calculated cell voltage for particular operating conditions directly influences the operating costs of electrolyzer. Lower cell voltages for particular current density are desired because it implies lower losses due to overpotentials and subsequently lower power consumption per mole of hydrogen produced. In this subsection, effects of temperature and pressure on cell voltage of electrolyzers as a function of current density are discussed. The general operating range of temperature and pressure of electrolyzers is given in Table 2.2.

1) Alkaline Electrolyzer
Temperature effects:
To study the temperature effects on operating cell voltage, the temperature was varied from 30 °C to 80 °C at 1 bar pressure and 30% electrolyte concentration. The effect of temperature on voltage is shown in Figure 7.1.It can be deduced from Figure 7.1 that increase in temperature reduces the cell voltage for particular current density.This is because the elevated temperatures lead to a decrease in open circuit voltage, activation overpotential, and ohmic losses. The reduction in activation overpotential is mainly due to the increase in exchange current densities. It was observed that bubble effect given by Equation 3.7 plays an important role in the reduction of ohmic overpotential due to increase in temperature. As the temperature is increased, value of θ in Equation 3.7 can be observed to be decreasing. As this leads to an increase in the conductivity of KOH electrolyte, the ohmic overpotentials decrease. Therefore, temperature of 80 °C which is the upper limit of operating temperature range of alkaline electrolyzer was considered for the economical analysis.
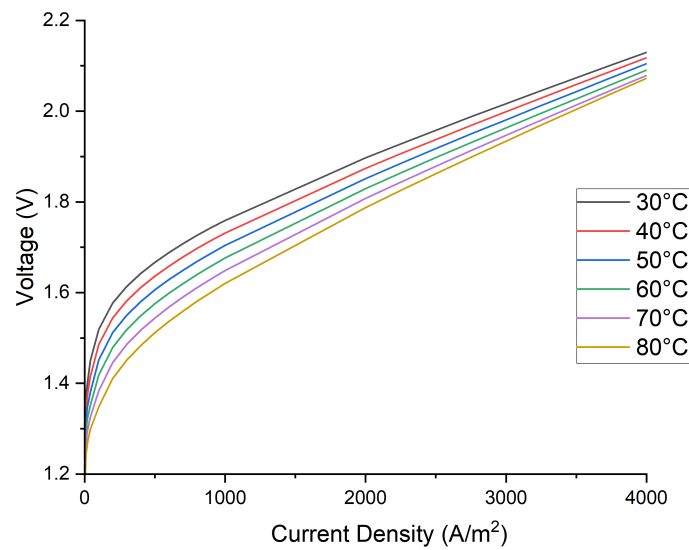
Figure 7.1: Effect of temperature on voltage - current density curve for alkaline electrolyzer at 1 bar pressure and 30% electrolyte concentration

Pressure effects:

By keeping the operating temperature constant at 80°C and varying the pressure, voltage-current density curve as shown in Figure 7.2 was obtained.
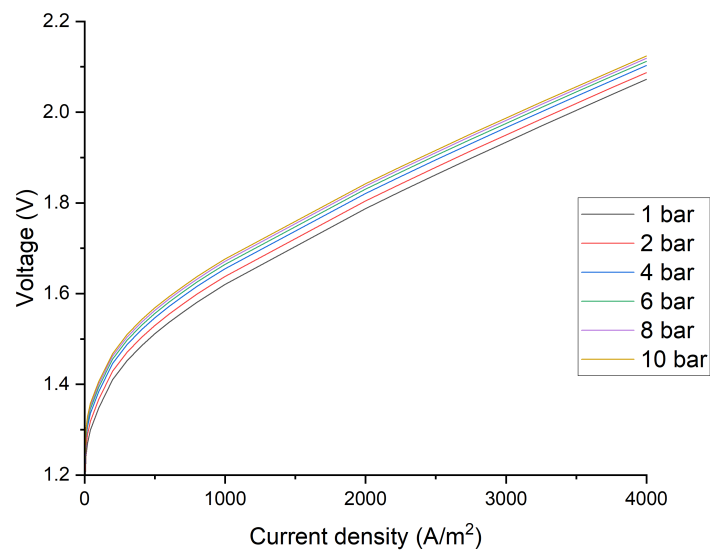
Figure 7.2: Effect of pressure on voltage - current density curve for alkaline electrolyzer at 80 °C temperature and 30% KOH concentration

As observed from Figure 7.2, the effects of pressure on voltage are not significant. But with increase in pressure, slight increase in voltage at particular current density is observed. This is because the open circuit voltage increases with increase in pressure. Although increase in pressure reduces the resistance

caused due to gas bubbles which in turn reduces activation and ohmic overpotentials, the decrease is quite insignificant as compared to impact on open circuit voltage. Operation at higher pressures would require modification of walls containing the electrolyzer assembly as well. For these reasons, operating alkaline electrolyzers at atmospheric pressure is deemed optimal and thus considered for the economic analysis.

Concentration effects

The concentration of KOH affects the conductivity of electrolyte which in turn impacts the ohmic overpotentials. The impact was analyzed for the concentration range of 20-40% of KOH in water and can be seen in Figure 7.3 at the operating temperature and pressure of 80 °C and 1 bar respectively.
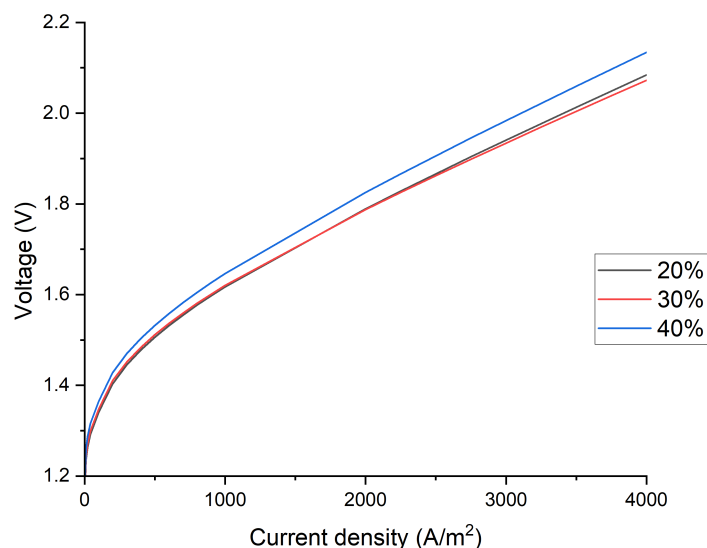
Figure 7.3: Effect of KOH concentration on voltage - current density curve for alkaline electrolyzer at 80 °C temperature and 1 bar pressure

It can be observed that cell voltage is highest for the entire operating current density range when KOH concentration is 40 %. For KOH concentration of 20% and 30%, the cell voltages are almost similar at lower current density. But at higher current densities, KOH concentration of 30% has slightly lower cell voltage values. This is because the conductivity of KOH solution was found to be higher at 30% concentration as compared to 20% KOH concentration. Therefore for the economical analysis, KOH concentration of 30% was considered.

2) PEM Electrolyzer
Temperature effects:
The effect of temperature variation on cell voltage of PEM electrolyzer can be seen in Figure 7.4. Similar to the alkaline electrolyzer model, increasing the temperature reduces the cell voltage. The difference in cell voltages at various temperatures can be seen to be more profound at higher current densities. This is mainly due to the fact that the Nafion membrane conductivity increases with temperature thereby reducing ohmic overpotentials. As ohmic overpotentials are product of total resistance and current density, increasing the current density has direct influence on cell voltage as well. Despite the reduction in cell voltage as temperature increases, Nafion membranes degrade quickly at temperatures above 85 °C [94]. Therefore, temperature was of 80 °C was considered in the economical analysis.
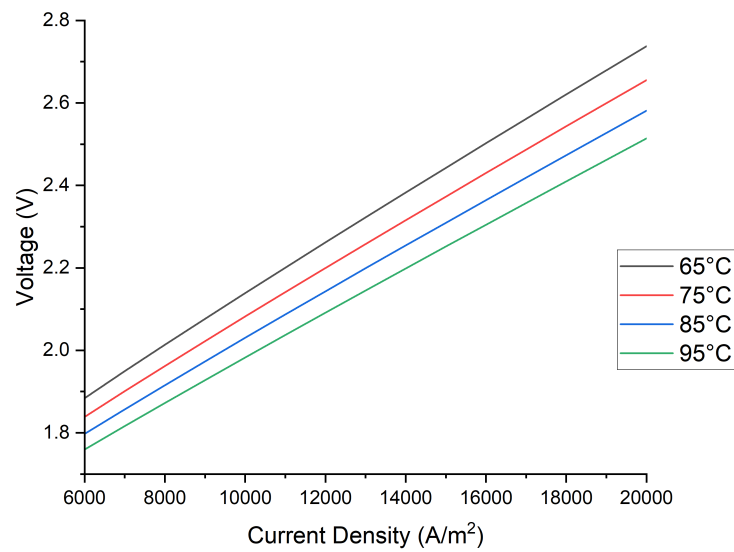
Figure 7.4: Effect of temperature on voltage - current density curve for PEM electrolyzer at 15 bar pressure

Pressure effects:

The pressure was varied from 15-30 bar at constant temperature of 80 °C to assess the impact on cell voltage and resulting curve can be seen from Figure 7.5. It was observed that the cell voltage increases with pressure but this increase was found to be insignificant. Therefore, operation at 15 bar pressure which is the lower limit of operating range was considered for economic analysis.
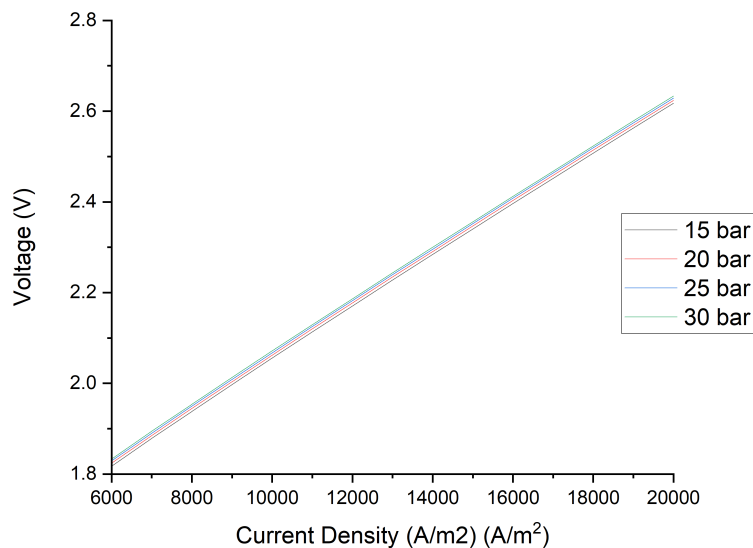
Figure 7.5: Effect of pressure on voltage - current density curve for PEM electrolyzer at 80°C

Membrane water content level:

The membrane content level (λ) directly influences the conductivity of membrane and therefore the ohmic

losses. λ is 12-14 for water saturated gas (100% relative humidity in the membrane) and 22 when exposed to liquid water [65]. The impact on cell voltage due to the membrane water content level is shown in Figure 7.6.
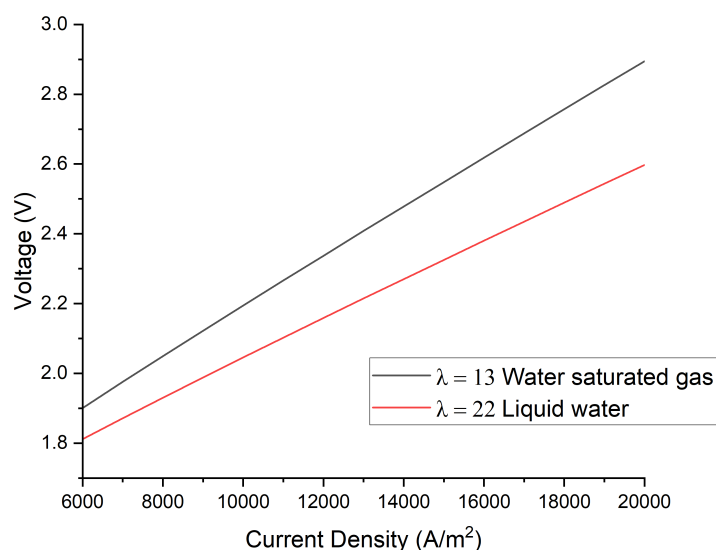
Figure 7.6: Effect of pressure on voltage - current density curve for PEM electrolyzer at 80°C

It can be observed that as water content is increases, the cell voltage reduces significantly. Moreover, the slopes of current density-voltage curve were also found to be slightly different. Higher slope for lower water content was observed implying higher rate of increase of overpotentials. This curve shows that maintaining water content level in Nafion membrane is crucial for maintaining lower cell voltage and thereby reducing the operating costs.

3) Solid oxide electrolyzer

Temperature effects:
The temperature effects on cell voltage of solid oxide electrolyzer were studied by varying the current density from 3000 A/m^2 to 10000 A/m^2. The temperature was varied from 600°C till 850 °C. The results can be seen from Figure 7.7. Similar to the alkaline and PEM electrolyzers, the cell voltage reduces as temperature is increased. As solid oxide electrolyzers operate at very high temperatures, overall influence of overpotential on cell voltage can be observed to be quite low. But, operation at higher temperatures is one of the main factors behind rapid degradation of electrodes and consequently the lifetime of solid oxide electrolyzer.
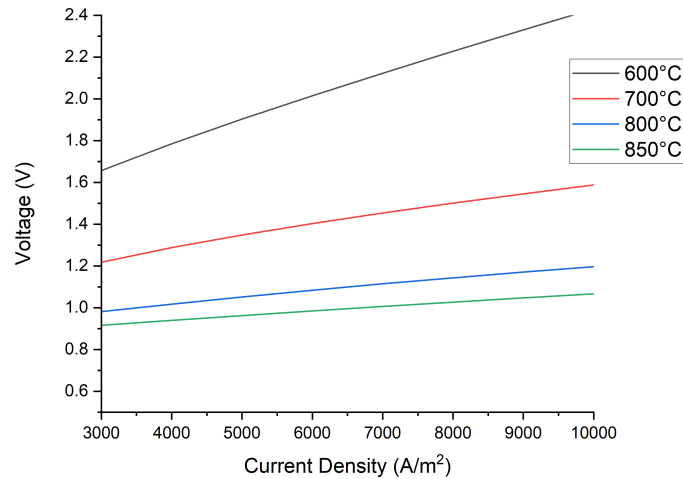
Figure 7.7: Effect of temperature on voltage - current density curve for solid oxide electrolyzer at 1 bar

Pressure effects:

Impact of pressure on cell voltage is quite low as seen from Figure 7.8. Difference of around 0.07 V can be observed in the cell voltage at 1 bar and 30 bar. Therefore, operating solid oxide electrolyzer at 1 bar pressure is more energy efficient as compared to high pressure operation.
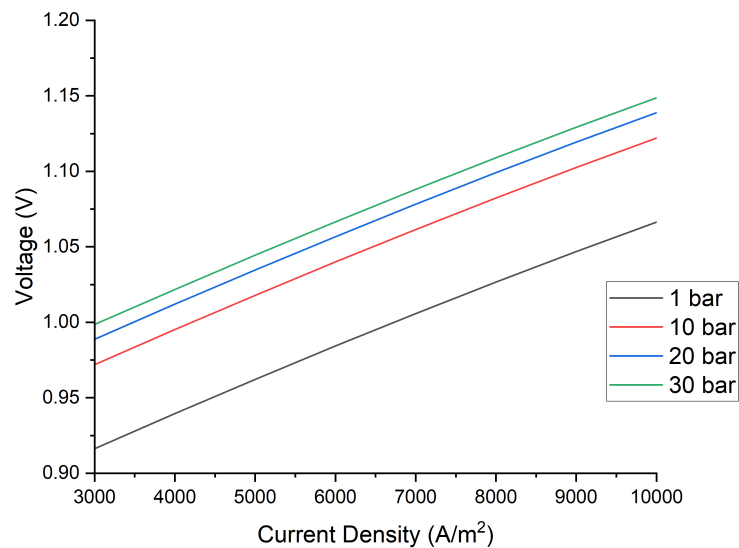
Figure 7.8: Effect of pressure on voltage - current density curve for solid oxide electrolyzer at 850 °C

7.1.2. Levelized cost of hydrogen production

In this subsection, effect of paramters such as operating current density, electricity costs etc. on levelized costs of hydrogen production are discussed. A summary of influencing paramters and their values/ranges used are given in Table 7.1.

Parameter	Alkaline Electrolyzer	PEM Electrolyzer	Solid Oxide Electrolyzer
Operating Temperature (°C)	80	80	850
Operating Pressure (bar)	1	15	1
Current Density (A/m^2)	2000-4000	6000-20000	3000-10000
Stack lifetime (hours)	60,000-90,000	40,000-65,000	20,000- 50,000
CAPEX ($/kW)	540-900	667-1450	677-2285
Electricity cost (€/MWh)	30-110		
Capacity factor	0.4		

Table 7.1: Operating parameters and their values used in cost analysis

Levelized costs on the basis of capital costs of electrolyzer stack
By taking mean operating values from Table 7.1 and considering three cases of capital costs of stack: low, mid and high, levelized costs were obtained and are given in Table 7.2 for a reference 1 MW capacity.

	Alkaline		PEM		Solid oxide	
	Capital cost ($/kW)	LCOH (€/kg)	Capital cost ($/kW)	LCOH (€/kg)	Capital cost ($/kW)	LCOH (€/kg)
Low	540	3.45	667	5.31	677	3.04
Mid	720	3.69	1058.5	6.64	1346	4.55
High	900	3.93	1450	7.98	2285	6.67

Table 7.2: Levelized costs of hydrogen production (€/kg) by considering three different cases of capital costs of stack in $/kW for 1 MW electrolyzer capacity and electricity price of 50 €/ MWh

In Table 7.2, capital costs of stack are in $/kW and levelized costs are given in €/kg. These LCOH were calculated for 1 MW electrolyzer capacity with 50 €/MWh of electricity costs. It can be observed that the LCOH are lowest for alkaline electrolyzers. This is mainly due to low capital costs of stack but also due to higher lifetime of electrolyzer stack. Between PEM and solid oxide electrolyzers, LCOH are lower for solid oxide electrolyzer if low and mid cases of capital costs are considered. This is due to reduced electricity consumption at higher temperatures. To better understand the division of annualized total costs, Figure 7.9 can be referred.

Alkaline Electrolyzer

1.8% 1.6%
31.3%
65.4%

PEM Electrolyzer

1.2% 2.6%
51.6%
44.6%

Solid Oxide Electrolyzer

1.3% 3.3%
29%
66.4%

CAPEX
Electricity
Desalinated water
Maintenance
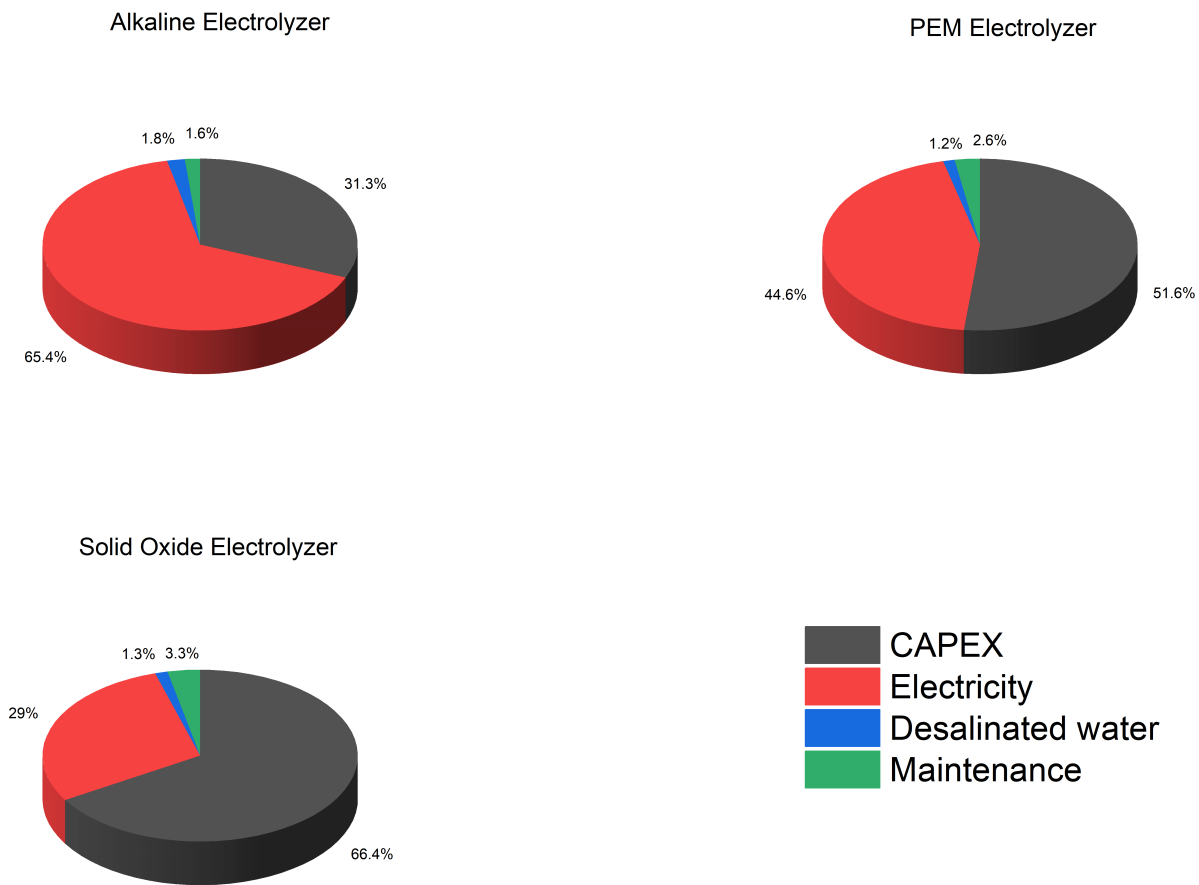
Figure 7.9: Total annualized cost distribution for alkaline, PEM, and solid oxide electrolyzers

It can be observed from Figure 7.9 that contribution of CAPEX costs to the total costs for alkaline electrolyzer is lower as compared to PEM and solid oxide electrolyzers. For alkaline electrolyzer, the total electricity costs contribute to around 65.4% of annual costs. Therefore, it can be inferred that LCOH for alkaline electrolyzer depend significantly on the electricity prices. On the other hand, CAPEX costs dominate the total annual costs of solid oxide electrolyzer. This is due to two reasons: higher capital costs of electrolyzer stack and lower operating cell voltage which reduces the contribution of electricity costs. For PEM electrolyzer, share of CAPEX was found to be 51.6% and that of electricity was found to be 44.6% to the total costs. In case of PEM, operating costs are somewhat similar to the operating costs of alkaline electrolyzer but capital costs of stack are higher.

Effect of electrolyzer capacity on levelized costs

In the economics section of electrolyzer modelling, it was explained that due to modular design of electrolyzers, the decrease in levelized costs as a function of electrolyzer capacity is small. This effect can be observed in Figure 7.10.
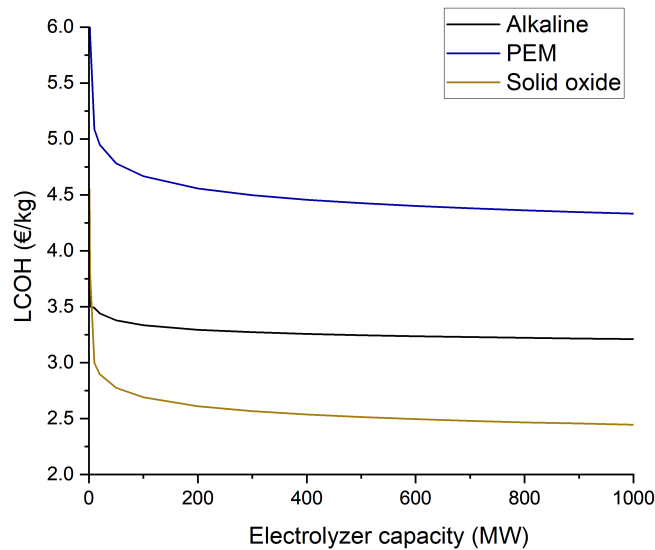
Figure 7.10: Impact of electrolyzer capacity on levelized costs of hydrogen production

The LCOH for solid oxide electrolyzer appear to be the lowest for larger electrolyzer capacities. This is mainly because six-tenth rule for scale factor was applied for capacity until 5 MW. At the same time, scale factors for alkaline and PEM electrolyzers were assumed to be much higher.

Effect of electricity costs on levelized costs of hydrogen production

Electricity costs were varied between 30 €/ MWh to 110 €/ MWh. This price range was chosen on the basis of levelized costs of green electricity from windfarms as reported by IRENA report [14]. The results are shown in Figure 7.11.
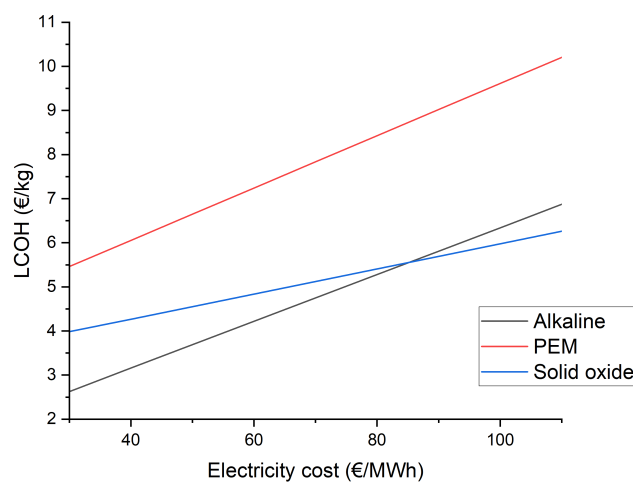
Figure 7.11: Levelized costs with respect to electricity prices

It can be seen from Figure 7.11 that levelized costs of hydrogen production are highest for PEM electrolyzer. Although alkaline electrolyzer has lower LCOH at lower electricity prices, solid oxide electrolyzer has slightly lower LCOH at higher electricity prices. This is because as operating cell voltage of solid oxide electrolyzer is lower, electricity consumption is lower as well. Also, slopes of the curve for alkaline and PEM electrolyzer are almost same and higher than the slope for solid oxide electrolyzer. This difference in slopes is mainly due to the difference in operating cell voltage of solid oxide electrolyzer as compared to PEM and alkaline electrolyzer.

7.1.3. Application of learning curves

As the commercial use electrolysis for hydrogen production is growing annually, the levelized costs of hydrogen production are expected to decrease due to improvement in certain areas such as reliability, decrease in construction costs etc. Thus, to predict this decrease in costs, learning rates are applied. The learning rate for the electrolyzers considered are given in Table 7.3 and are adapted from Patonia et al. [75].

Electrolyzer Type	Learning rate
Alkaline	16 ± 8
PEM	9 ± 2
Solid oxide	20 ± 8

Table 7.3: Learning rates used for the electrolyzers

It can be seen in Table 7.3 that solid oxide electrolyzer has the highest learning rate (12-24 %) while PEM has lowest (7-11%). Using the learning rate mentioned above, and applying Equations 2.11, 2.10 and 2.9, the levelized costs of hydrogen production till 2050 were predicted. It can be observed from Equation 2.9 that the initial cumulative production capacity and its trend across the years also needs to be known. For the cumulative production rates of alkaline electrolysis, projection given by Schmidt et al.[18] was used. For the PEM electrolyzer,15% increase in cumulative production rates between the years 2015 and 2020 and 20% increase between the years 2020-2050 was assumed with cumulative production capacity in year 2015 to be 10 MW. For solid oxide electrolysis, a steady 15% growth was assumed for 2015-2050 with the assumed cumulative hydrogen production capacity to be 100 kW. For the learning curve analysis discussed in this section, reference electrolyzer capacity of 5 MW was assumed with the electricity price of 50 €/MWh. On the basis of these assumptions, levelized costs for the three electrolyzers were predicted.

In Figure 7.12, the predicted levelized costs for alkaline electrolyzer are shown. In this curve, the upper limit of LCOH is for the learning rate of 8% and lower limit is for the learning rate of 24%. In case of high learning rate, the LCOH reduces from 3.7 /kg to 3.4 €/kg. It can be observed that although the learning rate is high, the decrease in levelized costs is limited. This is mainly due to the slow predicted increase in cumulative hydrogen production. By following Schmidt et al.'s [18] methodology, the predicted cumulative hydrogen production increased from 24 GW in 2015 to 47 GW in 2050. Therefore, although the learning rates for alkaline electrolyzer are high, the improvement in LCOH is only around 0.3 €/ kg over the span of 30 years.
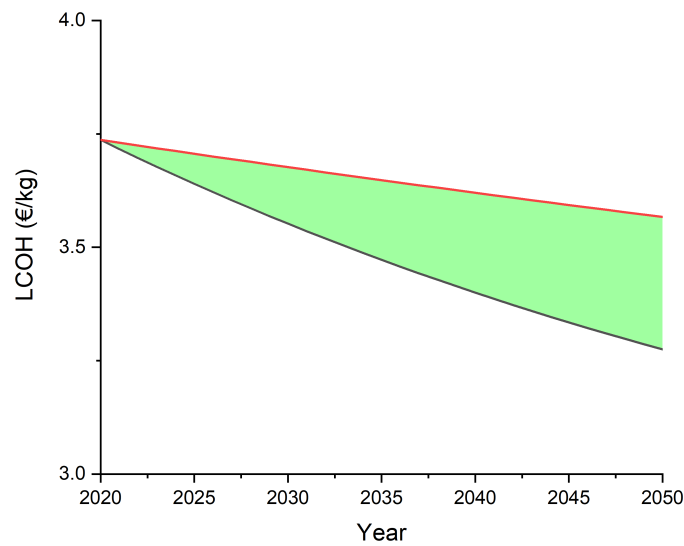
Figure 7.12: Prediction of LCOH for alkaline electrolyzer

In Figure 7.13, the predicted LCOH per year for PEM electrolyzer are given. In case of PEM electrolyzer, learning rates are between 7-11%. With these rates, a decrease of around 0.5 €/ kg can be observed in best case scenario. It can be also observed that LCOH for PEM electrolyzer in 2050 is still higher than LCOH for alkaline electrolyzer in 2020. This is mainly due to the lower learning rates associated with the PEM electrolyzer.
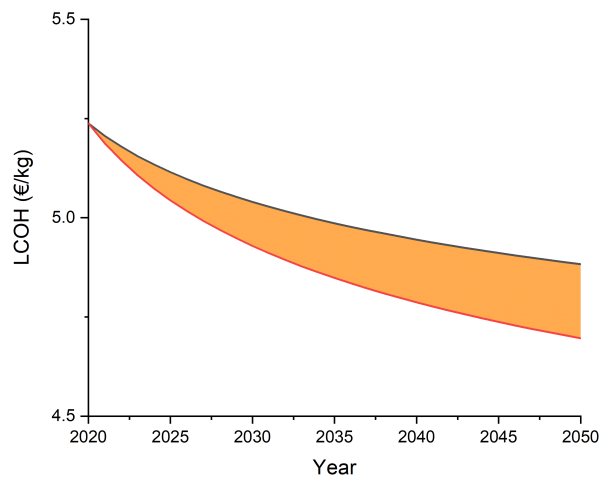
Figure 7.13: Prediction of LCOH for PEM electrolyzer

In case of solid oxide electrolyzer, the decrease in LCOH was found to be substantial as seen in Figure 7.14. This is due to two reasons: the learning rates for solid oxide electrolyzer used in the calculation are quite high as compared to PEM electrolyzer. The second reason is the prediction of cumulative hydrogen production increase which was assumed to 15% per year from 2020 to 2050. Because of the substantially higher rise in production rates is assumed when compared to the other two types of electrolyzers, the drop in LCOH is likewise rather considerable.
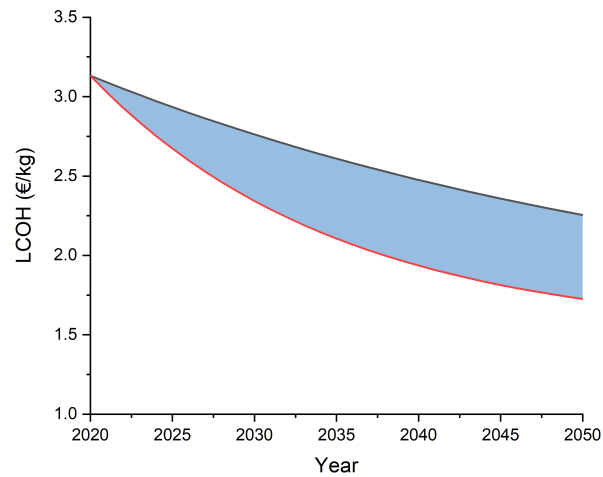
Figure 7.14: Prediction of LCOH for solid oxide electrolyzer

In summary, solid oxide electrolyzers show high potential for cost reduction in future with predicted LCOH range of 1.7-2.5 €/kg in 2050. The LCOH of hydrogen production will decrease for all the three electrolysis process but the cumulative hydrogen production for respective electrolysis process will be a major influencing parameter for the cost reduction.

7.2. Hydrogen Compression

Since hydrogen compression is involved in multiple stages along the supply chain, its influence on the levelized costs is quite significant due to energy intensive nature of hydrogen compression. In this section, the results obtained from the economic analysis for centrifugal and diaphragm compressors are explained.

7.2.1. Impact of flow rate on costs

Centrifugal compressor:

As centrifugal compressors are often used alongside the pipelines to handle large flow rates and for moderate discharge pressures (60-80 bar), the impact of the flowrates was analyzed for flowrates ranging between 30 tonnes of hydrogen per day till 350 tonnes of hydrogen compressed per day. The analysis was done for the discharge pressure of 70 bar and suction pressure of 20 bar. These values were chosen because the transmission pipelines usually operate around 70 bar pressure and along the length of pipeline, re-compression is performed if the pressure of gas in pipeline reaches the range of 20-30 bar [83] to maintain optimum flow rate.

In Figure 7.15 the variation of levelized costs of compression and total capital investments required as a function of flowrates is shown. It can be seen from Figure 7.15 (a), the levelized costs of compression reduce from 0.071 €/kg to 0.062 €/kg as flow rate is increased from 30 t/day to 350 t/day. The slope of levelized cost reduction was observed to reduce in value as flow rate is increased further.
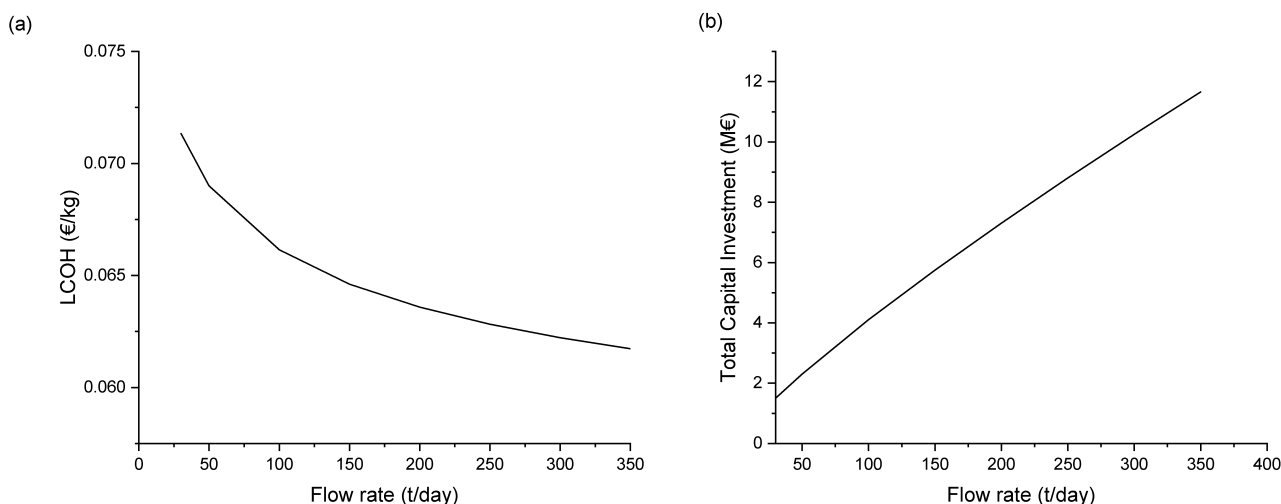
Figure 7.15: Impact of flow rate on levelized costs and total capital investment of centrifugal compressor

From Figure 7.15 (b), the total capital investments can be observed to increase almost linearly as the flowrates are increased.

Diaphragm compressor:

For the diaphragm compressors, two discharge pressure values were analyzed for the economics: 350 bar and 700 bar. This is because the diaphragm compressors are designed for higher compression ratios and relatively low flow rates. Therefore, they will be mainly used at refuelling stations for fuel cell vehicles. Due to space constraints in fuel cells vehicles, the pressure of stored hydrogen is higher: 700 bar for light duty vehicles and 350 bar for heavy duty vehicles [95]. The flow rate was assumed to be in the range of 100 kg/h to 12000 kg/h on the basis of case study done by Khan et al. [41]. The results are shown in Figure 7.16.
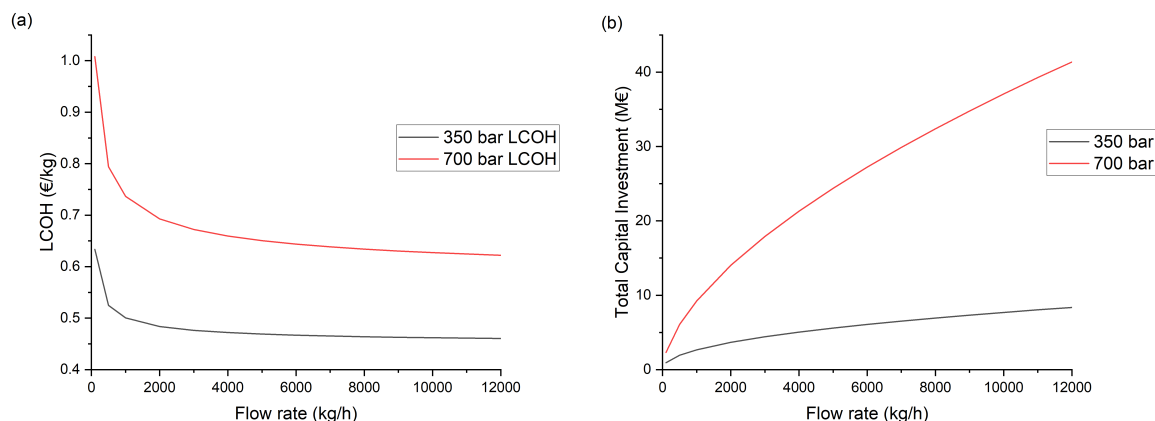
Figure 7.16: Impact of flow rate on levelized costs and total capital investment of diaphragm compressor

It can be observed from Figure 7.16 that levelized costs for high pressure-low flow rate compression are about 10 times higher than centrifugal compression. This is due to significantly increased power requirements and reduced flow rates. The total capital investments for high pressure compression are also in few multiples of moderate compression. The main reason for increase in capital costs is due to increase in the number of required compression stages. By observing Figure 7.16, levelized costs and capital investments are higher for 700 bar compression as expected. But a significant difference between capital investments of 700 bar and 350 bar can be observed. This is because the estimation of capital costs for compressors was based on the power requirements. As 700 bar compression is more energy intensive, the capital costs are subsequently higher.

7.2.2. Effect of suction pressure on costs:

Along the supply chain, the inlet pressure for the compression will vary significantly from alkaline electrolysis (at ambient pressure) to pipeline transport (at 70 bar pressure) to storage in salt cavern (around 140-250 bar). Therefore, the impact of suction pressure on levelized costs needs to be analyzed.

In Figure 7.17, the impact of suction pressure on levelized costs of compression by centrifugal is shown. In this case, the pressure was varied from 1 bar to 30 bar for a fixed flow rate of 150 t/day.
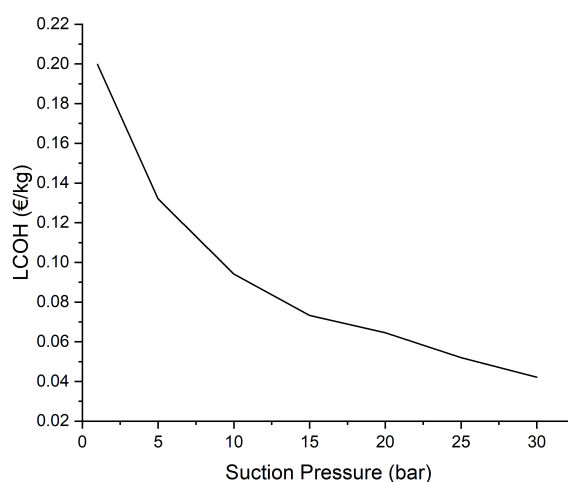
Figure 7.17: Impact of suction pressure on levelized costs of compression for centrifugal compressor

It can be observed from Figure 7.17 that levelized costs of compression decrease significantly from 0.2 €/kg to 0.04 €/kg as the suction pressure is increased.

Similarly, the effect of suction pressure on diaphragm compression to 350 and 700 bar was also analyzed and is shown on Figure 7.18. The suction pressure was varied from 1 bar to 145 bar.
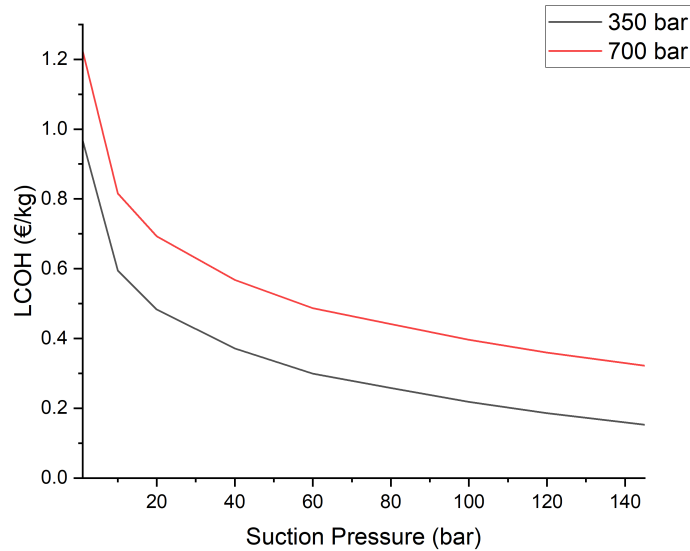
Figure 7.18: Impact of suction pressure on levelized costs of compression for diaphragm compressor

It can be seen that that compression costs for suction pressure at 1 bar are around 1 €/ kg for 350 and 700 bar discharge pressure. While at 145 bar, the levelized costs are about 50% of the costs at 1 bar. Given that the refueling stations where these compressors will be deployed will be supplied by pipelines, the suction pressure will most likely will be in the range of 30-70 bar. For this range, the levelized costs of compression are around 0.3-0.5 €/kg and 0.45-0.65 €/kg for 350 bar and 700 bar respectively.

7.2.3. Impact of electricity costs on levelized costs of compression:

To understand the effects of levelized costs of electricity on levelized costs of compression, electricity prices were varied from 30 €/ MWh to 110 €/MWh. The results for centrifugal and diaphragm compressors are shown in Figure 7.19, 7.20 respectively.
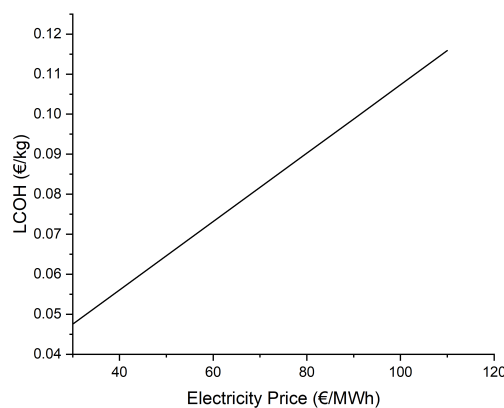
Figure 7.19: Impact of electricity price on levelized costs of compression for centrifugal compressor
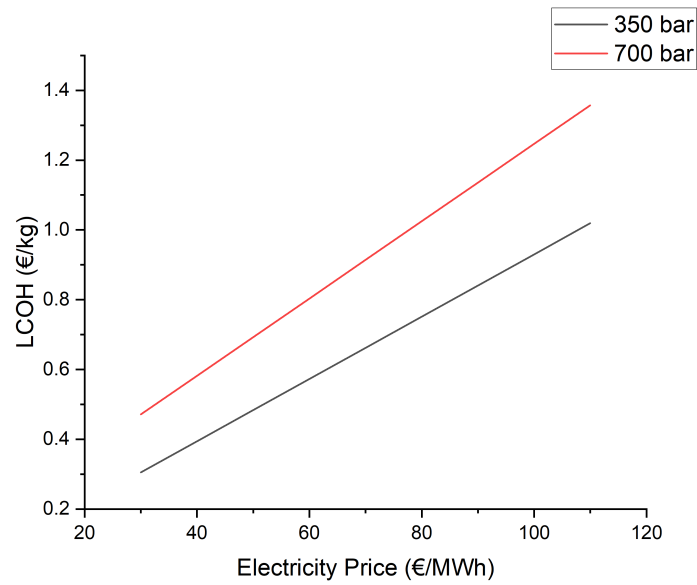
Figure 7.20: Impact of electricity price on levelized costs of compression for diaphragm compressor

It can be observed that electricity prices also have a significant impact on the levelized costs of compression.Thus as renewable energy costs are predicted to reduce in future, compression costs will also decrease.

7.3. Hydrogen Transport

In this section levelized costs of hydrogen transport by pipeline network and impact of some paramters such as diameter of pipe and utilization factor on the levelized costs are discussed. The analysis was performed by assuming project lifetime of 50 years and inlet pressure of 70 bar.

7.3.1. Impact of diameter on costs per kilometer

The internal diameter was varied from 24 inches to 36 inches and variation in levelized costs of transport and total capital investment per kilometer was analyzed. It was assumed that the utilization factor of the pipeline is 90% and inlet pressure of the pipeline is 70 bar. The results are shown in Figure 7.21.
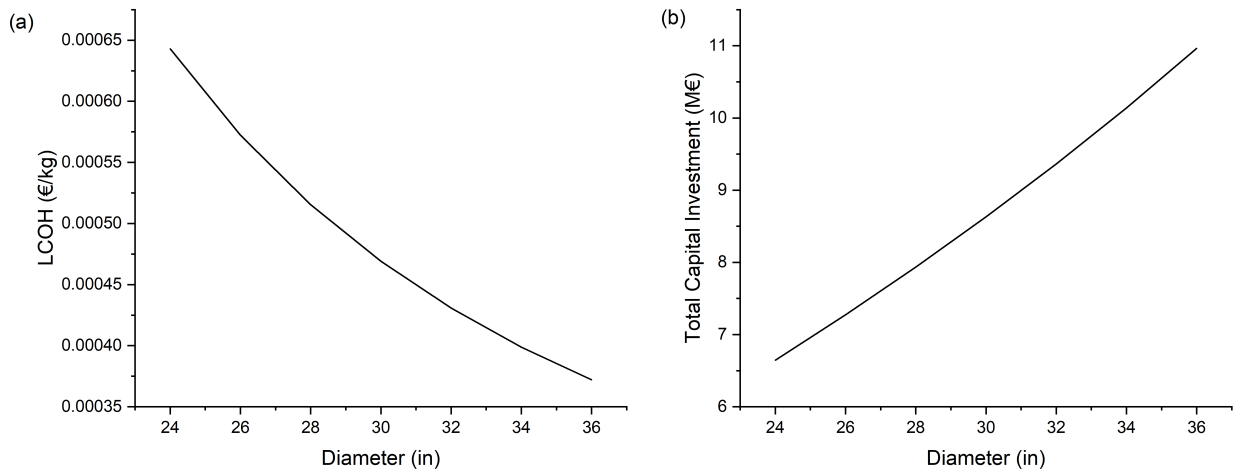
Figure 7.21: Levelized costs and total costs of pipeline per km as a function of pipeline diameter

It can be observed that levelized cost per kilometer travelled are in the range of 0.00037 to 0.00065 depending on the diameter. As the diameter was increased, the levelized cost decreased but capital investment increased almost linearly.

7.3.2. Capital cost distribution of pipeline network

The cost distribution of various parameters involved in the pipeline network is shown in Figure 7.22 for 34 inch pipeline.
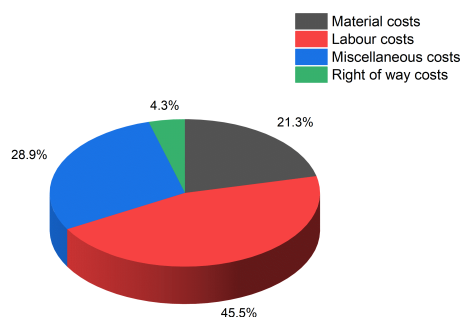
Figure 7.22: Capital cost distribution for the pipeline network

The labour costs seem to be the most influencing parameter on capital costs. This can be explained due to the time and complexity involved in the planning and construction of a pipeline network. Next largest influencing parameter is the miscellaneous costs which involve construction of fittings, valves etc. Although material costs for hydrogen pipeline are around 10% higher as compared to natural gas pipeline, overall impact on levelized costs appears to be low.

7.3.3. Effect of utilization factor on levelized costs

As the pipeline network involves very high capital investments, a through survey of demand and supply and some other factors is performed in the planning phase. But, the pipeline life is around 50 years and it is complex to predict the exact nature of demand and supply for this long duration. Moreover, green hydrogen production also has some intermittency. Due to this, daily and seasonal variation in hydrogen transport through the pipeline network will occur. To understand the effects, an utilization factor was introduced in the cost analysis. It was varied between 40% to 90% and results are shown in Figure 7.23.
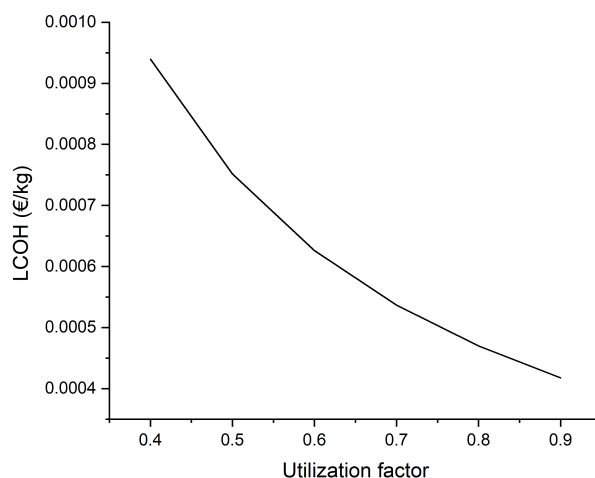
Figure 7.23: Effect of utilization factor on levelized costs of transport

It can be observed that levelized costs of transport are almost twice when utilization factor is low. Therefore, it is important to predict the demand and intermittency while choosing the diameter of pipeline to maintain the utilization factor close to 90% (Assuming around 10% downtime for maintenance) and consequently reduce the levelized costs of transport.

7.4. Hydrogen storage

In this section storage costs associated with salt caverns are discussed. For the salt cavern storage, there are also compression and pipeline costs involved. For the analysis, depth of salt cavern was assumed to be 1500 m and hydrogen production cost was assumed to be 5 €/ kg. Also, compression using diaphragm compressor was assumed with a constant flow rate of 2000 kg/hr. The total pipeline length per salt cavern was assumed to be 1.2 km [6]. The total project lifetime was assumed to be 50 years.

7.4.1. Impact of storage cycles on levelized costs

Amount of total hydrogen stored in a salt cavern in a year significantly impacts the levelized costs of storage as shown in Figure 7.24. The analysis was done by assuming cavern volume to be 500,000 m^3. The levelized costs shown include the capital and operating costs of cavern construction, gas cleaning, compression and required pipeline network.
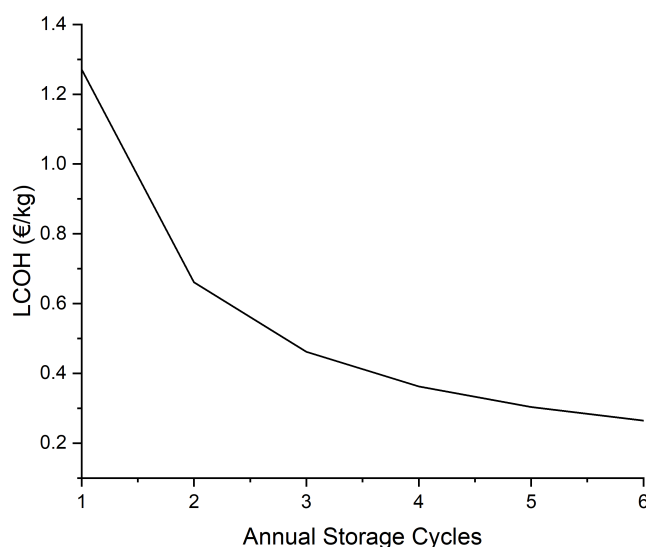
Figure 7.24: Levelized costs of hydrogen storage with respect to annual storage cycles for a salt cavern

For one annual storage cycle, the levelized costs are around 1.3 €/ kg. But the levelized costs drop by 50% by increasing the annual storage cycles and for 6 annual storage cycles, the levelized cost of storage is around 0.4 €/kg. In reality, 6 annual cycles is an optimistic value and there is no clear trend available in the literature. Moreover the levelized costs of storage reported by literature vary between 0.3 €/kg to 1.04 €/ kg [90] depending on the set of assumptions.

7.4.2. Capital cost distribution

For a cavern volume of 500,000 m^3, contribution of various paramters such as cavern construction, cushion gas costs etc. was analyzed and results are presented in Figure 7.25. It can be seen that factors involved with cavern construction (Mining, leaching, integrity tests and wellhead) make up about 79 % of total capital costs. The cavern construction costs were calculated to be 59 M€.
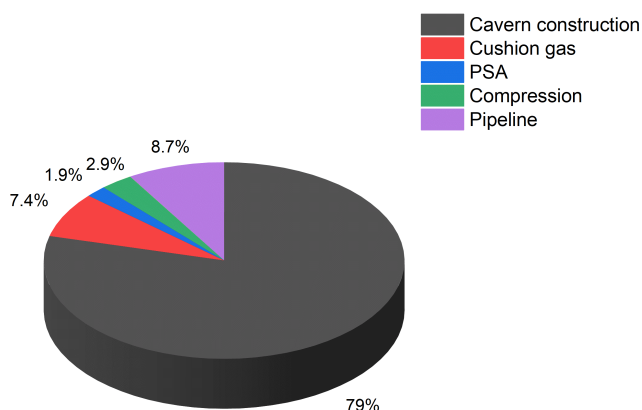
Figure 7.25: Capital cost distribution of a salt cavern

The next largest contributing factor to capital costs is the pipeline network costs closely followed by the cushion gas costs. Hydrogen was assumed to be cushion gas in these calculations. But nitrogen and carbon dioxide can also be used as cushion gas which could reduce the cushion gas costs. On the other hand, gas cleaning costs will increase as these gases will give rise to impurity levels in the hydrogen gas during withdrawal.

7.5. Total levelized costs of hydrogen

In the previous sections, levelized costs associated with hydrogen production, compression, transport and storage were analyzed in detail. In this section, total cost of hydrogen to the consumer under various scenarios is discussed. A summary of levelized costs of hydrogen production, compression etc. is given in Table 7.4.

		LCOH (€/kg)
Production	Alkaline Electrolyzer	3.45-3.93
	PEM Electrolyzer	5.31-7.98
	Solid Oxide Electrolyzer	3.04-6.67
Compression	Centrifugal compression	0.0625-0.071
	Diaphragm compression	0.55-1.2
Transport	Pipeline network	0.0004 - 0.00095 (per km)
Storage	Salt cavern	0.3-1.25

Table 7.4: Summary of levelized costs of hydrogen for different components of supply chain assuming electricity price of 50 €/ MWh

For the evaluation of scenarios, a simplified flow diagram as shown in Figure 7.26 was considered. In this flow diagram, two utilization scenarios are considered: 1) heating and industry 2) Fuel for fuel cell vehicles. For the refuelling scenario, an extra high pressure compression step is required. Initially, a base case scenario is considered with some assumptions. Then, optimistic and pessimistic scenarios are

considered by varying some of the inputs. By applying the learning curves, a comparison is then made between the levelized costs in 2022 and 2050.
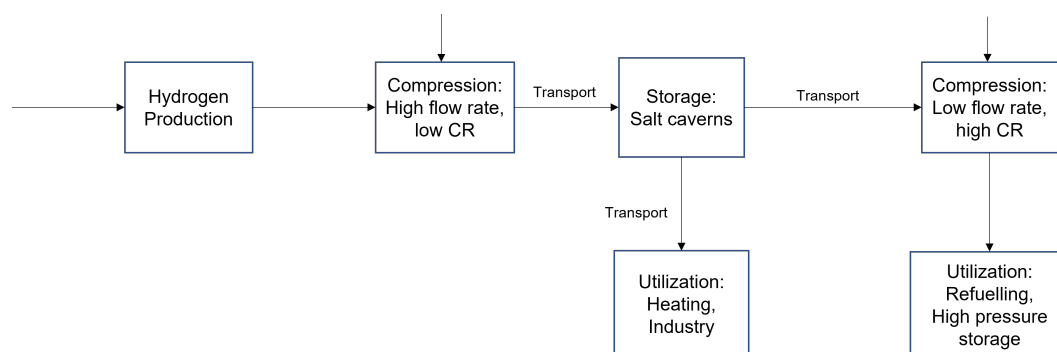
Figure 7.26: Simplified scenario diagram

There are several steps involved in the scenario. Their explanation and some assumptions made are given below:

1. **Electrolysis**: Electrolyzer size of 100 MW is assumed in the scenario with operation at mean current density of the operating range.

2. **Compression**: Compression is involved multiple times throughout the supply chain. But in this scenario, compression at three distinct stages is considered:

   - After hydrogen production (Centrifugal compressor): After hydrogen production at 1 bar, the hydrogen will be compressed to 70 bar pressure and injected into the pipeline network.

   - Before storage in salt cavern(Diaphragm compressor): Hydrogen will be transferred to the salt cavern location and compressed to cavern pressure (260 bar maximum) from pipeline pressure (Assumed to be 30 bar at the outlet of pipeline). A constant flowrate of 2000 kg/hr was assumed

   - For refuelling (Diaphragm compressor): Compression from 30 bar to storage pressure of vehicles (350 bar for heavy duty vehicles and 700 bar for light vehicles) is considered.

3. **Storage**: For storage in salt cavern, the cavern volume of 500,000 m^3 is assumed with the cavern depth of 1500 m. As explained in previous section, number of storage cycles play an important role in storage costs. For the salt cavern location, Groningen was chosen as per Figure 2.12.

4. **Pipeline network**: Although only levelized costs of hydrogen transport per kilometer were discussed in the previous section, total transport distance influence the costs. To better understand the impact, Gasunie's proposed pipeline network as shown in Figure 2.19 was used as a reference map of hydrogen pipeline network in the Netherlands. As the salt caverns are located in the north of the Netherlands and Rotterdam is one of the most important industrial cluster in the Netherlands, hydrogen transport from Groningen salt cavern to Rotterdam was assumed. But since the map in Figure 2.19 does not include the distances and pipeline network shown is not straight, mapping software ArcGIS Pro was used to estimate the total length of pipeline network between Groningen and Rotterdam and is estimated to be 422 km.

7.5.1. Base case scenario

In this scenario, electricity costs are assumed to be 50 €/ MWh. Capital costs of electrolyzer stacks are assumed to be mean values of the range. For centrifugal and diaphragm compressors at refueling stations, flow rate of 150 t/day and 2000 kg/hr are assumed respectively. For salt cavern, 3 annual storage cycles are assumed with compressor flow rate of 6000 kg/hr. For the pipeline network, a utilization factor of 70% is assumed with pipeline diameter of 34 inches. The results obtained for industrial utilization are given in Table 7.5. It can be seen that depending on the type of electrolyzer, the total levelized costs of hydrogen for industry/heating purposes in the base case scenario will range between 3.7 to 5.7 €/kg.

	Alkaline Electrolyzer	PEM Electrolyzer	Solid Oxide Electrolyzer
Production (€/kg)	3.34	4.66	2.69
Compression (€/kg)	0.48	0.48	0.48
Transport (€/kg)	0.167	0.167	0.167
Storage (€/kg)	0.384	0.384	0.384
Total (€/kg)	**4.37**	**5.69**	**3.72**

Table 7.5: Total levelized costs for industrial utilization in base case scenario

It can be observed that the base costs for hydrogen production given in Table 7.5 differ slightly from the levelized costs of hydrogen production discussed in Table 7.2. This is due to the difference in electrolyzer capacity assumed.

For utilization of hydrogen as fuel, extra compression costs are added and the total levelized costs for refueling are given in Table 7.6. For compression to 350 bar, the total LCOH are around 4.13 - 6.1 €/kg and for compression to 700 bar. the total LCOH are in the range of 4.33 - 6.3 €/kg. As compared to levelized costs for industrial purpose, the levelized costs for hydrogen as a fuel can be observed to be around 0.4-0.6 €/kg higher.

	Alkaline Electrolyzer	PEM Electrolyzer	Solid Oxide Electrolyzer
LCOH 350 bar (€/kg)	4.78	6.1	4.13
LCOH 700 bar (€/kg)	4.98	6.3	4.33

Table 7.6: Total levelized costs for hydrogen as a fuel in base case scenario

7.5.2. Optimistic scenario

In this scenario, electricity prices are assumed to be 30 €/ MWh and lower limit of capital costs for electrolyzer stack are used. Flow rates for centrifugal and diaphragm compressor at refueling station are assumed to be similar to base case scenario. Six annual storage cycles for salt cavern are assumed with compressor flow rate of 12000 kg/hr. The pipeline utilization factor of 90% is assumed. The results for optimum case scenario for industrial utilization are given in Table 7.7.

	Alkaline Electrolyzer	PEM Electrolyzer	Solid Oxide Electrolyzer
Production (€/kg)	2.12	2.88	1.53
Compression (€/kg)	0.3	0.3	0.3
Transport (€/kg)	0.13	0.13	0.13
Storage (€/kg)	0.19	0.19	0.19
Total (€/kg)	2.74	3.5	2.15

Table 7.7: Total levelized costs for industrial utilization in optimum case scenario

As seen from Table 7.8, the LCOH for production are significantly lower as compared to base case scenario. This reduction is largely attributable to the lower capital costs of the stack and the decreased electricity costs, which together result in the expectedly lower LCOH for hydrogen production. Total centrifugal compression LCOH also decreased from 0.48 €/kg to 0.3 €/kg. The change observed in transport costs is low mainly due to the fact that utilization factor was changed from 70% (base case) to 90% (optimum case).

For hydrogen as a fuel, the total levelized costs for optimum case scenario are given in Table 7.8. As compared to base case scenario, a significant drop in total LCOH can be observed. The majority of this reduction can be attributed to the decrease in hydrogen production costs. However, another influential factor contributing to the reduction in LCOH is the decline in diaphragm compression costs.

	Alkaline Electrolyzer	PEM Electrolyzer	Solid Oxide Electrolyzer
LCOH 350 bar (€/kg)	3.62	3.76	2.41
LCOH 700 bar (€/kg)	3.77	3.91	2.56

Table 7.8: Total levelized costs for hydrogen as a fuel in optimum case scenario

7.5.3. Pessimistic scenario

For this scenario, electricity prices are assumed to be 110 €/ MWh and upper limit of capital costs for electrolyzer stack are used. Only one annual storage cycle for salt cavern was assumed with compressor flow rate of 2000 kg/hr. The pipeline utilization factor of 40% is assumed. On the basis of these assumptions, the total levelized costs for industry are given in Table 7.9 while levelized costs for hydrogen as a fuel are given in Table 7.10.

	Alkaline Electrolyzer	PEM Electrolyzer	Solid Oxide Electrolyzer
Production (€/kg)	6.66	8.82	5.22
Compression (€/kg)	0.44	0.44	0.44
Transport (€/kg)	0.29	0.29	0.29
Storage (€/kg)	1.18	1.18	1.18
Total (€/kg)	**8.57**	**10.73**	**7.13**

Table 7.9: Total levelized costs for industrial utilization in pessimistic case scenario

As compared to base case scenario, the total LCOH in pessimistic case can be observed to be significantly high as seen from Table 7.7. The primary factor leading to the high LCOH for hydrogen production is the elevated upper limits of capital costs associated with the electrolyzer stack. On top of that, higher electricity prices are assumed in this scenario which causes increase in the LCOH as well. Although such high electricity prices are unlikely to happen in reality, this scenario shows the dependence of LCOH for green hydrogen on levelized costs of electricity.

	Alkaline Electrolyzer	PEM Electrolyzer	Solid Oxide Electrolyzer
LCOH 350 bar (€/kg)	9.43	11.59	7.99
LCOH 700 bar (€/kg)	9.76	11.92	8.32

Table 7.10: Total levelized costs for hydrogen as a fuel in pessimistic case scenario

7.5.4. Prediction of total levelized costs in 2050

As the levelized costs of hydrogen production are expected to decrease in the future, learning rates were applied to the electrolyzers to predict the change in costs. In Table 7.11, the hydrogen production costs in 2022 and predicted levelized costs in 2050 are shown.

	LCOH in 2022 (€/kg)	LCOH in 2050 (€/kg)
Alkaline Electrolyzer	3.34	3.24
PEM Electrolyzer	4.66	4.1
Solid Oxide Electrolyzer	2.69	1.72

Table 7.11: Comparison of levelized costs of hydrogen production in 2022 and 2050

By using the values given in the table above, it can be predicted that the total levelized cost of entire supply chain (assuming costs of other components stays constant) will decrease by 0.1 €/kg, 0.5 €/kg and 0.97 €/kg for alkaline, PEM and solid oxide electrolyzer respectively. But, it should be noted that the learning rates used and estimation of increase in the cumulative hydrogen production rates significantly influence the projected levelized costs.

7.5.5. Summary

In this subsection, a comprehensive summary of levelized costs calculated in the previous sections is given. To gain an understanding of influence of various paramters on the total LCOH, electricity prices were varied from 30 €/ MWh to 110 €/ MWh. Additionally, several other parameters, including the capital costs of the electrolyzer stack and the flow rates for compressors, were also varied. According to the optimistic and pessimistic scenarios, a range of LCOH for different components involved was obtained and is summarized below:

1. **Hydrogen production:** Due to wider capital cost estimates given in literature and also due to the energy intensive nature of the process, LCOH for production also has a wider range. For the alkaline electrolysis, the lower and upper capital cost estimates given in the literature have relatively lower difference as compared to solid oxide electrolysis mainly due to the tech maturity. The resulting range is given below:

   - Alkaline electrolysis: 2.74 - 6.66 €/kg
   - PEM electrolysis: 2.88 - 8.82 €/kg
   - solid oxide electrolysis: 1.53 - 5.22 €/kg

2. **Compression:**
   The total pipeline and salt cavern compression cost was found to be in the range of 0.3 - 0.44 €/kg. The flow rates and electricity prices were found to be the major influencing parameters.

3. **Transport:**
   For assumed pipeline length of 422 km and diameter of 34 inches, the LCOH for transport was found to be in the range of 0.13 - 0.29 €/kg.

4. **Storage in salt caverns:**
   Depending on the annual storage cycles, the LCOH for storage was found to be in the range of 0.19 - 1.18 €/ kg.

5. **Utilization scenario: Hydrogen as a feed**
   The range of total LCOH for hydrogen as a feed by considering different electrolyzers is given below:

   - Alkaline electrolysis: 3.36 - 8.57 €/kg
   - PEM electrolysis: 3.5 - 10.73 €/kg
   - Solid oxide electrolysis: 2.15 - 7.13 €/kg

6. **Utilization scenario: Hydrogen as a fuel**

   (a) **For heavy duty vehicles (Compression to 350 bar)**:

      - Alkaline electrolysis: 3.62 - 9.43 €/kg
      - PEM electrolysis: 3.76 - 11.59 €/kg
      - Solid oxide electrolysis: 2.41 - 7.99 €/kg

(b) **For light duty vehicles (Compression to 700 bar)**:

- Alkaline electrolysis: 3.77 - 9.76 €/kg
- PEM electrolysis: 3.91 - 11.92 €/kg
- Solid oxide electrolysis: 2.56 - 8.32 €/kg

8
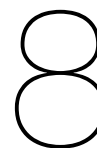
Conclusions and Recommendations

In this chapter, conclusions obtained from results are discussed. Based on the conclusions and limitations faced during modeling phase, recommendations for future research are given.

8.1. Conclusions

This study was done to analyze the techno-economic aspects of green hydrogen supply chain. The supply chain was split into several components such as hydrogen production, compression, storage and transport. a literature review was conducted to identify the most feasible technologies for production, compression, transport and storage. Based on this information, steady state 0-D mathematical models of these components were built on Python with main objective of calculating the levelized costs of each component. A summary and conclusion of each component involved is given below.

8.1.1. Hydrogen Production

Based on the literature review, it was determined that water electrolysis using alkaline, PEM (Proton Exchange Membrane), and solid oxide electrolyzers are viable methods for hydrogen production by considering factors such as tech maturity,reported levelized costs etc. One of the major cost driving factor for hydrogen production was identified to be cell voltage. Therefore, electrochemical models were built to identify the voltage. The voltage values were then validated with experimental/simulation results available in the literature. The analysis was then done to understand the effect of temperature and pressure on the cell voltage. It was found that increasing the temperature and decreasing the pressure reduces the cell voltage for particular current density i.e improves the efficiency. The voltage values were then used for the calculation of levelized costs of hydrogen production. From the results obtained for techno-economical aspects, conclusions obtained for each electrolyzer are explained below:

1. **Alkaline Electrolyzer**
   Operating temperature of 80 °C and pressure of 1 bar was found to be the most optimum by considering cell voltage. Effect of concentration of electrolyte (KOH) was also analyzed and 30% concentration was found to be most optimal. The capital costs of electrolyzer stack were found to be low as compared to PEM and solid oxide electrolyzer. In terms of levelized costs, the alkaline electrolyzer ranked lowest for 1 MW capacity mainly due to low capital costs. But at higher electricity prices, the operating costs increase significantly.

2. **PEM Electrolyzer**
   Similar to the alkaline electrolyzer, operating temperature of 80 °C was found to be most optimal. According to literature, PEM operates at 15-30 bar pressure and operation at 15 bar pressure yielded lower voltage value. Due to higher capital costs as compared to alkaline electrolyzer and higher cell voltages (i.e higher operating costs) as compared to solid oxide electrolyzer, the levelized costs of hydrogen production were found to be highest for PEM electrolyzer.

3. **Solid Oxide Electrolyzer**
   For solid oxide electrolyzer, operating temperature of 850 °C and pressure of 1 bar was found to be optimum from voltage analysis. Due to operation at higher temperature, the cell voltage and

consequently the operating costs were found to much lower than other two electrolyzers. Large variation in reported capital costs of solid oxide electrolyzer stack was found in literature. From the capital costs considered, it was found that levelized costs at 1 MW electrolyzer capacity are second lowest.

Scaling effects on levelized costs were also studied for the electrolyzers. Due to modular design, impact on levelized costs for alkaline and PEM electrolyzers was found to be low. But for the solid oxide electrolyzer, six-tenth rule was followed for scaling factor and due to this, relatively higher impact on levelized cost was observed.

Learning curves were applied to predict the costs of hydrogen production in 2050. During the analysis, it was observed that assumption of cumulative hydrogen production capacity for particular electrolysis method significantly influences the prediction of levelized costs. From the assumptions made for the increase in cumulative hydrogen capacity for the next 30 years, solid oxide electrolyzer shows the highest potential for cost reduction.

8.1.2. Hydrogen compression

After hydrogen production, hydrogen compression was found to be second most energy intensive process involved. As the compression is required multiple times during the supply chain, total compression costs are second biggest contributor in the entire supply chain even if energy costs are lower. Among the compression systems studied, centrifugal compression (High flow rate and moderate compression ratio) contributed the least to the total levelized costs while diaphragm compressors used at refueling stations have significant contribution to the costs. Due to these costs, it can be concluded that compressed hydrogen as a fuel for vehicles will remain expensive as compared to utilization of hydrogen in the industry.

8.1.3. Hydrogen transport by pipeline network

Although levelized costs of hydrogen transport are much lower as compared to hydrogen production, compression etc., the capital investment involved in the construction of hydrogen pipelines was found to be around 10 M€/km. Pipeline lifetime of 50 years was assumed for the analysis but an in-depth analysis is required to assess the impact of hydrogen embrittlement and leakages on total lifetime.

8.1.4. Hydrogen storage in salt cavern

There are some feasible salt cavern structures for hydrogen storage in the north of the Netherlands and also in the north sea. Therefore, salt cavern storage was considered for hydrogen. Not much effect on the levelized costs of storage was observed by changing the cavern volume but the most influencing factor on costs was found to be annual storage cycles.

8.1.5. Total levelized costs of supply chain

Depending on the type of electrolyzer, the levelized costs of hydrogen utilized in an industry are expected to range between 2.15 €/kg to 10.73 €/kg. For hydrogen as a fuel, the levelized costs would range between 2.41 to 11.92 €/kg depending on the type of electrolyzer and discharge pressure.

8.2. Recommendations

On the basis of analysis of obtained results and limitations and assumptions related to the mathematical model, following suggestions are made to model the process more accurately:

1. **Dynamic model of electrolyzers**
   The electrolyzers considered in this study have different start-up times. PEM electrolyzer is known for its faster dynamic response while solid oxide electrolyzer is reported to be sluggish in dynamic response. A dynamic model can be built on the basis of existing steady state model to study the effect of seasonal temperatures and renewable energy intermittency.

2. **Optimization of flow rate in pipelines**
   To estimate the levelized costs, several assumptions were made in the pipeline model. An initial discharge pressure was assumed and it was manually changed until the average velocity was lower than erosional velocity. Also, a steady state model was assumed with no leakages. In reality, some

leakages will be present in the system. More detailed modeling is required to study the effects of leakages and for optimization of flow rate.

3. **Elaborate scenarios**
   Only two major types of scenarios were assessed in this study. One potential scenario that could yield interesting results is centralized vs decentralized production of hydrogen.

References

[1] *Climate policy.* Government Document. 2019. URL: https://www.government.nl/topics/climate-change/climate-policy.

[2] "The Netherlands 2020: Energy Policy Review". In: (2020).

[3] *Netherlands' Electricity Fuel Mix,2021.* Web Page. 2021. URL: https://environmentalprogress.org/netherlands.

[4] Rodolfo Dufo-López et al. "Grid-Connected Renewable Electricity Storage: Batteries vs. Hydrogen". In: *Advances in Mechanical and Electronic Engineering.* Ed. by David Jin et al. Springer Berlin Heidelberg, pp. 221–225.

[5] Nikolay Rogalev et al. "Comparative Analysis of Energy Storage Methods for Energy Systems and Complexes". In: *Energies* 15.24 (2022), p. 9541. DOI: 10.3390/en15249541. URL: https://dx.doi.org/10.3390/en15249541.

[6] D.S. Eradus. "The techno-economic feasibility of green hydrogen storage in salt caverns in the Dutch North sea". Thesis. 2022.

[7] National Center for Biotechnology Information (2023). *PubChem Compound Summary for CID 783, Hydrogen.* Web Page.

[8] *Hydrogen Tools.* Web Page. URL: https://h2tools.org/hyarc/calculator-tools/lower-and-higher-heating-values-fuels.

[9] Etienne Rivard et al. *Hydrogen Storage for Mobility: A Review.* Electronic Article. 2019. DOI: 10.3390/ma12121973.

[10] Lucas Sens. *Hydrogen Supply Chains.* Web Page. URL: https://www.hoou.de/projects/green-hydrogen/pages/3-4-hydrogen-supply-chains.

[11] Adam Christensen. *Assessment of Hydrogen Production Costs from Electrolysis: United States and Europe.* Report. Three seas, 2020.

[12] Ralon Taylor et al. *Renewable Power Generation Costs in 2021.* Report. IRENA, 2021.

[13] IEA. *Renewables 2020.* Report. IEA, 2020. URL: https://www.iea.org/reports/renewables-2020.

[14] IRENA. *Future of wind: Deployment, investment, technology, grid integration and socio-economic aspects.* Report. IRENA, 2019. URL: https://www.irena.org/-/media/files/irena/agency/publication/2019/oct/irena_future_of_wind_2019.pdf.

[15] Leonardo Vidas et al. *Recent Developments on Hydrogen Production Technologies: State-of-the-Art Review with a Focus on Green-Electrolysis.* Electronic Article. 2021. DOI: 10.3390/app112311363.

[16] Jörn Brauns et al. "Alkaline Water Electrolysis Powered by Renewable Energy: A Review". In: *Processes* 8.2 (2020), p. 248. DOI: 10.3390/pr8020248.

[17] S. Shiva Kumar et al. "Hydrogen production by PEM water electrolysis – A review". In: *Materials Science for Energy Technologies* 2.3 (2019), pp. 442–454. DOI: https://doi.org/10.

1016/j.mset.2019.03.002. URL: https://www.sciencedirect.com/science/article/pii/S2589299119300035.

[18] O. Schmidt et al. "Future cost and performance of water electrolysis: An expert elicitation study". In: *International Journal of Hydrogen Energy* 42.52 (2017), pp. 30470–30492. DOI: https://doi.org/10.1016/j.ijhydene.2017.10.045. URL: https://www.sciencedirect.com/science/article/pii/S0360319917339435.

[19] M. Nasser et al. "A review of water electrolysis-based systems for hydrogen production using hybrid/solar/wind energy systems". In: *Environ Sci Pollut Res Int* 29.58 (2022). 1614-7499 Nasser, Mohamed Megahed, Tamer F Ookawara, Shinichi Hassan, Hamdy Orcid: 0000-0002-0156-7186 Journal Article Review Germany 2022/10/25 Environ Sci Pollut Res Int. 2022 Dec;29(58):86994-87018. doi: 10.1007/s11356-022-23323-y. Epub 2022 Oct 25., pp. 86994–87018. DOI: 10.1007/s11356-022-23323-y.

[20] Matheus T. de Groot et al. "Ohmic resistance in zero gap alkaline electrolysis with a Zirfon diaphragm". In: *Electrochimica Acta* 369 (2021), p. 137684. DOI: https://doi.org/10.1016/j.electacta.2020.137684. URL: https://www.sciencedirect.com/science/article/pii/S0013468620320776.

[21] H. Wendt et al. "Ceramic diaphragms for advanced alkaline water electrolysis". In: *Journal of Applied Electrochemistry* 19.4 (1989), pp. 605–610. DOI: 10.1007/BF01022121. URL: https://doi.org/10.1007/BF01022121.

[22] Peter de Laat. *Overview of Hydrogen Projects in the Netherlands*. Catalog. 2022.

[23] Gulru Babac et al. "Two-dimensional thermal analysis of liquid hydrogen tank insulation". In: *International Journal of Hydrogen Energy* 34.15 (2009), pp. 6357–6363. DOI: https://doi.org/10.1016/j.ijhydene.2009.05.052. URL: https://www.sciencedirect.com/science/article/pii/S0360319909007587.

[24] K. Mark Thomas. "Hydrogen adsorption and storage on porous materials". In: *Catalysis Today* 120.3 (2007), pp. 389–398. DOI: https://doi.org/10.1016/j.cattod.2006.09.015. URL: https://www.sciencedirect.com/science/article/pii/S0920586106006377.

[25] Etienne Rivard et al. "Hydrogen Storage for Mobility: A Review". In: 12.12 (2019). DOI: 10.3390/ma12121973.

[26] A. Valera-Medina et al. "Chapter 1 - Introduction". In: *Techno-Economic Challenges of Green Ammonia as an Energy Vector*. Ed. by Agustin Valera-Medina et al. Academic Press, 2021, pp. 1–14. DOI: https://doi.org/10.1016/B978-0-12-820560-0.00001-1. URL: https://www.sciencedirect.com/science/article/pii/B9780128205600000011.

[27] Siddharth Gumber et al. "Chapter 25 - Methanol Economy Versus Hydrogen Economy". In: *Methanol*. Ed. by Angelo Basile et al. Elsevier, 2018, pp. 661–674. DOI: https://doi.org/10.1016/B978-0-444-63903-5.00025-X. URL: https://www.sciencedirect.com/science/article/pii/B978044463903500025X.

[28] Cintia Goncalvez et. al Remco Groenenberg Joaquim Juez-Larré. *Techno-Economic Modelling of Large-Scale Energy Storage Systems*. Report. TNO, 2020.

[29] Fangxuan Chen et al. "Capacity assessment and cost analysis of geologic storage of hydrogen: A case study in Intermountain-West Region USA". In: *International Journal of Hydrogen Energy* 48.24 (2023), pp. 9008–9022. DOI: https://doi.org/10.1016/j.ijhydene.2022.11.292. URL: https://www.sciencedirect.com/science/article/pii/S0360319922056348.

[30] Dilara Gulcin Caglayan et al. "Technical potential of salt caverns for hydrogen storage in Europe". In: *International Journal of Hydrogen Energy* 45.11 (2020), pp. 6793–6805. DOI: `https://doi.org/10.1016/j.ijhydene.2019.12.161`. URL: `https://www.sciencedirect.com/science/article/pii/S0360319919347299`.

[31] Maarten Pieter Laban. "Hydrogen storage in salt caverns". Thesis. 2020.

[32] Miao Yang et al. "A review of hydrogen storage and transport technologies". In: *Clean Energy* 7.1 (2023), pp. 190–216. DOI: `10.1093/ce/zkad021`. URL: `https://doi.org/10.1093/ce/zkad021`.

[33] *Dutch infrastructure*. Web Page. 2007. URL: `https://www.biosng.com/existing-infrastructure/dutch-infrastructure/`.

[34] I.A. Gondal. "Hydrogen transportation by pipelines". In: *Compendium of Hydrogen Energy* (2016).

[35] *Making the Hydrogen Economy Possible: Acclerating Lean Hydrogen in an Electrified Economy*. Report. Energy Transitions Commission, 2021.

[36] Ruben Smit. "Hydrogen infrastructure development in The Netherlands". In: *International Journal of Hydrogen Energy* 32 (2006).

[37] *The Transportation of Natural Gas*. Web Page. URL: `http://naturalgas.org/naturalgas/transport/`.

[38] *Types Of Pipeline Every Oil and Gas Engineer Should Know About*. Blog. URL: `https://blog.enerpac.com/`.

[39] Harry Morgan. *The Netherlands pens the world's first national hydrogen network*. Web Page. 2022. URL: `https://rethinkresearch.biz/articles/the-netherlands-pens-the-worlds-first-national-hydrogen-network/`.

[40] *Hydrogen network Netherlands*. Web Page. URL: `https://www.gasunie.nl/en/projects/hydrogen-network-netherlands`.

[41] Mohd Adnan Khan. *The Techno-Economics of Hydrogen Compression*. Report. 2021.

[42] S. Orlova et al. "Compression of Hydrogen Gas for Energy Storage: A Review". In: *Latvian Journal of Physics and Technical Sciences* 60.2 (2023), pp. 4–16. DOI: `doi:10.2478/lpts-2023-0007`. URL: `https://doi.org/10.2478/lpts-2023-0007`.

[43] G. Sdanghi et al. "Review of the current technologies and performances of hydrogen compression for stationary and automotive applications". In: *Renewable and Sustainable Energy Reviews* 102 (2019), pp. 150–170. DOI: `https://doi.org/10.1016/j.rser.2018.11.028`. URL: `https://www.sciencedirect.com/science/article/pii/S1364032118307822`.

[44] Rahman M Shiddiqur. "Experimental and numerical study of snuber in hydrogen compressor". In: *International Journal of Science and Engineering* 3.2 (2012), pp. 21–25.

[45] Royce N Brown. *Compressors: Selection and sizing*. Gulf Professional Publishing, 1997.

[46] *Linde Introducing Ionic Compressor for Hydrogen Refueling Systems in US*. Web Page. 2009. URL: `https://www.greencarcongress.com/2009/03/linde-introducing-ionic-compressor-for-hydrogen-refueling-systems-in-us`.

[47] EBERHARD Schluecker et al. "New developments in pumps and compressors using Ionic Liquids". In: *Achema Worldwide News* 1 (2008), pp. 5–7.

[48] K.H. Lüdtke. *Process Centrifugal Compressors: Basics, Function, Operation, Design, Application*. Springer, 2004. URL: `https://books.google.nl/books?id=uRvqT3PromMC`.

[49] Syed Mohammed. "Techno-economic analysis of transporting hydrogen and hydrogen based energy carriers in the Netherlands". Thesis. 2019.

[50] R. K. Sinnott. *Chemical engineering design / Ray Sinnott, Gavin Towler*. 5th. Includes bibliographical references and index. Oxford: Oxford : Butterworth-Heinemann, 2009.

[51] Max S. Peters et al. *Plant design and economics for chemical engineers*. 2nd. (viaf). New York (N.Y.) : McGraw-Hill, 1968. URL: http://lib.ugent.be/catalog/rug01:000053778.

[52] Michael Tribe et al. "Scale economies and the "0.6 rule"". In: *Engineering Costs and Production Economics* 10 (1986), pp. 271–278. DOI: 10.1016/S0167-188X(86)80025-8.

[53] Andreas Zauner et al. "Innovative large-scale energy storage technologies and Power-to-Gas concepts after optimization". In: *Analysis on future technology options and on techno-economic optimization2019* (2019).

[54] Mark Bolinger et al. "Levelized cost-based learning analysis of utility-scale wind and solar in the United States". In: *iScience* 25.6 (2022), p. 104378. DOI: https://doi.org/10.1016/j.isci.2022.104378. URL: https://www.sciencedirect.com/science/article/pii/S2589004222006496.

[55] Grant Faber et al. "Adapting Technology Learning Curves for Prospective Techno-Economic and Life Cycle Assessments of Emerging Carbon Capture and Utilization Pathways". In: *Frontiers in Climate* 4 (2022). DOI: 10.3389/fclim.2022.820261. URL: https://www.frontiersin.org/articles/10.3389/fclim.2022.820261.

[56] K. Schoots et al. "Learning curves for hydrogen production technology: An assessment of observed cost reductions". In: *International Journal of Hydrogen Energy* 33.11 (2008), pp. 2630–2645. DOI: https://doi.org/10.1016/j.ijhydene.2008.03.011. URL: https://www.sciencedirect.com/science/article/pii/S0360319908002954.

[57] Edward S Rubin et al. "A review of learning rates for electricity supply technologies". In: *Energy Policy* 86 (2015), pp. 198–218.

[58] A Elia et al. "Impacts of innovation on renewable energy technology cost reductions". In: *Renewable and Sustainable Energy Reviews* 138 (2021), p. 110488.

[59] Nikolaos Kouvaritakis et al. "Modelling energy technology dynamics: methodology for adaptive expectations models with learning by doing and learning by searching". In: *International Journal of Global Energy Issues* 14.1-4 (2000), pp. 104–115.

[60] A Subedi S Niroula C Chaudhary et al. *Parametric Modelling and Optimization of Alkaline Electrolyzer for the Production of Green Hydrogen*. Conference Paper. 2023. DOI: 10.1088/1757-899X/1279/1/012005.

[61] Tohid Adibi et al. "Modeling of thermal performance of a commercial alkaline electrolyzer supplied with various electrical currents". In: *International Journal of Thermofluids* 13 (2022), p. 100126. DOI: https://doi.org/10.1016/j.ijft.2021.100126. URL: https://www.sciencedirect.com/science/article/pii/S266620272100063X.

[62] M. Hammoudi et al. "New multi-physics approach for modelling and design of alkaline electrolyzers". In: *International Journal of Hydrogen Energy* 37.19 (2012), pp. 13895–13913. DOI: https://doi.org/10.1016/j.ijhydene.2012.07.015. URL: https://www.sciencedirect.com/science/article/pii/S036031991201590X.

[63] Christian Henao et al. "Simulation tool based on a physics model and an electrical analogy for an alkaline electrolyser". In: *Journal of Power Sources* 250 (2014), pp. 58–67. DOI: https://doi.org/

10.1016/j.jpowsour.2013.10.086. URL: https://www.sciencedirect.com/science/article/pii/S0378775313017527.

[64] Kevin W Harrison et al. "Semiempirical model for determining PEM electrolyzer stack characteristics". In: (2006).

[65] Z. Abdin et al. "Modelling and simulation of a proton exchange membrane (PEM) electrolyser cell". In: *International Journal of Hydrogen Energy* 40.39 (2015), pp. 13243–13257. DOI: https://doi.org/10.1016/j.ijhydene.2015.07.129. URL: https://www.sciencedirect.com/science/article/pii/S0360319915019321.

[66] JJ Hwang et al. "Dynamic modeling of a photovoltaic hydrogen fuel cell hybrid system". In: *International Journal of Hydrogen Energy* 34.23 (2009), pp. 9531–9542.

[67] KS Agbli et al. "Multiphysics simulation of a PEM electrolyser: Energetic Macroscopic Representation approach". In: *International journal of hydrogen energy* 36.2 (2011), pp. 1382–1398.

[68] D. S. Falcão et al. "A review on PEM electrolyzer modelling: Guidelines for beginners". In: *Journal of Cleaner Production* 261 (2020), p. 121184. DOI: https://doi.org/10.1016/j.jclepro.2020.121184. URL: https://www.sciencedirect.com/science/article/pii/S0959652620312312.

[69] Thomas E Springer et al. "Polymer electrolyte fuel cell model". In: *Journal of the electrochemical society* 138.8 (1991), p. 2334.

[70] Burin Yodwong et al. *Faraday's Efficiency Modeling of a Proton Exchange Membrane Electrolyzer Based on Experimental Data*. Electronic Article. 2020. DOI: 10.3390/en13184792.

[71] Amin Mohammadi et al. "Techno-economic analysis of hydrogen production by solid oxide electrolyzer coupled with dish collector". In: *Energy Conversion and Management* 173 (2018), pp. 167–178. DOI: https://doi.org/10.1016/j.enconman.2018.07.073. URL: https://www.sciencedirect.com/science/article/pii/S0196890418308082.

[72] Meng Ni et al. "Energy and exergy analysis of hydrogen production by solid oxide steam electrolyzer plant". In: *International Journal of Hydrogen Energy* 32.18 (2007), pp. 4648–4660. DOI: https://doi.org/10.1016/j.ijhydene.2007.08.005. URL: https://www.sciencedirect.com/science/article/pii/S036031990700479X.

[73] Fu Wang et al. "Thermodynamic analysis of solid oxide electrolyzer integration with engine waste heat recovery for hydrogen production". In: *Case Studies in Thermal Engineering* 27 (2021), p. 101240. DOI: https://doi.org/10.1016/j.csite.2021.101240. URL: https://www.sciencedirect.com/science/article/pii/S2214157X21004032.

[74] J. Udagawa et al. "Hydrogen production through steam electrolysis: Model-based steady state performance of a cathode-supported intermediate temperature solid oxide electrolysis cell". In: *Journal of Power Sources* 166.1 (2007), pp. 127–136. DOI: https://doi.org/10.1016/j.jpowsour.2006.12.081. URL: https://www.sciencedirect.com/science/article/pii/S0378775307001103.

[75] Aliaksei Patonia et al. *Cost-competitive green hydrogen: how to lower the cost of electrolysers?* Report. The Oxford Institute For Energy Studies, 2022. URL: https://www.econstor.eu/handle/10419/253279.

[76] Hans Böhm et al. "Projecting cost development for future large-scale power-to-gas implementations by scaling effects". In: *Applied Energy* 264 (2020), p. 114780. DOI: https://doi.org/10.1016/j.apenergy.2020.114780. URL: https://www.sciencedirect.com/science/article/pii/S0306261920302920.

[77] Christoph Windmeier et al. "Ullmann's Encyclopedia of Industrial Chemistry: Oxygen". In: 2017, pp. 1–32. DOI: `10.1002/14356007.a18_329.pub2`.

[78] *Hydrogen Delivery Scenario Analysis Model (HDSAM)*. Web Page. 2006. URL: `https://hdsam.es.anl.gov/index.php?content=hdsam`.

[79] *Gases-Ratios of Specific Heat*. Web Page. URL: `https://www.engineeringtoolbox.com/specific-heat-ratio-d_608.html`.

[80] Michael Gustafson. "A Computational Approach to Simulating the Performance of a 24-Hour Solar-Fuel Cell-Hydrogen Electric Power Plant". Thesis. 2013.

[81] Ian H. Bell et al. "Pure and Pseudo-pure Fluid Thermophysical Property Evaluation and the Open-Source Thermophysical Property Library CoolProp". In: *Industrial Engineering Chemistry Research* 53.6 (2014). doi: 10.1021/ie4033999, pp. 2498–2508. DOI: `10.1021/ie4033999`. URL: `https://doi.org/10.1021/ie4033999`.

[82] E. Shashi Menon. "Gas pipeline hydraulics". In.

[83] Mohd Adnan Khan et al. "The Techno-Economics of Hydrogen Pipelines". In: *Transition Accelerator Technical Briefs* 1.2 (2021), pp. 1–40.

[84] W. M. Garrison et al. "12 - Hydrogen embrittlement of high strength steels". In: *Gaseous Hydrogen Embrittlement of Materials in Energy Technologies*. Ed. by Richard P. Gangloff et al. Vol. 2. Woodhead Publishing, 2012, pp. 421–492. DOI: `https://doi.org/10.1533/9780857093899.3.421`. URL: `https://www.sciencedirect.com/science/article/pii/B9781845696771500120`.

[85] Paul W. Parfomak. *Pipeline Transportation of Hydrogen: Regulation, Research, and Policy*. Report. Congressional Research Service, 2021. URL: `https://www.everycrsreport.com/files/2021-03-02_R46700_294547743ff4516b1d562f7c4dae166186f1833e.pdf`.

[86] Anna Huszal et al. *Studies of the Impact of Hydrogen on the Stability of Gaseous Mixtures of THT*. Electronic Article. 2020. DOI: `10.3390/en13236441`.

[87] Tongtao Wang et al. "Safety evaluation of gas storage caverns located close to a tectonic fault". In: *Journal of Natural Gas Science and Engineering* 23 (2015), pp. 281–293.

[88] Ahmet Ozarslan. "Large-scale hydrogen energy storage in salt caverns". In: *International journal of hydrogen energy* 37.19 (2012), pp. 14265–14277.

[89] Remco Groenenberg et al. *Techno-Economic Modelling of Large-Scale Energy Storage Systems*. Report. TNO, 2020.

[90] Seyed Hamidreza Yousefi et al. "Techno-economic analysis of developing an underground hydrogen storage facility in depleted gas field: A Dutch case study". In: *International Journal of Hydrogen Energy* 48.74 (2023), pp. 28824–28842. DOI: `https://doi.org/10.1016/j.ijhydene.2023.04.090`. URL: `https://www.sciencedirect.com/science/article/pii/S0360319923018256`.

[91] Joanna Benson et al. "Recovering hydrogen—And profits—From hydrogen-rich offgas". In: *Chem. Eng. Prog* 114.1 (2018), pp. 55–60.

[92] Fangxuan Chen et al. "Capacity assessment and cost analysis of geologic storage of hydrogen: A case study in Intermountain-West Region USA". In: *International Journal of Hydrogen Energy* 48.24 (2023), pp. 9008–9022. DOI: `https://doi.org/10.1016/j.ijhydene.2022.11.292`. URL: `https://www.sciencedirect.com/science/article/pii/S0360319922056348`.

[93]   Ali Mivechian et al. "Hydrogen recovery from Tehran refinery off-gas using pressure swing adsorption, gas absorption and membrane separation technologies: Simulation and economic evaluation". In: *Korean Journal of Chemical Engineering* 30 (2013), pp. 937–948.

[94]   Doo Hyun Mark Chung. "Techno-Economic Assessment of Electrolytic Hydrogen Production under Dynamic Operations". Thesis. 2022. URL: `https://dspace.mit.edu/bitstream/handle/1721.1/148613/chung-doochung-sm-sdm-2022-thesis.pdf?sequence=1&isAllowed=y`.

[95]   *Dual Pressure Hydrogen Refueling Station*. Web Page. URL: `https://hyfindr.com/dual-pressure-hydrogen-refueling-station/#:~:text=The%20main%20pressure%20combinations%20for%20dual%20pressure%20refueling%20is%20350,to%2050%20kg%20per%20refueling.`.

A

Appendix: CEPCI Indices

The CEPCI indices used in the economical modeling of various components of hydrogen supply chain are given in Table A.1.

Year	CEPCI
2022 Sep	821.3
2021	708.8
2020	596.2
2019	607.5
2018	603.1
2017	567.5
2016	541.7
2015	556.8
2014	576.1
2013	567.3
2012	584.6
2011	585.7
2010	550.8

Table A.1: CEPCI indices used in the economical modeling of supply chain

B

Appendix: Pipeline length calculations for scenario building

For the analysis of transport costs of hydrogen using pipeline network, Gasunie's proposed pipeline network plan for the Netherlands was considered. In Figure 2.19, Gasunie's proposed network connecting some major industrial and transport hubs in the Netherlands is shown. Unfortunately, the length of pipelines connecting these hubs was not available in the literature. Therefore to obtain the length of pipeline required, map shown in Figure 2.19 was carefully traced in ArcGIS software.Pipeline lengths were then obtained using polyline feature and some other tools available in ArcGIS. But some error is expected in the pipeline length estimation. This is due to the fact that image tracing requires fitting of an image over the map manually. Summary of pipeline length calculated between several nodes is shown in Figure B.1

Figure B.1: Length of pipeline network between several nodal points in km

In Figure B.1, the dark green line represents the traced pipeline network and numbers next to it represent the calculated pipeline length in km.